The characterisation of Eukaryotic-like serine/threonine kinases involved in antibiotic resistance in Gram Positive bacteria

Student Name: Tyler Charles Baverstock

Student ID: 1402448

Supervisor: Professor David Roper

Word Count: 27,458

May 2018

Dissertation submitted in partial fulfilment of the Master of Biology (Biochemistry) degree

School of Life Sciences

University of Warwick

Abstract

Gram-positive bacteria are becoming the major cause of multi-drug resistant bacterial infections. These include nosocomial infections from vancomycin resistant *Enterococcus faecalis* or the opportunistic colonisation of the bowel by *Clostridium difficile* post broad spectrum antibiotic treatments. Gram-positive bacteria have developed their own intrinsic resistances to antibiotics along with an enhanced range of mechanisms acquired from other resistant bacterial strains. Bacteria use transmembrane signalling systems to regulate a range of cellular processes including virulence, growth and antibiotic resistance. One such system, originally only thought to be present in Eukaryotes, Eukaryotic-like Serine/Threonine kinases (eSTKs) and their cognate phosphatases are known to regulate such cellular processes. These systems contain a cytosolic kinase domain which autophosphorylate upon detection of an extracellular signal using extracellular PASTA domains. In *Enterococcus faecalis*, there is an example of this system called IreK/IreP, but also similar systems are found in *Enterococcus faecium* and *Clostridium difficile*.

This project was a preliminary study into characterising the autophosphorylation activity of eSTK kinase domains from *E. faecalis*, *E. faecium* and *C. difficile*. Using phosphate detection methods, this work discovered eSTK kinase domains are phosphorylated during overexpression in *E. coli* and can be successfully dephosphorylated by general and cognate phosphatases. This led to the investigation of the effect of an ATP-competitive kinase inhibitor staurosporine on kinase function *in vivo* and *in vitro*. The inhibitor was found to reduce the autophosphorylation activity of IreK and bind with high affinity to the ADP-binding site of the kinase domain. During *in vivo* experiments, Staurosporine was discovered to reduce Cephalosporin resistance in *C. difficile* by over 100-fold. The project contributes to the growing research field of bacterial signalling systems and the prospect of using kinase inhibitors as a combinational therapy against multi-drug resistant bacteria.

Acknowledgments

I wish to take time to thank Professor David Roper for allowing me to take a Mbio project with him and for his insight and guidance throughout the project. I would also like to thank Dr Christopher Thoroughgood and Kathryn Maskew for their patience, teachings, ideas and kindness over the 6-month project. The people in C10 laboratory at Warwick University are also thanked for their welcoming nature, vast knowledge and generation of a friendly environment to work in. During mass spectrometry experiments, I acknowledge the work and help from the WPH Proteomics Facility RTP at the University of Warwick. Finally, I'd like to voice my appreciation for the work Dr Isabelle Carre does for running the Mbio course smoothly.

Table of Contents

List of Abbreviations

SDS	Sodium dodecyl sulfate
APS	Ammonium persulfate
TEMED	Tetramethylethylenediamine
EDTA	Ethylenediaminetetraacetic acid
PBS	Phosphate-buffered saline
eSTK	Eukaryotic-like Serine/Threonine Kinase
PCR	Polymerase chain reaction
E. faecalis	*Enterococcus faecalis*
E. faecium	*Enterococcus faecium*
C. difficile	*Clostridium difficile*
Bp	DNA Base Pair
PBP	Penicillin binding protein
CDC	Centres for Disease Control and Prevention
MICs	Minimal inhibitory concentrations
RT	Room Temperature
KD	Kinase Domain

1.0 Introduction

1.1 Gram-Positive Bacterial cell wall

Bacteria are divided into Gram-positive and Gram-negative categories which the nature of their cell walls are a part of their differentiation. The Gram-positive bacterial cell wall primarily composed of a crucial component, a polymer layer of peptidoglycan, containing glycan strands which are crosslinked by peptides. This polymer provides the cell its shape, structure and integrity as well as an anchoring point for various macromolecules including virulence factors. Peptidoglycan is a polymer unique to bacteria and thus of considerable fundamental and biomedical importance. The architecture and synthesis of the bacterial cell wall have been under continual scientific investigation due to its importance in cell survival and as target for existing and potentially new antibiotic targets.

1.1.1 Structure

The structure of a Gram-positive bacterial cell wall differs to that of its Gram-negative counterpart (**figure 1**). There is no outer membrane nor periplasmic space in Gram-positive bacteria, instead these bacteria have a comparatively larger peptidoglycan layer embedded with lipoteichoic acid and other macromolecules. This peptidoglycan layer is anchored to the cell membrane by diacylglycerol groups.

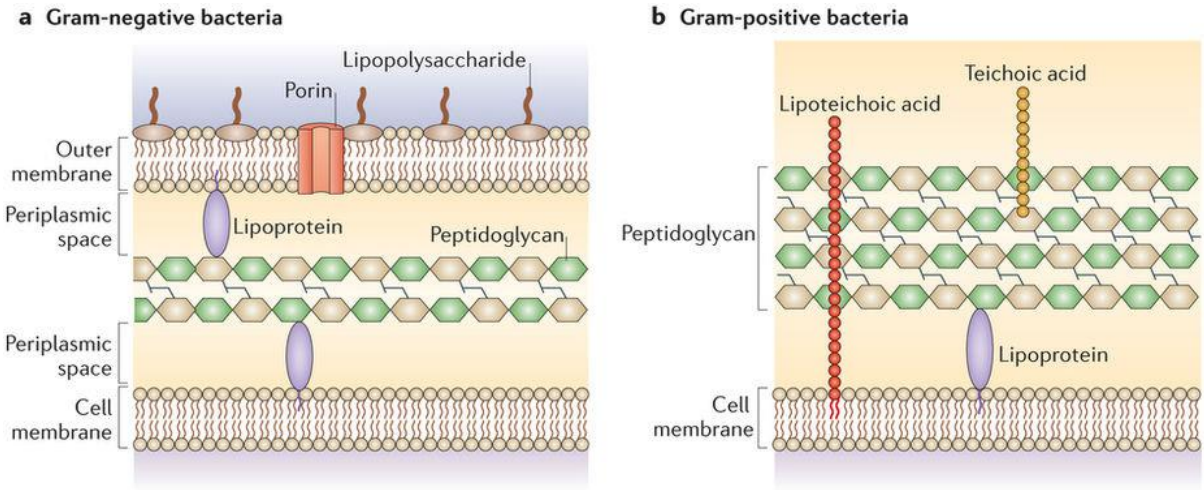

Figure 1: Comparison between structure of Gram-positive and Gram-negative bacterial cell walls. (Brown, Wolf, Prados-Rosales, & Casadevall, 2015)

The peptidoglycan layer is comprised of glycan chains of alternating units of N-acetylglucosamine and N-acetylmuramic acid. These units are crosslinked by two short peptide chains of flexible amino acids. This forms a hydrophilic lattice network which is resistant to hydrophobic compounds such as bile salts, present in the human digestive system. Teichoic acids, another cell wall component, are polymers of ribitol/glycerol linked by phosphodiester bonds and have a role in pathogenesis by virtue of their ability to promote adherence to host tissues during infection. (Beeby, Gumbart, Roux, & Jensen, 2013) (Brown, Wolf, Prados-Rosales, & Casadevall, 2015)

1.1.2 Cell wall synthesis

The cell wall synthesis pathway (**figure 2**) begins with the formation of UDP-MurNAc-L-Ala-D-iGlu-L-Lys-D-Ala-D-Ala (Parks nucleotide) in the cytoplasm from cell wall precursors. This peptidoglycan precursor is transferred to a lipid carrier present on the cytosolic side of the membrane. This creates lipid I. The MurNAc residue is modified into MurNAc-GlcNAc to form lipid II. After further modification, this lipid-anchored peptidoglycan precursor is translocated to the extracellular side of the membrane. Shortly after, this precursor is integrated into the peptidoglycan cell wall by transpeptidation and transglycosylation reactions. These reactions are performed by enzymes called penicillin binding proteins (PBPs). Lastly, the terminal D-alanine present in the wall pentapeptide can be substituted by cross-linking to other peptides or removed by D-alanyl-D-alanine carboxypeptidase. (Beeby et al., 2013) (Navarre & Schneewind, 1999)

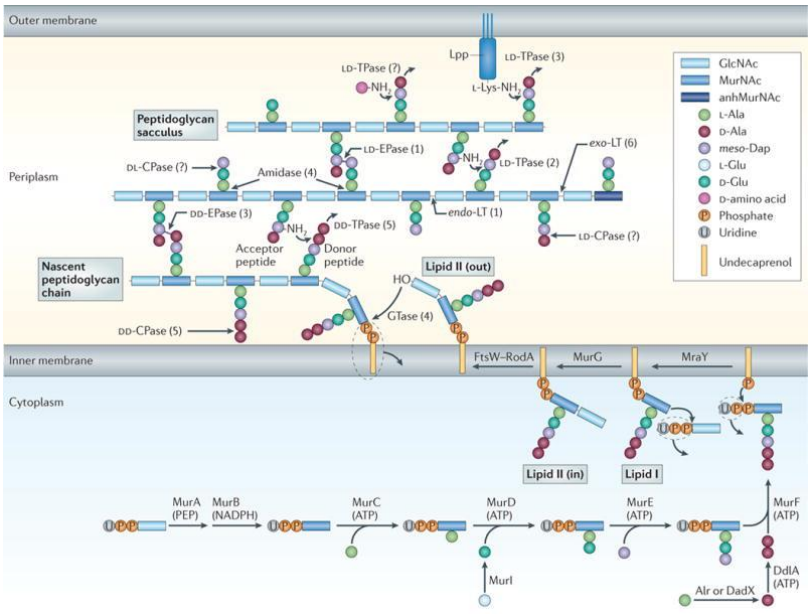

Figure 2: Cell wall synthesis pathway starting from the constituents in the cytoplasm to the extracellular space. (Typas, Banzhaf, Gross, & Vollmer, 2011)

1.2 Cell wall targeting antibiotics

As the cell wall is essential to the survival of bacteria in hostile environments by maintaining cell integrity, the synthesis pathway is a clear target for antibiotics. There are a range of cell wall targeting antibiotics which inhibit different enzymes at different stages of the cell wall synthesis pathway.

1.2.1 β-lactams

The β-lactam class of antibiotics is one of the first widely used classes in treatment of bacterial infections. Derived from the first of its kind penicillin, this class of antibiotics is especially useful due to their broad-spectrum activity against Gram-positive and Gram-negative bacteria. β-lactam molecular structures all contain a beta-lactam ring with a nitrogen bound to the beta carbon relative to the carbonyl ring (**figure 3**). This beta-lactam ring can covalently bind to the active site serine used in the transpeptidase activity of penicillin binding proteins including D-alanyl-D-alanine carboxypeptidases. The inhibition of these enzymes works by blocking substrate binding which results in preventing crosslinking reactions between peptidoglycan chains. This reduces the integrity of the bacterial cell wall. The complex formed between antibiotic and PBPs can stimulate the release of bacterial autolysins which degrade the peptidoglycan cell wall. Bacteria have high internal osmotic pressures and with damage to their cell wall synthesis mechanism, the cell will lyse due to the lower osmotic pressure in the environment (Kong, Schneper, & Mathee, 2010).

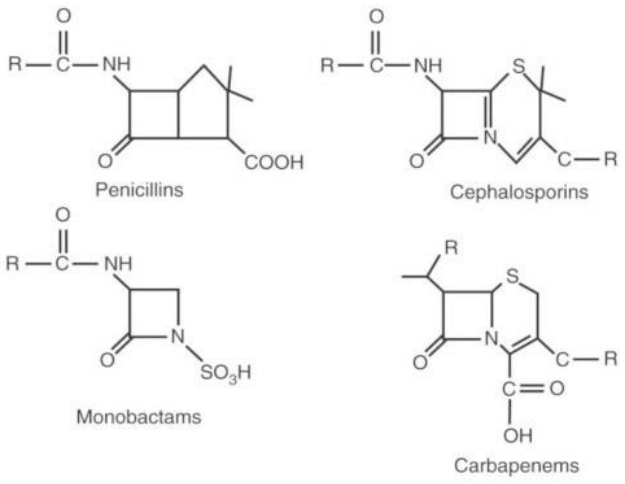

Figure 3: Structure of selected β-lactam antibiotic classes (Guéant, Guéant-Rodriguez, Viola, Valluzzi, & Romano, 2006).

β-lactam antibiotics target specific bacterial cell wall synthesis enzymes like penicillin binding proteins which are not present in human cells. This specific function of β-lactams makes them relatively safe to use, aside from dermatological hypersensitivity reactions and rare anaphylactic reactions (Kong et al., 2010,). Since their original discovery, the β-lactam class of antibiotic have been extensively chemically elaborated to provide several generations of compounds with different spectrums of activity against various bacterial pathogens.

1.2.1.1 β-lactam subclass: Cephalosporins

Due to the rise in antibiotic resistant bacteria, and to extend the spectrum of activity of those vital antibiotics, a range of β-lactam subclasses have been developed to overcome such resistance. One main subclass are called Cephalosporins. The structure of Cephalosporin antibiotics has been derived from the compound Cephalosporin C of the *Acremonium* genus. The main component is the 7-aminocephalosporanic acid core structure which allows the stability against acid hydrolysis and resistance to the action of β-lactamases (Yotsuji et al., 1988). β-lactamases are a set of enzymes which hydrolyse the β-lactam ring and significantly reduce the effectiveness of the antibiotic. There are other β-lactam subclasses including Penicillins, Monobactams, and Carbapenems; all which structural differences which alter their function. This includes a lone β-lactam ring in monobactams which are only effective against aerobic Gram-negative bacteria (Brewer & Hellinger, 1991) or Carbapenems which can inhibit β-lactamases because of an alteration in the carbon to carbon bonds in the β-lactam ring (See section **1.4**). (Papp-Wallace, Endimiani, Taracila, & Bonomo, 2011). The Cephalosporins antibiotic class however, along with glycopeptides, are currently WHO highest priority in critically important antimicrobials (**table 1**) (Kong et al., 2010).

Table 1: WHO Critically important antimicrobials 5th revision assessed on their importance to human medicine. ('WHO | Critically important antimicrobials for human medicine, 5th revision', 2016)

HIGHEST PRIORITY	HIGH PRIORITY	HIGHLY IMPORTANT
Cephalosporins (3rd, 4th and 5th generation)	Carbapenems and other penems	Cephalosporins (1st and 2nd generation) and cephamycins
Glycopeptides	Penicillins (natural, aminopenicillins, and antipseudomonal)	Penicillins (anti-staphylococcal)
Macrolides and ketolides	Aminoglycosides	Streptogramins
Polymyxins	Lipopeptides	Tetracyclines
Quinolones	Monobactams	Amidinopenicillins

1.2.2 Glycopeptides

Another class of cell wall targeting antibiotics is the Glycopeptide class with examples including vancomycin and teicoplanin. Glycopeptide antibiotics are only effective in treatment of Gram-positive bacteria because the antibiotic is unable to penetrate the outer membrane of Gram-negative bacteria. Glycopeptides are large "cup-shaped" natural product molecules which have peptide chains bonded to glycan groups. This structure contains a cleft which a specific bacterial peptide sequence D-alanine-D-alanine can fit. Glycopeptides can form hydrogen bonds with peptides with this specific configuration, resulting in a stable complex. When glycopeptides bind to these groups in cell wall synthesis precursors, it prevents the formation of peptidoglycan chains due to steric hinderance. The next stages of cell wall synthesis including transpeptidation, are therefore inhibited due to misalignment of transpeptidase enzymes. The result is the same as β-lactam treatment, leading to reduced cell wall integrity, that ends in cell lysis. As the binding of glycopeptide antibiotics to the peptidoglycan subunits occurs outside of the membrane, acquiring resistance to this class of antibiotic is more difficult to that of β-lactams for example. (Kang & Park, 2015; Reynolds, 1989)

Glycopeptides may have a high effectiveness against Gram-positive bacteria, however this antibiotic class does usually lead to several side effects. One example is vancomycin which is regarded as an antibiotic of last resort against bacterial infection. One reason for this is that vancomycin is only used to treat highly resistant bacterial strains such as *Clostridium difficile* which only a few antibiotics can treat effectively. The other reason is that vancomycin is a nephrotoxic agent and although it is usually removed by the kidneys, it can cause kidney damage in patients with impaired renal functions. Vancomycin and teicoplanin, another glycopeptide antibiotic, can cause hypersensitivity reactions including red man syndrome and anaphylaxis. Both are characterised by itching and flushing of face, neck and torso but anaphylaxis can lead to other symptoms such as shortness of breath, low blood pressure and death. (Kuriyama, Karasawa, & Williams, 2014; Pubchem, 2018)

1.3 Pathogenic Gram-Positive bacteria

Despite the current crisis regarding the lack of available antibiotics for Gram-negative infections, Gram-positive bacteria are associated with the majority of clinical infections resulting in morbidity and mortality (Eades, Hughes, Heard, & SP Moore, 2017). The severity of Gram-positive infections is exacerbated by the presence of multi-antibiotic resistant strains ranging from Methicillin-resistant *Staphylococcus aureus* (MRSA) and *Clostridium difficile* to highly resistant strains of *Enterococci*. This project focused on three specific pathogenic Gram-positive bacteria: *Enterococcus faecalis, Enterococcus faecium* and *Clostridium difficile*.

1.3.1 *Enterococcal* structure and metabolism

A part of the *Firmicutes* phylum, *Enterococcus faecalis* and *Enterococcus faecium* are commensal bacteria which reside in the gastro-intestinal tract of humans as a part of the natural intestinal flora. They are also present in soil, water and plants. Their cell structure is typical of *Enterococci*: they are spherical shapes that can exist as either short chains or reside in pairs. These bacteria can also express pili which promote cell to cell interaction to form biofilms, especially in *E. faecalis* strains which are known to cause endocarditis (Paulsen et al., 2003). The cells however are non-motile with no expression of flagella. (Gilmore, Clewell, & Courvalin, 2002)

E. faecalis and *E. faecium* can survive in a wide range of environments due to their flexible metabolism. These bacteria can produce lactic acid from fermentation and can catabolise a range of carbon sources such as carbohydrates, glycerol citrate and diamino acids (Maza, Pezzlo, & Shigei, 2004). *E. faecalis and E. faecium* can also tolerate oxidants like hydrogen peroxide which are produced as a part of oxidative phosphorylation. The bacteria can also tolerate azide detergents and ethanol. As a result of the accumulation of these tolerances, both *E. faecalis* and *E. faecium* can survive in bile salts, extreme pH conditions and grow at temperatures between 10 – 45 °C. (Werner et al., 2013) (Maza et al., 2004)

1.3.2 *Enterococcal* Pathology and treatment

These bacterial species are both present on the WHO pathogen watchlist of 2017 with a high priority for new antibiotic treatments (Tacconelli et al., 2018). This is due to a range of contributing factors. Firstly, *E. faecalis* and *E. faecium* are becoming the leading cause of nosocomial infections including local and systematic infections affecting the urinary tract and wounds but also causing bacteraemia and endocarditis (Huycke M, Sahm F, & Gilmore S, 1998). To promote hospital-based infections, both species can survive for long periods of

time in the environment promoting the faecal-oral route of transmission. Strains expressing the *Esp* gene for the *enterococcal* surface protein can aggregate and form biofilms, but this is usually not the case for commensal strains (Wamel et al., 2007).

Aside from potentially fatal infections, *E. faecalis* and *E. faecium* have become a challenge to treat due to intrinsic and acquired resistances to a wide range of antibiotics including β-lactams, aminoglycosides and glycopeptides (Kristich, Rice, & Arias, 2014). This is especially the case in vancomycin-resistant *Enterococci* which not only carry resistance to vancomycin but also to other antibiotic classes such as aminoglycosides and β-lactams like ampicillin. The concern for both *E. faecalis* and *E. faecium* infection is the transfer of resistance plasmids to other commensal bacteria in the gut and related bacterial species in the environment (Hollenbeck & Rice, 2012). Ultimately, both *E. faecalis* and *E. faecium* are becoming dangerous multi-drug resistant Gram-positive bacteria resulting in an increasing number of fatal hospital-based infections in humans.

1.3.3 *Clostridium difficile* structure and metabolism

Another Gram-positive bacterium from the *Firmicutes* phylum, *Clostridium difficile* is a spore forming anaerobic bacterium which is difficult to treat due to its intrinsic antibiotic resistance (Paredes, Alsaker, & Papoutsakis, 2005). It is a rod shaped or often spindle-shaped bacteria with a bulge at their terminus which aids in spore formation. *C. difficile* is also able to generate ATP from amino acid fermentation, like *Enterococci* (Jackson, Calos, Myers, & Self, 2006). When in the presence of sugars, *C. difficile* can grow exponentially to promote growth and colonisation while repressing the expression of virulence proteins, toxin A and B, for when colonisation is established (Dupuy & Sonenshein, 1998).

C. difficile's ability to survive in extreme environments is more enduring than *Enterococci* due to the ability to form spores. Should the bacteria be under extreme environmental stress from low pH or high heat, it can transfer into a dormant state and form spores (Rao, Jump, Pultz, Pultz, & Donskey, 2006). These spores can persist for up to two years and survive under more extreme conditions such as antibiotic treatment. If the environmental conditions improve, *C. difficile* can covert back to the active growth state in the more favourable conditions (Wilson, 1993). Another environment coping mechanism, *C. difficile* can also adhere to human tissue cells by increasing expression of surface adhesion proteins, which facilitate bacterial colonisation (Hennequin et al., 2001). The active form of *C. difficile* appears to be less tolerant of extreme temperatures when compared to *Enterococci*

however, although not a commensal bacterium, *C. difficile* grows optimally at 37 °C, human body temperature (Heinlen & Ballard, 2010).

1.3.4 *Clostridium difficile* Pathology and treatment

C. difficile is currently at hazard level urgent by the CDC due to its opportunistic infection to patients undergoing medical care that received antibiotic treatment, especially in elderly individuals. In a 2015 CDC study (CDC, 2016), *C. difficile* caused around half a million infections in the United States in a year which resulted in around 15,000 deaths directly linked to *C. difficile* infection. The bacteria are transferred person to person via the faecal-oral route, mostly in the hospital environment. *C. difficile* will inhabit the colon and gastro-intestinal tracts where it competes with commensal bacteria. If the patient however has recently taken antibiotic treatments, the nutrient and space competition for *C. difficile* is removed, enabling colonisation (Heinlen & Ballard, 2010). Once colonised, 70 % of strains will produce an enterotoxin (toxin A) and all strains will release a cytotoxin (toxin B). These toxins cause diarrhoea, mucosal injury and inflammation. This is because of the inactivation of Rho GTPases by glycosylation and disruption of tight junctions between intestinal epithelial cells leading to increased paracellular permeability (Gianfrilli et al., 1984). Toxin A can also interact with mast cells to release inflammatory granules and increase the expression of prostaglandins. This action is the major cause of antibiotic associated pseudomembranous colitis in most cases. (Gianfrilli et al., 1984)

C. difficile is becoming increasingly difficult to treat due to several factors. Firstly, the bacteria can express the *cdeA* gene which produces a multidrug efflux pump conferring resistance to multiple antibiotics (Dridi, Tankovic, & Petit, 2004). Secondly, the spore forming ability of this bacteria allows them to resist antibiotic treatment for a long time and then allow a secondary infection to occur when the bacteria convert back to their active form (Heinlen & Ballard, 2010). The current treatment for *C. difficile* is vancomycin or metronidazole but the bacteria may survive after spore formation (Freeman, Baines, Saxton, & Wilcox, 2007). Overall, *C. difficile* is becoming a dangerous bacterium to patients undergoing antibiotic treatment and, with other bacterial species like *E. faecalis* developing antibiotic resistance to vancomycin, *C. difficile* could become a highly resistant strain to complement its already resistant phenotype.

1.4 Gram-Positive bacteria resistance mechanisms

1.4.1 *Enterococci* Intrinsic resistance mechanisms

Enterococcus faecalis and *Enterococcus faecium* both have a set of intrinsic antibiotic resistances found in the genome of the species. They also can acquire resistance through random sporadic mutations in intrinsic resistance genes; the acquisition of genetic material from the environment; or through horizontal gene transfer from a related strain. It is possible that this ability of combining intrinsic and acquired resistance genes could lead to *Enterococci* becoming resistant to all effective antibiotics.

1.4.1.1 *Enterococci* Intrinsic resistance to β-lactam/Cephalosporins

As mentioned earlier in section **1.2.1**, β-lactam antibiotics target the transpeptidase enzymes called penicillin binding proteins (PBPs) which catalyse the cross-linking reactions between peptidoglycan chains. The binding of β-lactam antibiotics inhibits the action of PBPs leading to impaired cell wall synthesis.

Enterococci can express PBPs that have a low affinity to β-lactam binding, such as; PBP4 in *E. faecalis* and PBP5 in *E. faecium.* This results in normal transpeptidase activity in the presence of β-lactam treatment. Because of this, the minimum inhibitory concentrations (MICs) of both *E. faecalis* (2-8 μg/ml) and *E. faecium* (8-16 μg/ml) for penicillin is greater than other Gram-positive bacteria which do not have low affinity PBP genes in their genome (Sifaoui, Arthur, Rice, & Gutmann, 2001).

Another resistance mechanism against penicillins is the expression of the enzyme superoxide dismutase. During antibiotic-induced bacterial stress, superoxide is produced which at high concentrations, is toxic to the cell. Superoxide dismutase breaks down superoxide molecules into oxygen and hydrogen peroxide. The harmful increase in hydrogen peroxide is prevented by peroxidase and catalase reactions (Bizzini, Zhao, Auffray, & Hartke, 2009).

1.4.2 Routes of acquired resistance

The first route of acquired resistance is sporadic mutations in the resistance genes that, for example, produces a PBP with an even lower affinity for β-lactam binding, leading to a greater chance of cell survival. The second route of acquired resistance is the taking up of foreign genetic material through pheromone-sensitive or broad host range plasmids or through the movement of transposons (Palmer, Kos, & Gilmore, 2010).

In *E. faecalis*, pheromone-responsive plasmids are used to transfer genetic material at high frequency but only to the same species. This works by recipient cells releasing lipoprotein fragments (pheromones) to attract donor cells and stimulate aggregation. Recipient-donor contact is stimulated by *enterococcal* binding substance on the cell membrane. This facilitates highly efficient genetic exchange. Broad host range plasmids can transfer genetic material to other Gram-positive strains but at a low frequency to pheromone-responsive plasmids. This route is how some *Staphylococcus aureus* strains have started to acquire vancomycin resistance from *Enterococci* (Palmer et al., 2010). Lastly, transposons are the majority cause of gene mobility in *Enterococci*. Transposons like the Tn*3* family contain multiple resistance genes including those conferring glycopeptide resistance. Composite transposons are mobile insertion sequences that promote the mobility and integration of plasmid resistance genes into the genome (Hegstad, Mikalsen, Coque, Werner, & Sundsfjord, 2010).

1.4.2.1 *Enterococci* acquired resistance to β-lactam/Cephalosporin antibiotics

E. faecalis and *E. faecium* can obtain enhanced resistance to β-lactam treatments from plasmids from *S. aureus*. *E. faecalis* has been known to develop increased resistances to penicillins through β-lactamase expression and PBP4/5 sporadic mutations. β-lactamases are hydrolases which target amide and ester bonds present in all penicillins, third generation Cephalosporins, aztreonam however β-lactamases are ineffective against Cephamycins and Carbapenems. These enzymes cleave the amide bond in the β-lactam ring, significantly reducing the effectiveness of the antibiotic (Bonnet, 2004).

The most common cause of penicillin resistance in *Enterococci* is the generation of a number of point mutants in the β-lactam binding site of PBP5 (Zapun, Contreras-Martel, & Vernet, 2008) which is a functional homologue of the methicillin resistance PBP2a in *S. aureus*. These point mutations increase in frequency because of selective pressure from antibiotics. The chromosome based transfer of low affinity *pbp5* genes is another route to acquire low affinity PBP5 (Rice et al., 2005).

1.4.2.2 *Enterococci* acquired resistance to Glycopeptide antibiotics

As previously outlined in **1.2.2**, glycopeptide antibiotics like vancomycin, function by binding to the D-ala-D-ala terminus of the pentapeptide precursor which results in the inhibition of cell wall synthesis (Watanakunakorn, 1984). In *Enterococci* glycopeptide-resistant strains these terminal domains are replaced by D-lac or D-ser. The modified termini of pentapeptide precursors have a 1,000-fold reduced binding affinity to glycopeptide antibiotics. A gene cassette called Van contains operons called VanA, H, X, Y, Z, R and S. This cassette is located in a Tn*3* transposon family transposon Tn*1546* which confers different types of glycopeptide resistance including the modified termini precursor. The VanA and VanB operons are the most prevalent in glycopeptide resistant *Enterococci* strains. (Eliopoulos & Gold, 2001)

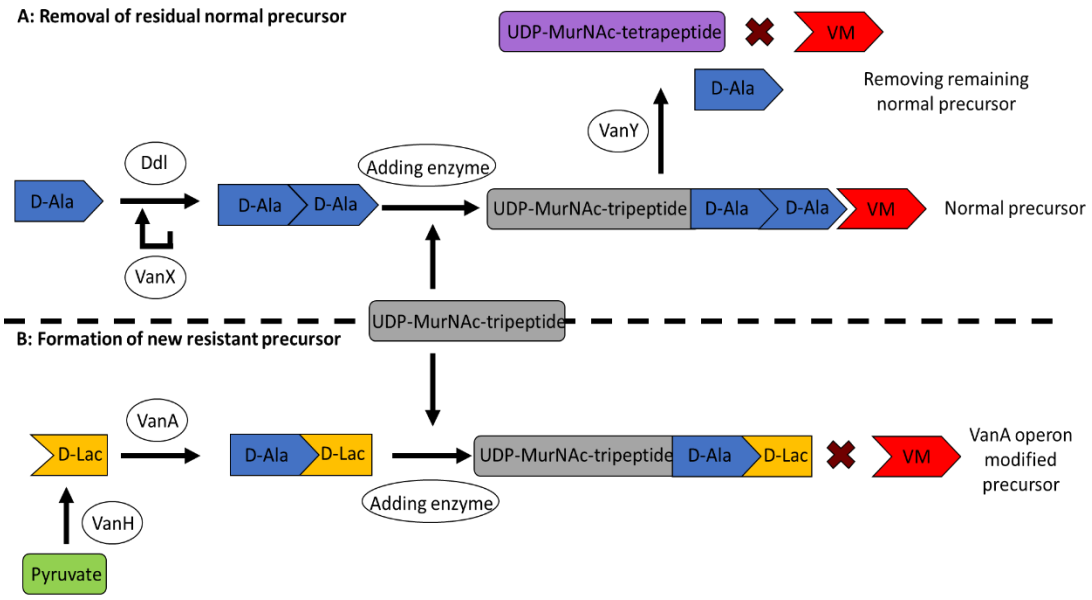

Figure 4: Mechanisms of vancomycin resistant peptidoglycan precursor synthesis in VanA *Enterococci*. Adapted from (Eliopoulos & Gold, 2001)

The function of each gene in the operons can be shown using VanA as a model for the other operons (**figure 4**). Firstly, pyruvate is converted to D-lactate using VanH hydrogenase and then VanA ligase ligates D-ala and D-lac together. *Enterococcal* host enzymes then ligase D-ala-D-lac to the tripeptide precursor which results in the low affinity pentapeptide precursor. The normal D-ala-D-ala precursors are also removed to confer full glycopeptide resistance. VanX hydrolyses D-ala-D-ala into amino acids which results in only D-ala-D-lac being the substrate of cell wall precursors. To remove any normal precursors remaining in the cell, VanY hydrolyses the terminal D-ala present on normal precursors, which makes them unusable to the cell. VanZ has an unknown function but has appeared to increase resistance to teicoplanin (Eliopoulos & Gold, 2001; Gagnon et al., 2011).

The Van gene cluster is regulated by a part of the VanA operon: VanR and VanS which compose a two-component sensor-transducer system (section **1.5.2**). If glycopeptide antibiotics are present in the environment, VanS activates, and autophosphorylates, and then phosphorylates VanR. The phosphorylated VanR interacts with specific promoter regions of VanH, A, X, Y, Z, R and S and enhance their transcription. *Enterococci* VanR and VanS mutants become susceptible to vancomycin and teicoplanin treatments suggesting that VanR is required for optimum expression of the VanA operon (Eliopoulos & Gold, 2001; Gagnon et al., 2011; Healy, Lessard, Roper, Knox, & Walsh, 2000).

1.4.3 *Clostridium difficile* resistance mechanisms

The antibiotic resistance mechanisms of *C. difficile* are significantly less characterised in comparison to *Enterococcus*, perhaps because until recently, *C. difficile* has not been an important clinical target. Now however, as the number of effective antibiotics against *C. difficile* infection decreases, investigation of this Gram-positive bacterium's resistance mechanisms has become a new priority. It recently been discovered that *C. difficile* is in fact becoming resistant to a wide range of different antibiotic classes; β-lactams, cephalosporins (2^{nd} and 3^{rd} Generation), aminoglycosides, lincomycin, tetracyclines, erythromycin, clindamycin and fluoroquinolones (Spigaglia, 2016). All these antibiotics are usually used to treat bacterial infections which makes treating *C. difficile* difficult. *Clostridium difficile* has both intrinsic abilities to resist antibiotic treatment and acquired mechanisms transferred from several other resistant bacterial strains.

1.4.3.1 *Clostridium difficile* intrinsic resistance mechanisms

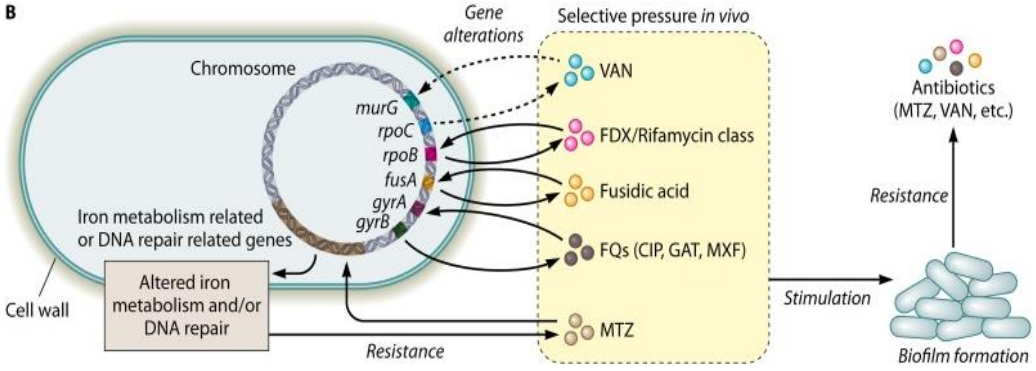

Figure 5: Intrinsic resistance in *C. difficile* utilising biofilm formation and the expression of β-lactam resistance genes (Peng et al., 2017)

C. difficile harbours a large range of antibiotic resistance genes as shown in **figure 5**. A very effective resistance mechanism of *C. difficile* is the formation of biofilms and spores. It is known that the process is primarily intrinsically controlled using Cwp84, flagella and LuxS however are promoted by antibiotic treatments (Đapa et al., 2013). *C. difficile* forms a multi-layered biofilm which includes a thick matrix containing proteins, DNA and polysaccharides. In general, pathogenic bacteria will form biofilms to survive extreme environments and antibiotic pressures. How forming a biofilm in *C. difficile* increases antibiotic resistance is not well characterised with the current hypothesis indicating the biofilm matrix performs as a protective barrier and alters the physiological state to dormant, all of which will increase antibiotic resistance. Under antibiotic selection pressure, mutations in biofilm formation genes cause them to start to become activated when specific antibiotics are used in treatment. (Vuotto, Moura, Barbanti, Donelli, & Spigaglia, 2016)

Another intrinsic mechanism present in the *C. difficile* genome is the expression of β-lactam resistance genes, like *Enterococci*. *C. difficile* however contains the genes to express both low affinity PBPs and β-lactamases (**figure 6**). As previously stated **1.4.1**, low affinity PBPs can function normally in the presence of β-lactams and β-lactamases hydrolyse the β-lactam ring and render the antibiotic useless. A number of resistance mechanisms however are received from resistant donor strains interacting with *C. difficile*. (Spigaglia, 2016)

1.4.3.2 *Clostridium difficile* acquired resistance mechanisms

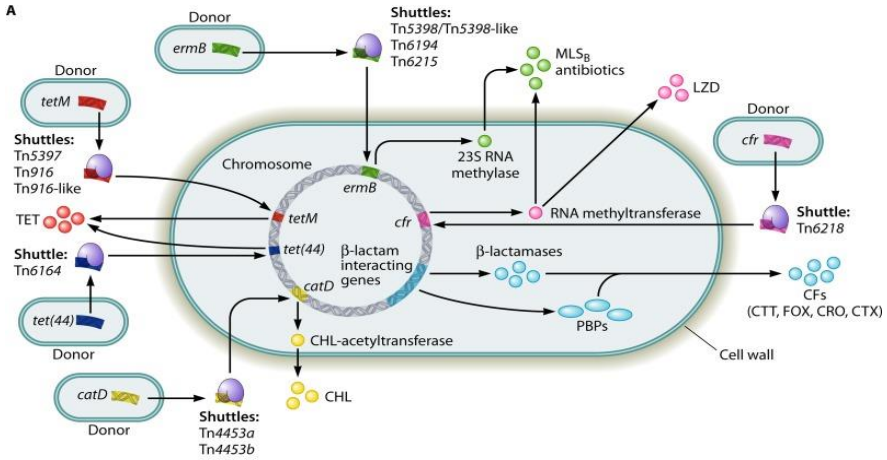

Figure 6: Acquired resistance genes, their source and their action in *C. difficile*. (Peng et al., 2017)

C. difficile can accumulate several resistance mechanisms from other Gram-positive strains (**figure 6**). This occurs through a number of processes including conjugation, transduction, and transformation of mobile genetic elements. The main resistances *C. difficile* has been shown to accumulate include macrolide-lincosamide-streptogramin B (MLS_B), tetracycline, chloramphenicol, and linezolid (Spigaglia, 2016).

The source of MLS_B resistance involves four transposons including Tn5398, Tn5398-like derivatives, Tn6194 and Tn6215. This class of antibiotics target different sites of 50S bacterial ribosome subunits, thus inhibiting protein synthesis (Ungureanu, 2010). These transposons initiate the movement of the *ermB* gene which is used to express a 23S RNA methylase that induces resistance to MLS_B antibiotics. The *ermB* gene has been found to transfer between *C. difficile, Bacillus subtilis* and *E. faecalis* (Spigaglia, Carucci, Barbanti, & Mastrantonio, 2005). Another resistance mechanism includes expressing an RNA methyltransferase which modifies the bacterial 23S rRNA that leads to increased resistance to MLS_B treatment. Chloramphenicol resistance is conferred by the *catP* gene which encodes a chloramphenicol acetyltransferase that attaches an acetyl group to chloramphenicol which prevents the antibiotic from binding to the ribosome subunits (Wasels et al., 2014) (S. Tsutsumi, B. Owusu, G. Hurdle, & Sun, 2014). Lastly, tetracycline resistance in *C. difficile* is conferred through obtaining the *tet* gene cluster from transposons such as Tn5397, Tn916 and Tn6164. Tetracycline is another protein synthesis inhibitor that acts by binding to the 30S ribosomal subunit thus inhibiting the binding of aminoacyl-tRNA to the mRNA-ribosome complex. The cluster encodes for energy- dependent efflux pumps, ribosomal protection proteins, and tetracycline inactivating enzymes (Roberts, 2005). *C. difficile*'s ability to harbour this

significant number of resistance genes from a range of Gram-positive bacteria is increasing its clinical threat and reducing the treatment options.

1.5 Bacterial cell signalling

To survive and respond to both chemical and physical changes in the environment, bacteria use multiple transmembrane signalling systems to detect and trigger cellular responses to extracellular stimuli. Because they are unicellular, bacteria are more susceptible to environmental changes, therefore rapid detection and response is required for survival. Due to the presence of a cell membrane, bacteria must detect signals of nutrients, pathogens, other cells and DNA information then transfer this across the membrane in a signalling cascade. These detector systems could also be used to detect antibiotics in the environment and signal the cell to activate resistance mechanisms to survive. Bacteria are known to use one- and two-component transmembrane signalling systems to respond to their environment. However, a new signalling system known as eukaryotic-like serine/threonine kinases have been discovered which also allow bacteria to respond to the environment.

1.5.1 One-component system

There are three main types of transmembrane signalling systems in bacteria; one- and two-component systems and Eukaryotic-like Serine/Threonine kinase systems (**figure 7**).

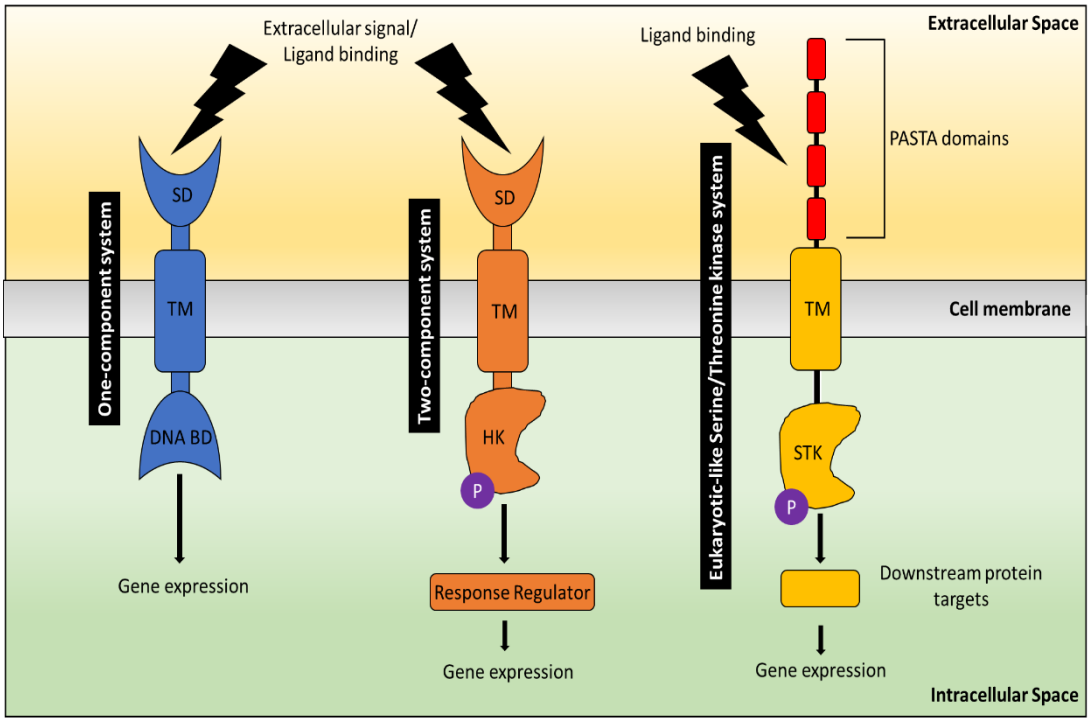

Figure 7: Main transmembrane signalling systems in bacteria. TM: Transmembrane domain, SD: Sensor domain, HK: Histidine kinase, STK: Serine/Threonine kinase. Adapted from (Jung, Fabiani, Hoyer, & Lassak, 2018; Pereira, Goss, & Dworkin, 2011)

The simplest of the three signalling systems, membrane-integrated one-component systems (or ToxR-like receptors) have only three components. The receptors are bitopic membrane proteins that consist of a periplasmic sensor domain, a transmembrane domain and an intracellular winged helix-turn-helix DNA-binding domain. These receptors do not however contain a phosphostransfer, histidine kinase nor receiver domains but instead directly interact with DNA to control transcription (Jung, Fabiani, Hoyer, & Lassak, 2018). This family of receptors are named according to the *Vibrio cholerae* main regulator of virulence, ToxR (Miller, Taylor, & Mekalanos, 1987). ToxR is a subclass of one-component systems, where 97 % of these systems are in fact cytosolic-based rather than membrane-embedded (Ulrich, Koonin, & Zhulin, 2005). An example of a membrane-integrated one-component system is CadC in *E. coli* which acts as a pH sensor to detect and respond to changes to internal and external pH changes (De Biase & Lund, 2015). Because of their simplicity, one-component systems are more widely spread among bacterial species and are older in terms of evolution in comparison to two-component systems

1.5.2 Two-component system

The two-component transmembrane systems (TCSs) have a greater complexity than one-component systems, perhaps because they control important gene expression they, therefore need to be tightly regulated.

The main membrane component (**figure 8**) is a membrane-integrated histidine kinase which is composed of an extracellular sensor domain, transmembrane helices, a N-terminal signal transduction domain, a cytoplasmic sensor domain and lastly a C-terminal catalytic kinase domain. If a signal is detected by the extracellular sensor domain, transmission of the signal reaches the kinase domain and causes activation. The activated kinase autophosphorylates either on Histidine or Aspartate residues and then the kinase phosphorylates a downstream cognate soluble response regulator (e.g. transcription factor) which can regulate gene expression. Two-component systems are responsible for regulating a range of bacterial cellular processes including virulence, metabolism and antibiotic resistance. The signal transduction process has four main steps: signal detection, kinase activation, phosphotransfer and response generation. (Zschiedrich, Keidel, & Szurmant, 2016)

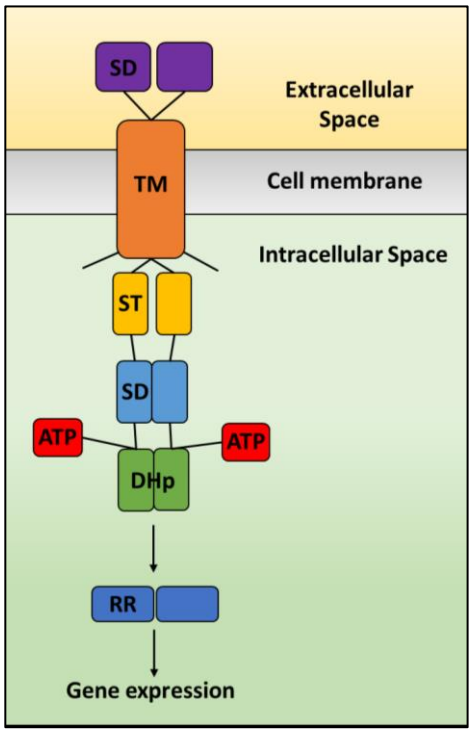

Figure 8: Typical modular domain structure of a bacterial two-component system. Adapted from (Zschiedrich, Keidel, & Szurmant, 2016)

1.5.3 Eukaryotic Serine-Threonine kinases

Originally, only two-component transmembrane systems were thought to regulate bacterial signal transductions to respond to both extracellular and intracellular stimuli (Stock, Stock, & Mottonen, 1990). Genomic studies have discovered Serine/Threonine kinases and cognate phosphatases present in bacteria. It has been revealed that the genomic sequences of both kinases and phosphatases have homology to their eukaryotic counterparts (Bakal & Davies, 2000). The first eukaryotic-like serine/threonine kinase (eSTKs) characterised was Pkn1 from *Myxococcus xanthus* (Muñoz-Dorado, Inouye, & Inouye, 1991). Pkn1 and a transmembrane eSTK Pkn2 also from *M. xanthus*, were shown to not be essential to cellular growth (Udo, Munoz-Dorado, Inouye, & Inouye, 1995). The first structure of a bacterial eSTK was deduced in *Mycobacterium tuberculosis*, PknB (Ortiz-Lombardía et al., 2003; Young et al., 2003). Genomic studies found that only a few eSTKs are encoded in the average bacterial genome differing to their histidine kinase counterparts. As a result of this, investigation has been performed on the structure and function of these eukaryotic-like serine/threonine kinases and their role in the physiology of the bacterial cell.

1.5.3.1 Eukaryotic Serine-Threonine kinase Structure and functions

The structure of a bacterial eukaryotic serine-threonine kinase is somewhat simpler than the two-component system (**figure 9**). The modular structure of an eSTK slightly differs between species but tends to be only in the extracellular domains. The sensing extracellular domains are a set of differing numbers of penicillin-binding protein and Serine/Threonine associated repeats (PASTA). These are attached to a single transmembrane domain which is linked to a cytosolic catalytic serine-threonine kinase domain (Pensinger, Schaenzer, & Sauer, 2018).

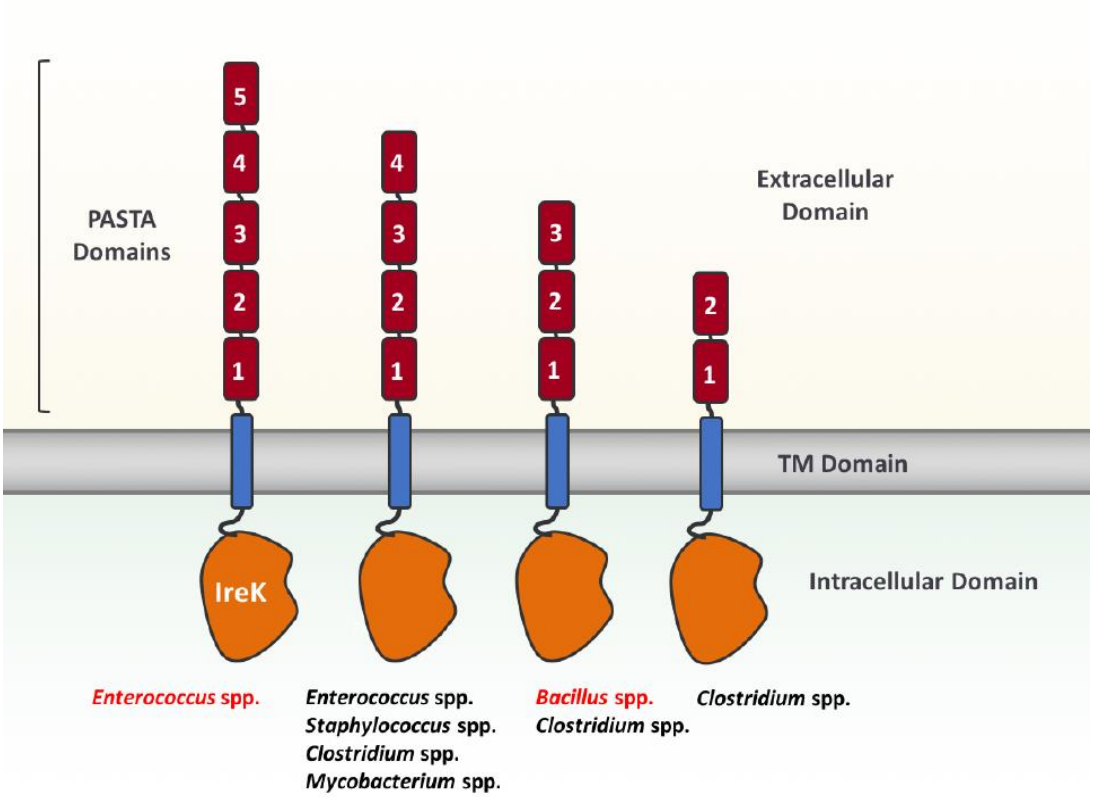

Figure 9: Modular structure of eSTKs in Gram-positive bacteria. Modules include a set of PASTA domains in the extracellular space, a transmembrane domain and a Serine/Threonine kinase in the cytoplasm. (Thoroughgood, 2018)

This modular structure of the eSTK indicates the regulation by either ligand binding or protein-protein interactions. The ligand binding on the extracellular side would be performed by the PASTA motifs. These are ~ 70-amino acid long repeats which form into a $\beta_3\alpha$ (if bound antibiotic/peptidoglycan) or a linear conformation (if in an unbound state). The bound state is observed in crystal structures of PBP2X of *Streptococcus pneumoniae* bound to β-lactam (Dessen, Mouz, Gordon, Hopkins, & Dideberg, 2001) and PrkC from *Bacillus subtilis* bound to peptidoglycan (Shah, Laaberki, Popham, & Dworkin, 2008). PknB from *M. tuberculosis* and its PBP2X homolog crystal structures show an unbound PASTA domain in its linear conformation (Barthe, Mukamolova, Roumestand, & Cohen-Gonsaud, 2010).

The kinase domain was another modular component of this signalling system under investigation. The main crystal structure used was of PknB of *M. tuberculosis* in a complex with an ATP analog (Ortiz-Lombardía et al., 2003). The PknB catalytic domain showed a two-lobed structure where the ATP analog was bound in the catalytic cleft in between the lobes and in close contact with the regulatory elements. This structure appeared very similar to mouse cyclic AMP-dependent protein kinase (PKA) in the activated form (Madhusudan, Akamine, Xuong, & Taylor, 2002). The position of ATP analog binding and conformation of both lobes and regulatory structural elements indicate similarity to eukaryotic Serine/Threonine kinases. There were though a couple of differences including the PknB αC helix was residing away from the active site, similar to the inactive site of the eukaryotic kinase. Secondly the PknB activation loop was disordered, also characteristic to the inactive eukaryotic kinase state. Conserved structural interactions in PknB were maintained however between residues Glu59 and Lys40 along with the α- and β-phosphates of the ATP analog (Huse & Kuriyan, 2002).

The dimerisation and phosphorylation also thought to be important in the comparison between PknB and eukaryotic PKA. PknB was crystallised in the dimeric form with interactions between 'back to back' sides of the N-terminal lobes of the two catalytic regions (Ortiz-Lombardía et al., 2003). A eukaryotic double stranded RNA-activated protein kinase PKR was also crystallised in the 'back-to-back' dimeric form (Dar, Dever, & Sicheri, 2005). Interestingly, PKA is activated by a ligand-induced dimerisation mechanism (Cole, 2007). This suggests that eSTKs may activate using a similar mechanism considering the structural similarities between PknB and eukaryotic serine/threonine kinases. If PknB is overexpressed in *E. coli*, four residues of the activation loop (Ser166m Ser169, Thr171 and Thr173) are phosphorylated (Young et al., 2003). In comparison to PKA, the phosphoreceptor residue Thr 197 is autophosphorylated during kinase activation, and Thr197 corresponds to Thr171 in PknB. Additionally, extensive conservation was discovered between PknB orthologs and PKA in terms of the ATP binding cleft, residues adjacent to the ATP γ-phosphate binding site and the corresponding region to the PKA substrate-binding groove (Madhusudan et al., 2002). Both crystal structure dimerisation and phosphorylation sites further suggest a common activation mechanism of eukaryotic and bacterial Serine/Threonine kinases.

1.5.3.2 Eukaryotic Serine-Threonine kinase activation mechanism

A model for the activation of Eukaryotic-like Serine/Threonine kinases was created with *M. tuberculosis* PknB as a model (**figure 10**). The model begins with the extracellular PASTA motifs exposed to a ligand in the environment. The binding of a single ligand to two or more PASTA domains brings the cytosolic kinase domains together which results in the formation of the symmetric 'back-to-back' dimer. The dimer then activates and autophosphorylates and can either phosphorylate downstream protein targets or activate a soluble kinase by forming an asymmetric 'front-to-front' dimer. The activated soluble kinase then phosphorylates further downstream targets in a signalling cascade pathway. (Pereira, Goss, & Dworkin, 2011)

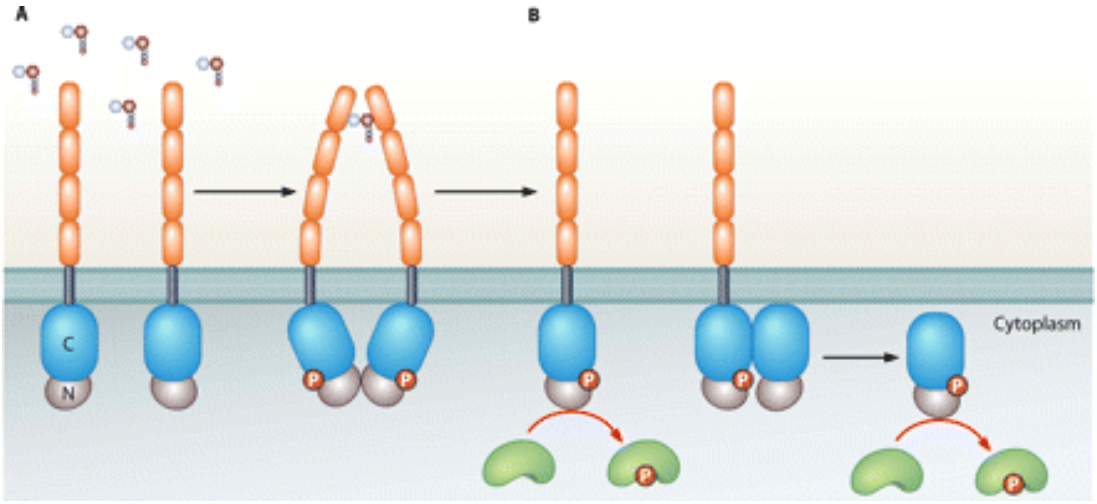

Figure 10: Mechanism of activation of Eukaryotic-like Ser/Thr kinase PknB from *M. tuberculosis* as a model. (Pereira et al., 2011)

The crystal structures of *M. tuberculosis* PknB and the eukaryotic PKA supported the idea of activation by dimerisation and autophosphorylation. The mechanism of autophosphorylation however is still largely unknown. The kinases do not appear to phosphorylate each other as the dimer active sites of the kinase domains face away from each other in the 'back-to-back' structure. A possible mechanism of phosphorylation is the allosteric regulation of the kinase domain post-dimerisation or phosphorylated by another kinase. This is supported by *M. tuberculosis* kinase domain PknD catalytic site mutants which are inactive but for a dimer with a wild-type PknD monomer to activate the wild-type catalytic domain (Greenstein, Echols, Lombana, King, & Alber, 2007). Further studies are required to identify the exact mechanism of autophosphorylation which occurs after dimerisation.

The ligand-induced dimerisation mechanism is another aspect of eSTK activation under investigation. As a contrast to this model, the *M. tuberculosis* PknD kinase domain is active as a monomer and a dimer to the same degree (Greenstein et al., 2007). There are also eSTKs which do not contain a ligand-binding domain however. In an attempt understand how these eSTKs are regulated, *M. tuberculosis* PknB mutant kinase was co-crystallised with an ATP competitive inhibitor (Mieczkowski, Iavarone, & Alber, 2008). This structure revealed a second dimerisation interface where two of the mutant monomers bound to the inhibitor, forming an asymmetric front-to-front dimer. The front-to-front dimer facilitated this dimerisation interface by interacting the αG helix and activation loop of one kinase with the αG helix of the other kinase. The conformations which both kinases take indicate that one acts as an activator and the other the activator substrate. In the same study, G-helix residue substitutions were performed in active and inactive kinase domains which support the idea that the asymmetric dimer mimics a trans-autophosphorylation complex (Mieczkowski et al., 2008).

1.5.3.3 Eukaryotic Serine-Threonine kinase physiological functions

As with two-component signalling systems, eukaryotic-like serine/threonine kinases regulate a range of essential processes, however many eSTKs have redundant or non-essential functions. The signalling networks initiated by eSTKs control complex cellular processes.

eSTKs have been found to regulate essential cellular processes such as development, cell division and cell wall synthesis. In terms of cell division, *S. pneumoniae* StkP has been found to have a complex function in coordinating cell division (Manuse, Fleurie, Zucchini, Lesterlin, & Grangeasse, 2016). It was discovered that this eSTK phosphorylates DivIVA, MapZ and FtsZ targets which are involved in peptidoglycan synthesis. MapZ is also responsible for moving FtsZ to the mid-cell leading to the closure of the FtsZ ring.

Some bacterial species rely on eSTKs to respond to the environment for survival. *Bacillus subtilis* will form spores when the environment is unfavourable with limiting nutrients. When conditions improve, the dormant spores activate again and resume growth. These cells rely on the transmembrane eSTK PrkC to trigger this cellular activation. This happens by the binding of the extracellular PASTA domains to peptidoglycan fragments which leads to germination by the phosphorylation and activation of GTPase elongation factor EF-G used in translation (Shah et al., 2008).

eSTKs have also been found to regulate virulence and antibiotic resistance mechanisms. A key example for the role of eSTKs in virulence is eSTK YpkA in *Yersinia pseudotuberculosis*. YpkA is activated from an inactive form when secreted into the infected host cell. The interaction with the host actin filaments leads to cytoskeleton disruption, and in macrophages this can inhibit their function during host infection (Juris, Rudolph, Huddler, Orth, & Dixon, 2000). Another eSTK important in infection is PrkC in *M. pneumoniae* which phosphorylates cytadherence proteins which promotes adhesive growth and cytotoxicity (Schmidl et al., 2010). There are homologs of PrkC found in *E. faecalis* and *S. pyogenes*.

S. aureus has been found to harbour two eSTKs, Stk1 (PknB) and Stk2, which regulate virulence and antibiotic resistance pathways (Didier, Cozzone, & Duclos, 2010). Firstly, Stk1 has been shown to phosphorylate VraR which is part of the two-component regulatory system VraS/VraR that control cell wall peptidoglycan biosynthesis (Canova et al., 2014). VraR is overexpressed in *S. aureus* strain Mu50 which leads to vancomycin resistance (Kuroda, Kuwahara-Arai, & Hiramatsu, 2000). Stk1 can also phosphorylate CcpA which controls various virulence determinants such as biofilm formation (Kalantari, Mijakovic, Shi, & Derouiche, 2015). Lastly, both Stk1 and Stk2 target SarA which is part of the SarA/MgrA family which regulates over 100 genes in *S. aureus* which is directly regulated by eSTK phosphorylation. SarA controls the expression of virulence genes such as *hla* (α toxin), *spa* (Spa immune evasion molecule) and master virulence-controlling quorum sensing locus agr (Kalantari et al., 2015).

1.5.3.4 Eukaryotic-like Serine-Threonine Phosphatases

In two-component signalling systems in bacteria, regulation appears to be a relatively simple mechanism of rapid hydrolysis of either phosphorylated histidine or aspartate residues (Sickmann & Meyer, 2001; C.-C. Zhang, 1996) and does not require a cognate phosphatase. In contrast, however, eukaryotic-like serine/threonine kinases use phosphorylated serine, threonine and tyrosine residues in the signalling process, which are more difficult to hydrolyse. To regulate the signalling cascade caused by eSTKs, the kinases require cognate phosphatases (Alber, 2009). These are bacterial homologs of four eukaryotic protein phosphatase superfamilies, including low molecular weight protein tyrosine phosphatases, phosphoprotein phosphatases (PPPs) and metal-dependent phosphatases (PPMs) (Shi, Potts, & Kennelly, 1998). The PPPs are specific for the dephosphorylation of serine and threonine residues but tend to also dephosphorylate phosphohistidine and phosphotyrosine residues (Barford, 1995). The PPMs present in bacteria are serine/threonine Mg^{2+} or Mn^{2+} dependent phosphatases which share a catalytic domain with eukaryotic PP2C that have 11-13 motifs

containing eight conserved residues (Shi et al., 1998) (W. Zhang & Shi, 2004) (Bork, Brown, Hegyi, & Schultz, 1996). As a general rule, there is one kinase per cognate phosphatase and these phosphatases are usually encoded on the same operon as the cognate eSTK. There are exceptions however, such as in *M. tuberculosis*, where there are eleven eSTKs to a single cognate phosphatase (Av-Gay & Everett, 2000; Koul et al., 2000).

The structure of eukaryotic-like serine threonine phosphatases (eSTPs) is very similar to the eukaryotic PP2C especially in the catalytic domains. PP2C has a conserved catalytic core composed of a central β-sandwich that is made of two five-stranded antiparallel β sheets, each flanked by a pair of antiparallel α helices (Das, Helps, Cohen, & Barford, 1996). Because of the high level of conservation of active site residues between eukaryotic and bacterial phosphatase homologs the mechanism of action is assumed the same. It is thought to use a metal activated water nucleophilic attack onto the phosphorus atom. There are a few structural differences between eukaryotic PP2C and bacterial eSTPs deduced by comparison of crystal structures of *M. tuberculosis* PstP (Wehenkel, Bellinzoni, Schaeffer, Villarino, & Alzari, 2007) and *Thermosynechococcus elongatus* PphA (Schlicker et al., 2008). The main difference is the flap subdomain which in bacteria, is placed away from the active site and mutation studies of this flap found residue Arg169 has a significant effect on the phosphatase activity and structural organisation. This indicates the flap region could act as a mobile element that may facilitate substrate binding and/or dictate the specificity dephosphorylation of substrates.

The function of eSTPs are to regulate the autophosphorylation state of their cognate kinases. The eSTPs physiological role however is not as well characterised compared to eSTKs. There are multiple examples of eSTPs regulating the physiological functions of eSTKs. As previously stated, some eSTKs regulate cell division and peptidoglycan synthesis in species such as *Mycobacteria* and *Streptomyces* (Manuse et al., 2016). In a mutation analysis study, STP from *S. aureus* was deleted leading to thicker and cell wall defects (Beltramini, Mukhopadhyay, & Pancholi, 2009) (Ohlsen & Donat, 2010). The eSTP Pph1 from *M. xanthus* mutant indicated growth defects in swarming and glycerol spore formation along with failure to form viable spores under starving conditions (Treuner-Lange, Ward, & Zusman, 2001). Lastly, eSTPs role in virulence is not well understood, however further mutation studies have suggested some physiological functions. For example, *B. anthracis* STK/STP double mutant had an impaired ability to survive in macrophages after infection (Shakir et al., 2010). Another example which only removes the phosphatase for a clearer interpretation, the inactivation of *S. aureus* eSTP

Stp1 reduces hemolysin expression which are exotoxins key to the pathogenesis of *S. aureus* infection (Burnside et al., 2010).

1.5.3.5 Convergence of Two-component and Eukaryotic-Like Serine/Threonine signalling systems

There have been several documented cases where both two-component and eukaryotic-like Ser/Thr kinase signalling systems intertwine resulting in similar responses to the environment. In *Enterococcus faecalis*, a two-component system called CroS (histidine kinase) and CroR (response regulator) modulate gene expression upon detection of cell-wall targeting antibiotics. A eukaryotic-like Ser/Thr kinase and phosphatase system called IreK (transmembrane kinase) and IreP (cognate phosphatase) which also regulate antibiotic resistance to cell-wall targeting antibiotics. It was discovered that IreK positively regulates CroR dependent gene expression by phosphorylating CroS to further upregulate antibiotic resistance in *E. faecalis*. (Kellogg & Kristich, 2018)

The two bacterial signalling systems can also regulate cytotoxin expressions in *Streptococcus agalactiae*. This human pathogen only encodes a single eSTK, Stk1, which was found to regulate expression towards resistance to human blood, neutrophils and oxidative stress. Stk1 positively regulates the expression of the cytotoxin β-haemolysin/cytolysin which is necessary for resistance to oxidative stress. A two-component regulator CovR is required for positive regulation of this cytotoxin expression. Stk1 phosphorylates CovR *in vitro* which suggests the eSTK phosphorylation affects CovR-mediated regulation of *Streptococcus agalactiae* gene expression. (Rajagopal, Vo, Silvestroni, & Rubens, 2006)

The convergence of these bacterial signalling systems have also been documented to regulate processes such as growth and dormancy. This is the case for the regulation of the dormancy regulon in *Mycobacterium tuberculosis*. Through kinase assays and mass spectrometry, it was found that eSTK PknH phosphorylates response regulator DosR for full induction of the dormancy DosR regulon to regulate growth.

These three examples highlight that cellular processes are controlled by a set of bacterial signalling systems. In terms of antibiotic resistance therefore, simply inhibiting one signalling system may result in the other system to compensate to produce the same antibiotic resistant phenotype.

1.5.3.6 Eukaryotic-like Serine-Threonine kinases in *Enterococcus*

As previously mentioned (section **1.3**), *enterococcus faecalis* and *enterococcus faecium* are becoming multi-drug resistant pathogens and are deadly in nosocomial environments. Investigation into how these commensal strains reside in the intestinal tract and mediate antibiotic resistance has therefore become an increasingly important research area. The identification of eukaryotic-like serine/threonine kinases in bacteria has caused research into how these signalling systems could regulate key processes in pathogenic bacteria.

After genomic studies into open reading frames of the *E. faecalis* V583 genome, a serine/threonine kinase was found called IreK which has a homolog from *Bacillus subtilis*, PrkC and has all the highly conserved regions required for catalytic activity (Paulsen et al., 2003). IreK is part of a eukaryotic-like serine/threonine kinase signalling system and appears to be present in many Gram-positive bacteria with both low and high GC content (Kristich, Wells, & Dunny, 2007). The structure of IreK is typical of an eSTK, has five extracellular PASTA domains, a transmembrane domain and a cytosolic kinase domain. The PASTA domains in this system are proposed to bind to free D-ala-D-ala (Kristich et al., 2007)termini present on uncross-linked peptidoglycan. IreK was found to mediate adaptive responses to cell-envelope stress which can be caused by β-lactam antibiotics. This eSTK promotes high-level colonisation of antibiotic-resistant enterococci which leads to *E. faecalis* infection (Kristich et al., 2007).

E. faecalis has an intrinsic resistance to β-lactam and its subclass, cephalosporin antibiotics (Hollenbeck & Rice, 2012). IreK and its cognate PP2C-type protein phosphatase IreP, has been found to regulate the intrinsic cephalosporin resistance in *E. faecalis*. In IreK deletion mutants were found to remove resistance to cephalosporins specifically in *E. faecalis* wild type (Kristich, Little, Hall, & Hoff, 2011). Interestingly, sensitivity to ampicillin did not change significantly even though ampicillin is also part of the β-lactam antibiotic family. As the IreK deletion mutant is significantly susceptible to cephalosporins, it must have a role in the promotion and regulation of intrinsic cephalosporin resistance mechanisms (Kristich et al., 2011). The exact protein and gene regulatory targets of IreK are not adequately understood however with only IreB, a negative regulator of cephalosporin resistance, known to become reversibility phosphorylated by IreK (C. L. Hall, Tschannen, Worthey, & Kristich, 2013).

IreP mediates the activity of IreK as in deletion mutants of IreP, *E. faecalis* becomes hyper resistant to cephalosporins (Kristich et al., 2011). This could be due to enhanced phosphorylation of IreK, in the activation loop, leading to enhanced cephalosporin resistance through phosphorylation of as yet unidentified, downstream elements. Although the removal of IreP causes hyper resistance, *E. faecalis* exhibits a fitness defect in IreP deletion mutants. In the absence of cephalosporins, the IreP mutants are less fit compared to wild type *E. faecalis* (Kristich et al., 2011). The growth rate of bacteria in a culture medium is commonly used as a model for evaluating fitness as a measure of reproductive potential (Bennett, Dao, & Lenski, 1990; Nguyen, Phan, Duong, Bertrand, & Lenski, 1989; Pope, McHugh, & Gillespie, 2010). Cephalosporin resistance therefore must present a significant fitness cost to the cell, although the molecular basis for this is unclear. The IreK/IreP signalling system is therefore an adaptation to control cephalosporin resistance in the absence of antibiotic and to promote survival in the presence of antibiotic. If this signalling system could be inhibited therefore, it should significantly reduce resistance to cephalosporin treatments of *E. faecalis* (Kristich et al., 2011). There are several interesting and significant biological questions which arise from these observations therefore:

What is the mechanism of resistance that ireK is controlling in this context?

What are the cellular targets of IreK?

How are these targets related to cephalosporin resistance?

Since IreK "over-activity" results in a fitness cost, what is the molecular nature of that fitness cost?

1.5.3.7 Staurosporine effect on eukaryotic-like serine threonine kinases

Staurosporine, an anti-cancer drug too toxic for human use, is now universally used as a kinase inhibitor in research (Meggio et al., 1995). Despite a lack of similarity between the structures of ATP and the drug, Staurosporine mimics ATP very effectively. This microbial alkaloid, isolated from *Streptomyces stauroporeus*, is a general small ATP-competitive inhibitor which binds to the ATP/ADP binding site of kinases, preventing phosphorylation (Tanramluk, Schreyer, Pitt, & Blundell, 2009).

Staurosporine has been co-crystallised in mouse PKA catalytic subunit, mimicking adenosine binding when bound to the adenosine pocket (Prade et al., 1997). The inhibitor has been documented to inhibit PknD kinase domain from *M. tuberculosis in vitro* (Mieczkowski et al., 2008) and *M. tuberculosis* PknB at micromolar concentrations *in vivo* (Fernandez et al., 2006). A bulky active site mutation has been observed to reduce the inhibitors effect to higher concentrations by *in vitro* binding studies in Stk1 from *Staphylococcus epidermis* containing a Phe in the active site instead of a Thr (Liu et al., 2011). The active site of multiple eSTK kinase domains appear to be conserved and an active site mutation does introduce a resistance to Staurosporine.

1.6 Project Aims and Objectives

The threat of multi-drug resistant Gram-positive bacteria is on the rise according to WHO. The ability of *Enterococci, Clostridium* and *Streptococcus*, for example, to survive in hostile environments and live through antibiotic treatments is troubling. The molecular basis of antibiotic resistance in Gram-positive bacteria is still under investigation. An emerging area of research is the complex signalling systems which bacteria use to sense the environment and respond to survive. It has been shown that bacteria use eukaryotic-like serine/threonine kinases to regulate essential cellular functions such as cell division, but also virulence and antibiotic resistance. A known system of this is the IreK/IreP eSTK system which is known to regulate cephalosporin resistance in *E. faecalis*. If a similar system in other *Enterococci* strains and Gram-positive bacteria is present, they could be a key target of kinase inhibitors to reduce antibiotic resistance levels in highly resistant strains.

The aim of this project was to investigate the phosphorylation and kinase inhibitory characteristics of Eukaryotic-like serine threonine kinases in Gram-positive bacteria using *Enterococcus faecalis*, *Enterococcus faecium* and *Clostridium difficile* as focus strains.

Objectives:

1) Clone, express and purify eSTK kinase domains from *Enterococcus faecalis*, *Enterococcus faecium* and *Clostridium difficile*

2) Investigate the phosphorylation state of the kinases in terms of oligomerisation and the effect of dephosphorylation using Native-Page analysis with Pro-Q Diamond phosphatase staining

3) Determine the autophosphorylation activity and the effect of kinase inhibitors on kinase activity using Pro-Q Diamond phosphate staining technology

4) Measure the dissociation constants of kinase inhibitor ligands to the kinases using Microscale Thermophoresis

2.0 Materials and Methods

2.1 Chemical and reagent suppliers

All reagents used were obtained from the following suppliers if not stated otherwise; New England Biolabs (USA), Sigma-Aldrich (USA), Integrated DNA technologies (USA), Invitrogen (USA), Thermofisher scientific (USA), Fisher Scientific (UK), Merck (Germany), Promega (USA), Cleaver scientific (UK), VWR (USA), Sartorius stedim biotech (Germany), Nanotemper Technologies (Germany), Biotium (USA), GE Healthcare (USA), Roche (Switzerland). All chemical reagents used were analytical grade.

2.2 Buffer solutions

All buffer solutions were prepared using purified water from a Purite Prestige deionised water system. All buffers used in chromatography were filtered using a Millipore 0.2 µM filter. Other buffers involved in *E. coli* competent cell preparation or bacterial growth were filtered using a Minisart 0.2 µm syringe filter.

2.3 Bacterial growth and manipulation

2.3.1 Bacterial growth media

Luria-Bertani (LB) liquid medium (Bertani, 1951) was prepared by dissolving 10 g Tryptone, 10 g NaCl, 5 g Yeast in a final volume of one litre and autoclaved. The appropriate antibiotic was then added prior to bacterial inoculation.

SOC outgrowth medium (2 % Vegetable Peptone, 0.5 % Yeast Extract, 10 mM NaCl, 2.5 mM Kcl, 10 mM $MgCl_2$, 10 mM $MgSO_4$ and 20 mM glucose) used in *E. coli* transformation was bought from NEB.

LB agar plates were prepared by autoclaving LB media supplemented with 20 g of agar per litre. When cooled to 50°C, the appropriate antibiotic was added, and plates poured into sterile petri dishes at around 25 ml per 100 mm plate and stored at 4°C for later use.

2.3.2 Bacterial strains

The bacterial strains used in this project are presented in **table 2**. NEB Alpha 5 *E. coli* cells were used for cloning and BL21 (DE3), C41 (DE3) and C43 (DE3) *E. coli* cells were used for recombinant protein expression. The *C. difficile* ATCC 9689 clinical strain was used as a source of template DNA for PCR gene amplification and *in vivo* minimal inhibitory concentration assays.

Table 2: Clinical and expression bacterial strains used for protein expression, cloning and minimum inhibitory assays

Strain	Characteristics	Reference
Expression Strains		
BL21 (DE3)	F- ompT hsdSB(rB-, mB-) gal dcm(DE3)	(Studier & Moffatt, 1986)
NEB Alpha 5	F' proA+B+ lacIq Δ(lacZ)M15 zzf::Tn10 (TetR) / fhuA2Δ(argF-lacZ)U169 phoA glnV44 Φ80Δ(lacZ)M15 gyrA96 recA1 relA1 endA1 thi-1 hsdR17	New England Biolabs (NEB)
C41 (DE3)	F – ompT hsdSB (rB- mB-) gal dcm (DE3)	(Miroux & Walker, 1996)
C43 (DE3)	F – ompT hsdSB (rB- mB-) gal dcm (DE3)	(Miroux & Walker, 1996)
Clinical Strains		
C. difficile ATCC 9689	Cytotoxin A and B	(I. Hall & O'Toole, 1935)

2.3.3 Bacterial vectors

All plasmid constructs used in this project are listed in **table 3**. Both of the *Enterococcal* kinase constructs were obtained from Dr Christopher Thoroughgood and the *C. difficile* construct was created during this project.

Table 3: All plasmid constructs used in protein expression in *E. coli*

Construct	Features	Content	Cloning (Type and Features)	Source and primers	Reference	Vector
pLG226	T7-6x His-IreK KD (AmpR)	*E. faecalis* IreK soluble kinase domain	-	-	(Thoroughgood, 2018), (Goss, 2013)	pETDuet
pLG234	T7-6x His-IreK KD (AmpR)	*E. faecium* IreK soluble kinase domain	-	-	(Thoroughgood, 2018), (Goss, 2013)	pETDuet
pCD001	trc-TEV-6x His-eSTK kinase domain (AmpR)	*C. difficile* eSTK soluble kinase domain	Gibson cloning (NEBuilder), Dpn1	Clos STK pProEx F, Clos STK pProEx R, *C. difficile* eSTK gBlock	This project	pProEx HTa

2.3.4 Preparation of *E. coli* competent cells for DNA transformation

BL21 (DE3) and NEB alpha 5 chemically competent cells were made used an adapted protocol from (Hanahan, 1983). An overnight growth of a single colony was created using 2.5 ml LB broth and incubated at 37 °C with shaking at 180 RPM. This culture was added to 250 ml LB media which contained 20 mM $MgSO_4$. The growth was performed in a 1 L flask to each A_{600} of 0.4 to 0.6. The cells were then pelleted by centrifugation at 4,500 x g for 5 minutes at 4 °C. The supernatant was discarded, and the cell pellet was resuspended in 40 ml TFB1 (**table 5**) buffer which was incubated on ice for 5 minutes. The resuspended pellet was centrifuged again at 4,500 x g for 5 minutes at 4 °C. Again, the cells were re-suspended in 4 ml TFB2 (**table 5**), incubated on ice for 60 minutes and aliquoted into 200 µl volumes in 1.5 microcentrifuge tubes and frozen at -80 °C.

2.3.5 Bacterial DNA transformation

The transformation method was derived from New England Biolab protocol (REF). For the purposes of cloning NEB alpha 5 *E. coli* cells were used and BL21 (DE3) *E. coli* cells were used for protein expression. Other *E. coli* strains including C41 and C43 were used in protein expression trials. The protocol started with adding 1-100 ng of plasmid DNA to 100 µl of thawed Cryo-stored competent cells. Cells were incubated on ice for 30 minutes and then heat shocked at 42°C for 30 seconds followed by 5 minutes on ice. The cells were then diluted to 1 ml with pre-warmed SOC medium and incubated for 1 hour at 37°C with shaking at 180 RPM. After, 100 ul of diluted cells were spread on pre-warmed agar plates with appropriate antibiotics and incubated overnight at 37°C.

2.3.6 Preparation of *E.coli* glycerol stocks

After the transformation protocol in **2.3.5**, 250 ul of diluted transformed cells were mixed with 250 ul of autoclaved 20% glycerol and flash frozen in liquid nitrogen. The glycerol stocks were stored at -80°C

2.4 DNA manipulation techniques

2.4.1 Primer and Gblock design

Primer oligonucleotides were designed based of their targeted plasmid or gene with restriction sites analysed to prevent problematic digestion during cloning. All primers were ordered from Integrated DNA technologies (IDT). The list of primer names and sequences are present in **table 4**. Synthetic DNA gBlocks were designed and ordered from IDT. The gBlocks were codon optimised for *E.coli* expression. Only one gBlock named *C. diffcilile* eSTK KD was created in this project and its sequence is presented in section **5.2**, appendix.

Table 4: Primers used in the linearisation of pProEx HTa, sequencing and for the creation of gene inserts for Gibson cloning

Primer Name	**5'-3' Sequence**
Sequencing	
pProEx Forward	AGC GGA TAA CAA TTT CAC ACA GGA
PProEx Reverse	GGC AAA TTC TGT TTT ATC AGA CCG CTT C
Linearisation of pProEx	
pProEx F	CAT GGC GCC CTG AAA ATA C
pProEx R	TGA TAC AGA TTA AAT CAG AAC G
PCR amplification of gene inserts	
Clos STK pProEx F	TGT ATT TTC AGG GCG CCA TGG GAG ATA CAA TTT TAG GAA ATC
Clos STK pProEx R	TTC TGA TTT AAT CTG TAT CAT TTT AAT CTT CTT CTA GAT TTT GG

2.4.2 Polymerase Chain Reaction

PCR reactions were performed on a SureCycler 8800 Thermal cycler with conditions optimised using the online NEBuilder tool (NEB). PCR reaction mixtures followed the manufacturers protocol for Phusion and *Taq* polymerases (NEB). All designed primers used were manufactured by IDT. Optional DMSO was added to the reaction at 3 % of total reaction volume for optimum amplification.

2.4.3 Linearisation of vectors

Using the prementioned PCR protocol, only the pProEx HTA expression plasmid was used as a template for vector linearisation. Linearised vector was run on an agarose gel (**2.4.4**) and purified using the protocol in **2.4.5**.

2.4.4 Agarose gel electrophoresis

Agarose gels were 0.8% and prepared with TAE buffer (Table etc) and Gel Red (Biotium). DNA samples were prepared with 6 x DNA loading buffer (NEB) and run for 1 hour at 120 V for optimal band separation. Gels were imaged using a UV transilluminator.

2.4.5 Purification of PCR products

Linearised vectors were purified using Monarch® DNA Gel Extraction Kit (NEB) following the manufacturers protocol.

2.4.6 Gibson Cloning

Gibson cloning was performed using NEBuilder® HiFi DNA Assembly Cloning Kit (NEB) following the manufacturer's protocol. The cloning reaction composition used a 1:2 ratio of vector to insert respectively. The vector amount was 12.94 pmoles with a 2 fold excess of insert DNA. Total reaction volume was 20 ul with 10 ul NEBuilder HiFi DNA Assembly Master Mix and the reaction was incubated at 50 °C for 15 minutes. To prevent false positive colonies from template DNA in transformation, Dpn1 restriction digestion at 37 °C for 1 hour was performed. Post-digestion, 2ul of cloning reaction used in the transformation of NEB 5-alpha cells using the protocol in **2.3.5**.

2.4.7 Preparation of plasmid DNA

After successful transformation of the cloning product in **2.4.6**, a 5 ml LB broth with appropriate antibiotic was inoculated with successful colonies and grown overnight at 37 °C. Bacterial cells were pelleted by centrifugation at 4,000 RPM for 10 minutes. Plasmid extraction was performed using Monarch® Plasmid Miniprep Kit (NEB) following the manufacturer's protocol. Purified recombinant plasmid DNA was stored at -20 °C

2.4.8 Quantifying DNA

All DNA samples were quantified using a Nanodrop (Thermofisher) by measuring the absorbance at 260 and 280 nm. DNA purity was calculated using the ratio of absorbance between 260/280 nm. Sufficient purity DNA has a ratio between 1.6 to 2.0.

2.4.9 Sequencing plasmid constructs

To validate recombinant constructs, plasmid DNA was checked using Sanger sequencing. Sequencing reaction composition included 5 ul of 80-100 ng DNA with 5 ul of 10 µM primer (GATC-Biotech).

2.5 Protein Expression and Purification

2.5.1 *E.coli* recombinant protein overexpression with ITPG

All protein expression was performed in LB media, the appropriate antibiotic, 20% glucose and overnight cultures. Overnight cultures were grown at 37°C using LB media with the appropriate antibiotic. All large-scale cultures were grown in 1 L flasks up to a total of 6 L and grown to OD 0.6 before inducing with 1 mM ITPG. Induction temperatures and timescales varied depending on the protein being expressed. IreK from *E. faecalis and E. faecium* was induced for 4 hours at 37°C. The eSTK from *C. difficile* was induced multiple times at either 4 hours 37°C or overnight at 23°C or 17°C in the expression trials. All protein inductions were stopped by collecting the cell pellets after centrifugation at 5,000 rpm for 10 minutes and then flash freezing them with liquid nitrogen for purification later.

2.5.2 Preparation of crude cell lysates

Cell pellets were thawed and resuspended in the IMAC binding buffer. Resuspended pellets were sonicated at 70% power for 5-10 30 second bursts with 30 second cooldown on ice between each burst. Sonicated mixtures were centrifuged at 50,000 x g for 30-45 minutes. The supernatant was kept as this is the protein crude extract. For all cellular extraction steps, the sample was kept at 4°C.

2.5.3 Immobilised Metal Affinity Chromatography

HisTrap™ high performance (GE Healthcare) nickel columns were stripped, cleaned and recharged before all Immobilised Metal Affinity Chromatography (IMAC). The protocol involves running solutions through the column at 1ml/min using a peristaltic pump and for the duration of the nickel column size; 5 min for 5 ml column and 1 min for 1 ml column per solution. Columns were washed with water, stripping buffer (**table 5**), binding buffer (**table 5**), water, 0.1M $NiSO_4(H_2O)_6$ and lastly, water.

Crude extracts were run though a 5 ml nickel column at 1 ml/min using a peristaltic pump and the flow-through was collected. The protein containing nickel column was run through an equilibrated ÄKTA chromatography system (GE Healthcare) with IMAC binding buffer. Elution buffer (**table 5**) is used to create an imidazole gradient from 0-50% up to 250 mM. 5 ml fractions were collected corresponding to possible protein peaks at 280 nm on the chromatogram. Selected fractions, crude and flow-through extracts were analysed on a 12% SDS-PAGE gel. The purest fractions were pooled together and concentrated to 5 ml total volume using a Vivaspin™ concentrator spin column (GE Healthcare). All purification steps were run at 4^OC

2.5.4 Gel filtration Chromatography

When purity of the protein from SDS-PAGE analysis was insufficient for binding studies, further purification by gel filtration was also performed. Using a 125 ml gel filtration column, using an ÄKTA, the column was equilibrated firstly with water and then exchange buffer (**table 5**). The 5 ml of concentrated pooled IMAC fractions were added to the gel filtration column and 5 ml fractions collected corresponding to protein peaks at 280 nm on the chromatogram. Selected fractions were analysed on SDS-PAGE gel and the purest fractions were pooled together and concentrated to 200 ul for a protein concentration of around 20-100 mg/ml. Purified protein was aliquoted and flash frozen in liquid nitrogen and stored at -80 ^{O}C.

2.5.5 Reverse Immobilised Metal Affinity Chromatography

In the further purification of the eSTK from *C. difficile*, Reverse Immobilised Metal Affinity Chromatography (reverse IMAC) and dephosphorylation were performed. The reaction mixture involved all the pooled eSTK protein was incubated at 4^{O}C with 80 ug TEV protease in a volume of 1 ml for 4 hours then a 1-hour incubation with 90 ug IreP phosphatase from (Thoroughgood, 2018) at 30^{O}C with 1mM $MnCl_2$. The whole mixture is run through a 1 ml nickel column on an ÄKTA equilibrated with exchange buffer. 1 ml fractions are collected and analysed on SDS-PAGE gel then purified fractions are pooled and concentrated. The same gel is stained using Pro-Q diamond staining protocol stated in section **2.7.1**. Reverse IMAC is run at 4^{O}C.

Table 5: Buffers and solutions used in competent cell making and protein purification

Buffer	**Composition**
Competent cell making	
Transformation buffer 1 (TBF1)	30 mM potassium acetate, 10 mM $CaCl_2$, 50mM $MnCl_2$, 100 mM RbCl, 15 % glycerol
Transformation buffer 2 (TBF2)	10 mM MOPS, 75 mM $CaCl_2$, 10 mM RbCl, 15 % glycerol
Recombinant protein purification buffers	
Binding buffer	500 mM NaCl, 20 mM Na_3PO_4, 20 mM imidazole, 10 % glycerol, 0.2 mM PMSF, 1 µm leupeptin, 1 µm pepstatin, pH 7.4
Elution buffer	500 mM NaCl, 20 mM Na_3PO_4, 500 mM imidazole, 10 % glycerol, 0.2 mM PMSF, 1 µm leupeptin, 1 µm pepstatin, pH 7.4
Exchange buffer	10 mM HEPES, 150 mM NaCl, 0.2 mM PMSF, 1 µm leupeptin, 1 µm pepstatin, pH 7.4
Stripping buffer	500 mM NaCl, 20 mM Na_3PO_4, 50 mM EDTA, pH 7.4

Table 6: Buffers and solutions used in DNA suspension, Agarose gel analysis, acrylamide gel analysis, kinase activity and phosphate gel staining

Buffer	**Composition**
DNA suspension buffers	
TE	10 mM Tris-HCl, 1 mM EDTA, pH 8.0
Agarose gel running buffers	
TAE	1 x 40 mM Tris acetate, 1mM EDTA
Acrylamide gel analysis	
Resolving Gel	Per 12 % gel: 1.41 ml 1.5 M Tris-HCl pH 8.8, 2.3 ml 29 % (w/v) Acrylamide, 1.9 ml distilled water, 57.5 µl 10 % (w/v) SDS, 57.5 µl 10 % (w/v) APS, 5 µl TEMED
Stacking Gel	Per 12 % gel: 1.25 ml 0.5 M Tris-HCl pH 6.8, 0.5 ml 29 % (w/v) Acrylamide, 3.25 ml distilled water, 50 µl 10 % (w/v) SDS, 50 µl 10 % (w/v) APS, 7.5 µl TEMED
SDS-PAGE loading dye	1x: 50 mM Tris-HCl pH 6.8, 2 % SDS, 10 % glycerol, 1 % β-mercaptoethanol, 12.5 mM EDTA, 0.02 % bromophenol blue
SDS-PAGE running buffer	1x: 25 mM Tris, 192 mM glycine, 0.1 % (w/v) SDS
Native-PAGE loading dye	2x: 62.5 mM Tris-HCl pH 6.8, 40 % glycerol, 0.01% bromophenol blue
Native-PAGE running buffer	1x: 25 mM Tris, 192 mM glycine, pH 8.3
Phosphate-buffered saline	137 mM NaCl, 2.7 mM KCl, 10 mM Na_2HPO_4, 1.8 mM KH_2PO_4
Pro-Q Diamond Staining Solutions	
Fixing solution	50 % Methanol, 10 % acetic acid
Destain solution	20 % Acetonitrile, 50 mM sodium acetate, pH 4.0
Kinase autophosphorylation buffers	
Assay buffer	250 mM Hepes, 250 mM KCl, 5 mM MgCl, pH 7.5
Kinase buffer	50 mM HCl, 50 mM KCl, 10 mM $MgCl_2$ and 0.5 mM DTT

2.6 Protein analysis and detection

2.6.1 Protein quantification

All protein samples had their concentrations determined using a Nanodrop ND-1000 Spectrophotometer (Nanodrop Technologies). Protein was measured at 280 nm absorbance with the molecular weight and molar extinction coefficient for accuracy.

2.6.2 SDS-Polyacrylamide gel electrophoresis

SDS-Polyacrylamide Gel Electrophoresis (SDS-PAGE) was used to separate and visualise proteins in denaturing conditions. All gels made were 12% acrylamide and prepared on a Mini-PROTEAN tetra system (BIORAD). Resolving gel (**table 6**) was added to the system and topped with 100% ethanol to level out the setting gel. Once the resolving gel was set, the ethanol is removed and 5 % stacking gel (**table 6**) is added with a well separating comb and left to set. All protein samples and low molecular weight calibration ladder (Phosphorylase b, Bovine Serum Albumin, Ovalbumin, Carbonic anhydrase, Trypsin inhibitor, β-Lactalbumin) (GE Healthcare) were prepared with SDS-loading dye (**table 6**) and heat denatured for 10 minutes at 95 °C. The prepared acrylamide gel was placed into an electrophoresis unit Mini-PROTEAN tetra system (BIORAD) with 20 µl of protein sample and 10 µl protein ladder added to their specified wells. SDS-PAGE running buffer (**table 6**) was added and gel was run at 180 V for 50 minutes for optimum separation. To visualise total protein, gels were incubated overnight with instant blue (Expedeon) and then kept in water. Gels were imaged with Gel Doc™ XR+ Gel Documentation System (BIORAD).

2.6.3 Western blotting

For detection of recombinant protein expression, protein samples were analysed by SDS-PAGE analysis (**2.6.2**). The gel was then transferred to a polyvinylidene difluoride (PVDF) using a BioRad Mini Transfer Blot. The membrane was blocked overnight in 10 % skimmed milk powder in phosphate-buffered saline (PBS). The following day, the His-tagged protein is detected by an anti His-6 mouse monoclonal Ab (Roche) (1:500 in 0.1 % skimmed milk powder in PBS) with a 1-hour incubation. This was followed by three washes in Tris buffered Saline (TBS)-0.1 % Tween-20 for 20 minutes each. Anti-mouse IgG HRP conjugate secondary antibody was added) (Promega) (1:2500 in 0.1 % skimmed milk powder in PBS) and incubated for 1-hour incubation at room temperature. Lastly, the membrane was washed in TBS-Tween three times for 20 minutes each. To prepare for imaging, the membrane is washed with a 10 ml 50/50 mixture of hydrogen peroxide and luminol

enhancer solution (Amersham – GE Healthcare). The membrane chemiluminescence was imaged using an ImageQuant LAS 4000 imager (GE Healthcare).

2.6.4 Native-polyacrylamide gel electrophoresis

Proteins were separated and visualised according to their conformations in Native-polyacrylamide electrophoresis (Native-PAGE). Only Mini-PROTEAN® TGX Stain-Free™ 4-20 % gradient gels were used due to their absence of SDS. The gels were loaded into an SDS-free electrophoresis Mini-PROTEAN tetra system (BIORAD). Protein samples were prepared with Native-PAGE loading dye (**table 6**) to 1 mg/ml concentration. Protein size ladders included BSA prepared at 8 mg/ml in PBS and a protein solution of Bovine-serum Albumin (BSA), β-Amylase and Thyroglobulin at 1 mg/ ml per protein. Both ladders were also prepared in Native-PAGE loading dye (**table 6**) to 1 mg/ml 20 µl per lane of protein samples and ladders were added. Native-PAGE running buffer (**table 6**) was added to the electrophoresis unit. Gels were run at 100 V for 3.5 hours on ice to retain native protein conformation. To visualise total protein, gels were incubated overnight in Instant Blue (Expedeon) and subsequently stored in water. Gels were imaged with a Gel Doc™ XR+ Gel Documentation System.

2.6.5 Mass spectrometry

To detect phosphorylated sites proteins, Electrospray ionisation mass spectrometry (ESI-MS) was used. Sample preparation began by dicing Coomassie blue-stained bands excised from an SDS-PAGE gel and placing in a 1.5 ml Eppendorf tube. All following buffer steps use a volume sufficient to cover the gel bands. The gel is destained using 50 % ethanol, 50 mM ammonium bicarbonate (ABC) for 20 minutes, RT at 650 rpm, repeated 3 times. The protein gel is dehydrated using 100% ethanol for 5 minutes, RT at 650 rpm. This was followed by reduction and alkylation using 10 mM tris(2-carboxyethyl)phosphine (TCEP) and chloroacetamide (CAA) for 5 minutes, 70 °C with gentle vortex. Washing follows with 50 % ethanol and 50 mM ABC for 20 minutes, RT at 650 rpm, repeat twice. The protein was rehydrated and digested with 2.5 ng/µl trypsin solution for 10 minutes at RT. To fully cover gel bands, 50 mM ABC is added and incubated overnight at 37 °C. The next day the peptides were extracted using 25 % acetonitrile, 5% formic acid solution and sonicated in a bath twice for 5-10 minutes at RT. The resulting solution was concentrated in a speed-vac at 13,000 rpm for approximately 40 minutes to bring the volume to 20 µl. Lastly, the peptides are resuspended using 2.5 % acetonitrile, 0.05 % Trifluoroacetic acid (TFA) to bring the volume to 50 µl. The sample is then transferred for mass spectrometry analysis by the proteomics team. Analysis is performed using Scaffold proteome software.

2.7 *In vitro* Kinase Phosphorylation assays

2.7.1 Invitrogen Pro-Q Diamond Staining

Pro-Q Diamond stain is a method to detect phosphorylated proteins in acrylamide gels. The protocol followed is a published variation of the manufacturers protocol (Ganesh Kumar Agrawal & Thelen, 2009). All staining steps were performed with gentle agitation on a gel rocker. After running SDS-PAGE or NATIVE acrylamide gels according to (**2.6.2**, **2.6.4**), the gels were incubated in fixing solution for 2 X 30 minutes, followed by 3 X 10 minute washes in distilled water. Pro-Q Diamond stain solution was diluted 3-fold to a total volume of 30 ml. All following staining and destaining steps were performed in darkness and during wash changes, light exposure was minimised. Diluted stain was added to the gel and heated in a microwave to 65-80 °C, incubated for 7 minutes and reheated to 65-80 °C in a microwave and again incubated for 7 minutes. The gel was then incubated with Pro-Q destain solution for 2 x 30 minutes. Lastly, it was washed with distilled water twice for 5 minutes. The stained gel was imaged using Typhoon FLA 9500 with filters LBP, LPR(ch2), LPG and IP at 532 nm. For clearer viewing of phosphoproteins, the image produced was modified in the program ImageJ using a filter called Green Fire Blue. To confirm the presence of total protein, the imaged gel was stained using Coomassie blue protein stain.

2.7.2 Dephosphorylation assay

Dephosphorylation of the kinase domains was performed using either IreP or Lambda Protein Phosphatase (NEB). For optimised phosphatase activity, the reaction composition included 1 mM $MnCl_2$, 1 X NEBuffer Pack for Protein MetalloPhosphatases. Lambda phosphatase was added at a ratio of 10,000 units per 1 mg of phosphorylated protein. IreP was added at an equivalent concentration to the phosphorylated protein. Kinase concentrations added to the reaction ranged from 50-100 μM. Dephosphorylation reaction was performed at 30 °C for 1.5 hours with gentle agitation.

2.7.3 Small scale dephosphorylation and purification

Loose recharged nickel Sepharose beads were used to purify kinase domains after the dephosphorylation assay with lambda phosphatase as described in **2.7.2**. All following centrifugation steps were run for 1 min at 13,000 rpm. Purification began by mixing 30 μl Sepharose bead suspension with 50 μl of dephosphorylation reaction mixture and incubating for 30 minutes at room temperature. The breads were washed by centrifugation and removing the supernatant. The beads were resuspended in 100 μl binding buffer (**table 5**), then washing was repeated twice. To elute the protein off the Sepharose beads, 50 μl elution

buffer was added and left at room temperature for 30 minutes. The eluted proteins were separated by centrifugation and protein containing supernatant was collected. A buffer exchange was performed in a concentration column to store protein in exchange buffer (**table 5**). The total volume was concentrated down to 50 µl.

2.7.4 Kinase autophosphorylation assay

Autophosphorylation kinase assay was performed in a kinase buffer adapted from (Goss, 2013) (**table 6**). A 5X version of the kinase buffer was created for the assay. Reactions were set up using 25 µM kinase with 1 mM ATP. The assay was performed at 37 °C for 0-60 minutes. Reactions were terminated by adding 4X SDS-PAGE loading dye (**table 6**) and heat denatured at 95 °C for 10 minutes. Reaction samples were analysed by SDS-PAGE analysis (**2.6.2**) and stained using the Pro-Q Diamond phosphate stain (**2.7.1**).

2.7.5 Staurosporine competition assay

Staurosporine competition assay was performed using the exact conditions described in **2.7.4.** However, before the addition of ATP, staurosporine was added at concentrations ranging from 0-100 µM and incubated at 37 °C for 15 minutes.

2.8 *In vitro* Biophysical assays

2.8.1 Microscale thermophoresis

A Monolith NT.115 (NanoTemper Technologies) was used to determine the dissociation constant between *E. faecalis* IreK and kinase inhibitor Staurosporine. The protein was labelled using red (MO-LOO8 NT-647) using a Monolith NT protein labelling red-NHS (Nanotemper Technologies) according to the supplied manufacturers protocol. The red label dye covalently binds to the x6 His tag of the recombinant protein during a 30-minute incubation at room temperature. The unlabelled kinase inhibitor and protein were serially diluted in DMSO supplemented with PBS-T. The total reaction mixture was 10 µl for each reaction with the protein at 50 µM. Individual reactions were loaded into standard capillaries (Nanotemper Technologies) and loaded into a Monolith NT.115.

2.9 *In vivo* kinase inhibitor assays

2.9.1 Minimum inhibitory concentration

Minimum inhibitory concentrations (MICs) in definition is the lowest concentration of antibiotic that will inhibit the visible growth of a micro-organism after overnight incubation. All MIC work was primarily undertaken by John Moat and Dr Christopher Thoroughgood to conform to health and safety conditions when working with pathogenic organisms. The antibiotic concentration range used to determine the MIC is universally accepted to be in doubling dilution steps. All MIC testing performed was according to CSLI standards or adapted when stated. The MIC defined here is 95 % inhibition. In *C. difficile* MIC testing, the standard growth media was modified to accommodate the anaerobic nature of the microorganism. The growth media for *C. difficile* composed of Bursella (Vicente et al., 2014) media supplemented with hemin.

3.0 Results and discussion chapter 1: *C. difficile* kinase cloning, expression and purification

3.1 Introduction

This chapter involves first aim of the project, the sequence analysis, Gibson cloning and protein expression of three eukaryotic serine/threonine (eSTK) domains from *E. faecalis*, *E. faecium* and *C. difficile*. These pathogenic organisms all have intrinsic antibiotic resistance mechanisms which are suggested to be controlled by these kinase domains. Both the cloning and protein expression processes had several challenges, especially with an anaerobic organism such as *C. difficile*. This work is the expansion on the experiments performed in (Goss, 2013) but expanding the kinase domain repertoire into from *E. faecalis* to *E. faecium* and *C. difficile*.

3.2 Kinase domain sequence alignment analysis

To investigate the biological relevance of comparing eSTK kinase domains between different species, a sequence alignment analysis was performed. Using the online tool Clustal Omega, the kinase domain protein sequences were aligned and quantified between the eSTK kinase domains of *E. faecalis*, *E. faecium* and *C. difficile* and the *homo sapiens* CDK2, which is closest protein relative (**table 7**). The full sequence protein sequences can be found in the appendix. An eSTK present in *C. difficile* was found in ATCC 9689 strain containing a kinase domain, transmembrane domain and two extracellular pasta domains. As shown in **table 7**, this kinase domain has sequence similarity to both *E. faecalis* and *E. faecium* IreK kinase domains.

Table 7: Sequence percentage similarity between kinase domains from *E. faecalis*, *E. faecium*, *C. difficile* and *homo sapiens*

Sequence	*Homo sapiens* CDK2	*E. faecalis* IreK	*E. faecium* IreK	*C. difficile* eSTK KD
Homo sapiens CDK2	100.00	30.28	30.68	29.47
E. faecalis IreK	30.28	100.00	82.95	49.61
E. faecium IreK	30.68	82.95	100.00	49.61
C. difficile eSTK KD	29.47	49.61	49.61	100.00

The sequence similarity output raises several points. The kinase domain between *E. faecalis* and *E. faecium* is nearly 83 % which considering that same species, is expected. This means the characteristics between the two kinase domains should be relatively similar. Considering *C. difficile* is a different species and an anaerobic organism, unlike *Enterococci*, a near 50 % sequence alignment suggests perhaps similar structures and functions of these kinase domains between Gram-positive bacteria. This is however only based on genomic information. All three of the bacterial kinase domains have around 30 % alignment to the closest human homolog, CDK2, indicating some possible sequence conservation between eukaryotes and prokaryotes. Due to their sequence conservation and possible antibiotic regulation roles, the kinase domains are an important aspect to investigate.

3.2 Gibson cloning

3.2.1 High-fidelity PCR

The recombinant expression pETDuet plasmid constructs coding *E. faecalis* and *E. faecium* kinase domains (**table 3**) were originally obtained by Dr Christopher Thoroughgood from collaborators at Columbia university in New York (Goss, 2013) and verified by DNA sequencing (**2.4.9**). Gibson cloning requires two components, linearised vector and gene insert, both containing complementary overhangs to promote annealing. Firstly, high-fidelity PCR was performed to create the gene insert encoding the kinase domain from an eSTK from *C. difficile* (**figure 11**). This was performed using Clos STK pProEx F and Clos STK pProEx R primers (**table 4**).

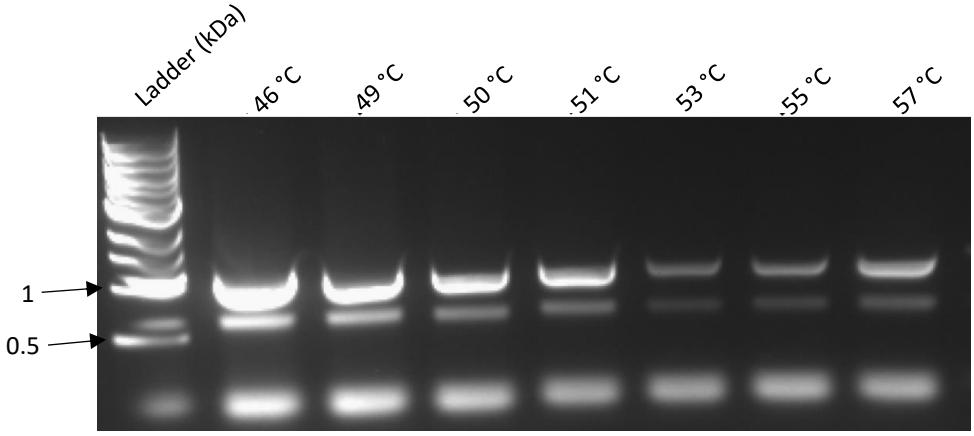

Figure 11: Gradient PCR of eSTK *C. difficile* gene insert on 0.8 % agarose gel. Annealing temperatures ranged from 46-57 °C. Gene insert from annealing temperatures 46-51 °C were cut out and purified.

The amplified gene insert bands from temperatures 46-51 °C were cut out and purified using the protocol in **2.4.5**. The template DNA used in the reaction was originally planned to be *C. difficile* chromosomal DNA however this was unsuccessful because of the difficult nature to grow large cultures *C. difficile* in the laboratory. The second attempt was made using chromosomal DNA obtained directly from a cell colony in the PCR reaction which was successful in **figure 11**.

3.2.2 gBlock gene design

To minimise the problems which can arise in cloning, a gBlock (IDT) was created of the *C. difficile* eSTK kinase domain for cloning into a linearised pProEx HTa expression plasmid vector. The gBlock was codon optimised for expression in *E. coli* BL21 (DE3) strains. The full gBlock sequence is present in **7.2**, appendix. The designed gBlock contains complementary overhangs to sticky ends of linearised pProEx expression plasmid (indicated by bolded sections in the sequence). The gBlock was resuspended in TE buffer (**table 6**) and ready for Gibson cloning if required.

3.2.3 Linearisation of pProEx HTA

For successful Gibson cloning, linearised vector containing complementary overhangs to the insert are required. Using designed primers; pProEx F and pProEx R (**table 4**), a high-fidelity gradient PCR was performed (**figure 12**).

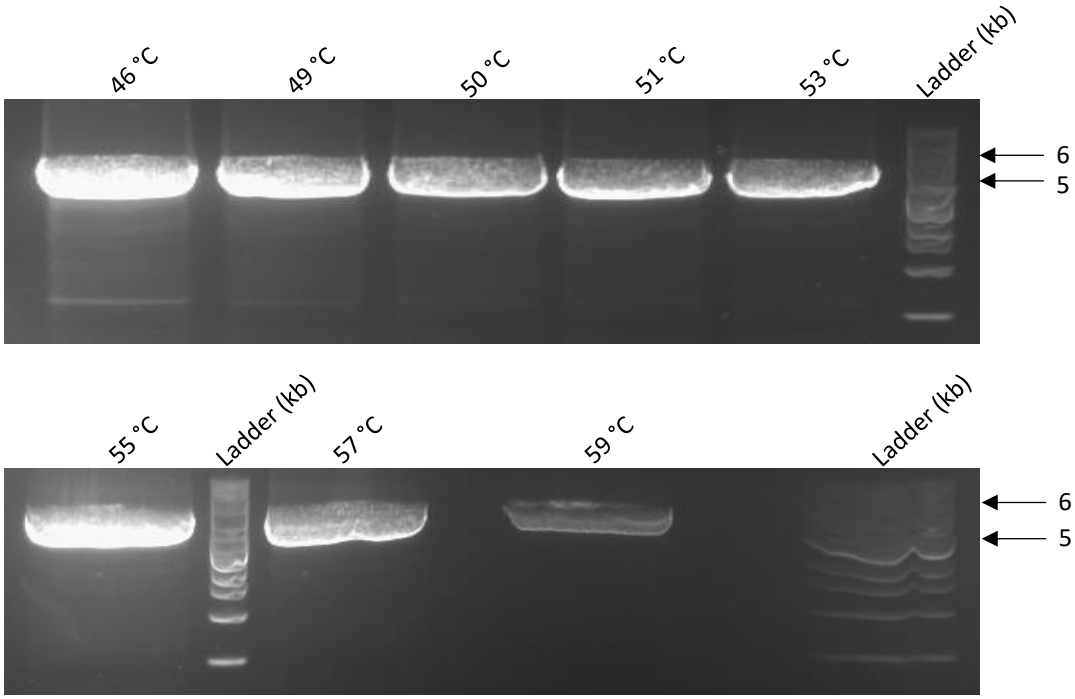

Figure 12: Gradient high-fidelity PCR of pProEx HTA on 0.8% agarose gel. Lanes Include Linear pProEx at increasing annealing temperatures from 46-59 °C. Linear pProEx from annealing temperatures 46-55 °C were cut out and purified.

The optimum annealing temperatures of primers pProEx F and pProEx R were deduced. The optimum annealing temperature is 46 °C with the strongest band signal. The linearised pProEx in wells 46-55 °C were cut out and purified using the protocol in **2.4.5**. Annealing temperatures at 57 and 59 °C produced a lower concentration of linearised vector, possibly not full length, resulting in them being discarded. If required further linearised vector could be obtained by running another high-fidelity reaction at an annealing temperature at 46 °C, sufficient plasmid was obtained from this reaction only however. The *C. difficile* gBlock insert and linearised vector were then ready for Gibson cloning.

3.2.4 Gibson cloning reaction and validation of successful cloned constructs

Gibson cloning only requires the gene insert and a linearised vector both with complementary sticky ends. The first attempt of Gibson cloning used the amplified gene insert from PCR amplification and linearised vector. A colony PCR was performed to detect positive clones by analysing ten positive colonies and a control construct pProEx PBP2 (**figure 13**). The primers used were pProEx Forward and pProEx Reverse, sequences presented in **table 4**.

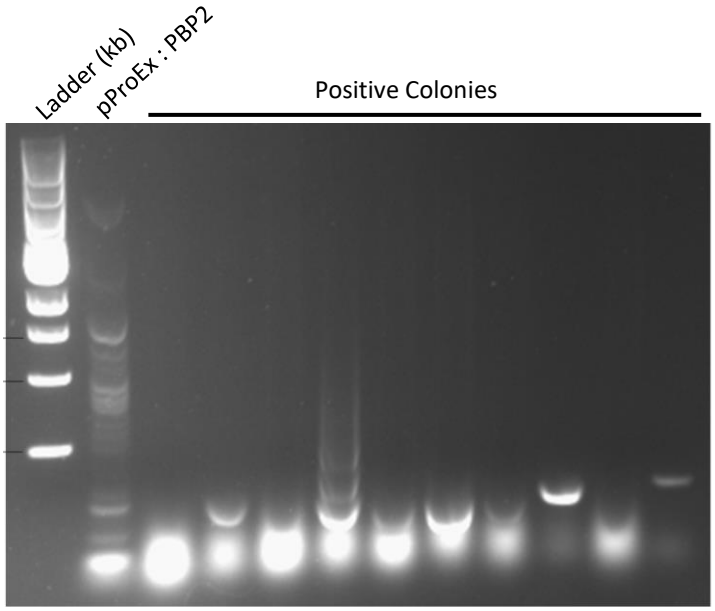

Figure 13: Colony PCR of pProEX : eSTK (*C. difficile*) on 0.8% agarose gel. Lanes left to right: Control pProEx:PBP2 (*Staphylococcus aureus* Mu50), Colonies 1-10 of potential pProEX : eSTK construct.

For a positive pProEx eSTK construct, there should be a band present at approximately 1,200 base pairs. Unfortunately, all positive colonies don't appear to have the construct, only with a few containing a band at around 200 base pairs. The pProEx:PBP2 control is possibly contaminated with unspecific primer annealing resulting in multiple bands throughout the lane, dismissing the validity of the control unfortunately. The failure of the Gibson cloning could be due to minimal concentrations of linearised vector after gel purification or the amplified gene insert.

In a second attempt at Gibson cloning, the designed gBlock was used and agarose gel analysis was performed (**figure 14A**) to ensure the presence and validity of purified linearised pProEx vector and *C. difficile* kinase domain gBlock. Both vector and gene insert were pure and at a sufficient concentration for cloning.

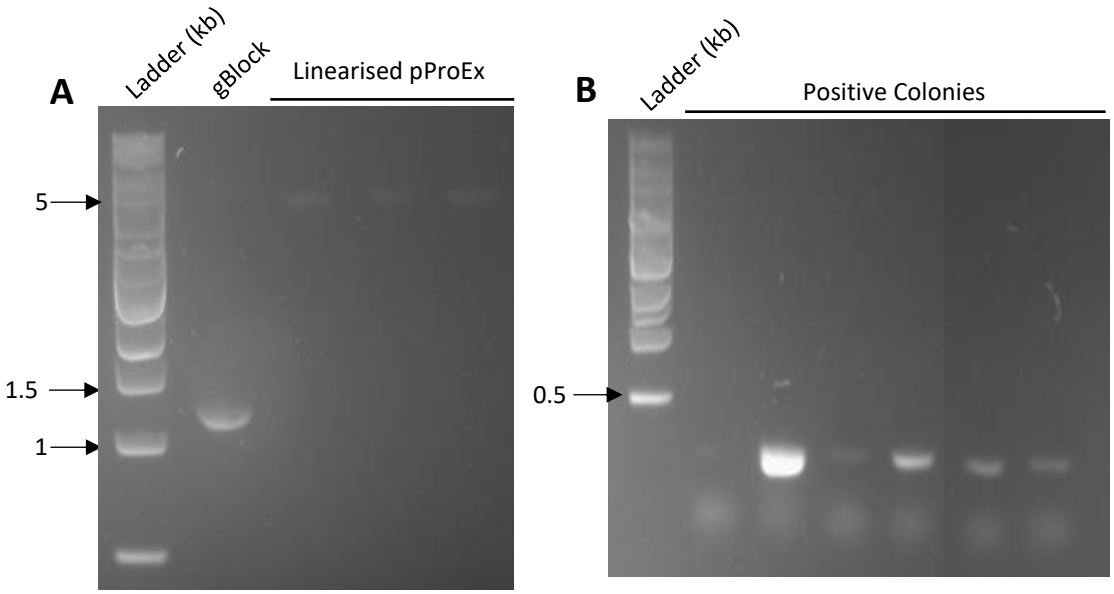

Figure 14: High Fidelity PCR of pProEx HTA (left) and colony PCR of pProEx:eSTK construct (C. d*ifficile*) on 0.8% agarose gel. Lanes left to right: (**A**) eSTK (*C. difficile*) gblock insert, linear pProEx samples, Gblock pProEx:eSTK construct colonies, (**B**) Colonies of potential pProEX : eSTK construct.

To prevent false positives, post-cloning, the reaction was incubated with Dpn1 to digest any remaining template DNA. To validate successful colonies after transformation, colony PCR was performed (**figure 14B**). The expected successful gene length was 1200 bp however colony PCR only showed ~200 bp products again, which also occurred during cloning repeats. To confirm the whether the cloning was successful, the colonies which produced the strongest 200 bp bands in colony PCR were sent off for sanger sequencing (**2.4.9**). All plasmid constructs returned with high sequence similarity to the *C. difficile* kinase domain gene, indicating a possible lack of specificity with the primers (**table 4**) used in colony PCR. The plasmid construct with the correct aligned sequence was selected, matching the sequences in **table 9**, appendix. The three constructs in **table 3** were used in kinase domain protein expression in *E. coli*.

3.3 Kinase domain protein expression and purification

3.3.1 *E. faecalis* IreK kinase domain

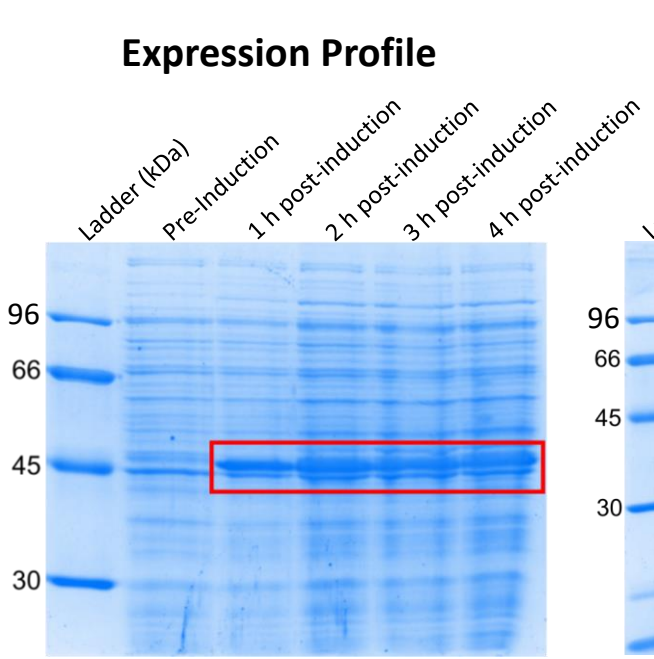

Figure 15: Expression profile of IreK Kinase Domain from *E. faecalis* BL21 (DE3) cells on a 12% SDS-PAGE gel. Cells were normalised to OD 0.6 at 600 nm for gel analysis. Lanes left to right: 0 h pre-induction (0.689 OD_{600}), 1 h post-induction (1.167 OD_{600}), 2 h post-induction (1.554 OD_{600}), 3 h post-induction (1.818 OD_{600}) and 4 h post-induction (1.990 OD_{600}).

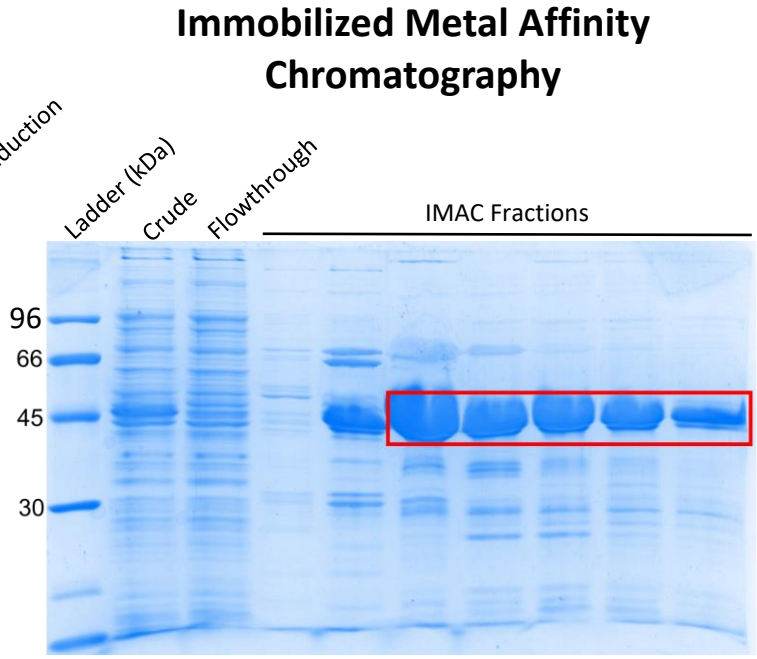

Figure 16: IMAC selected fractions of IreK Kinase Domain from *E. faecalis* on a 12% SDS-PAGE gel. Samples were normalised up to 40 µg for gel analysis. Lanes left to right: Crude extract, Flow through after column run, Protein containing IMAC fractions. Pooled fractions are highlighted in red.

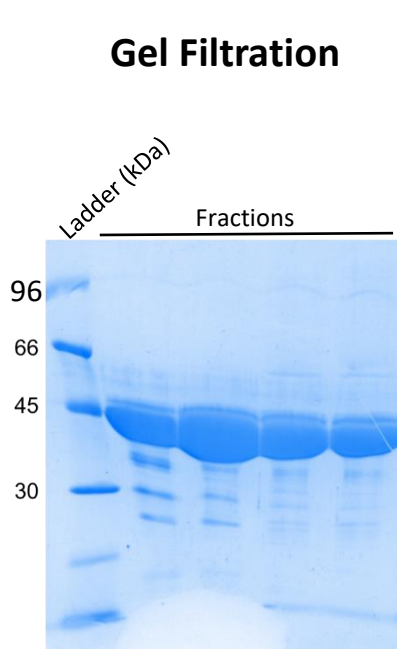

Figure 17: Gel filtrated select fractions of IreK Kinase Domain from *E. faecalis* on a 12% SDS-PAGE gel. Samples were normalised up to 40 µg for gel analysis. Lanes left to right: *E. faecalis* IreK protein containing fractions. All factions were pooled and concentrated.

3.3.2 *E. faecium* eSTK kinase domain

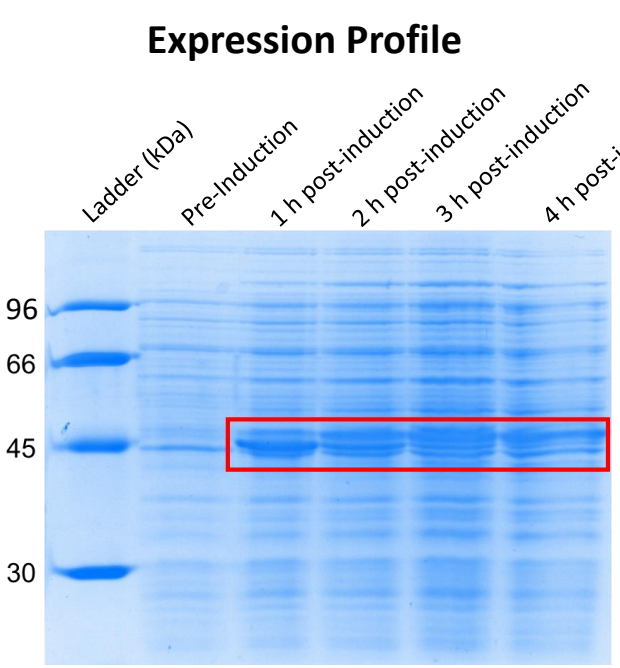

Figure 18: Expression profile of IreK Kinase Domain from *E. faecium* in BL21 (DE3) cells on a 12% SDS-PAGE gel. Cells were normalised to OD 0.6 at 600 nm for gel analysis. Lanes left to right: 0 h pre-induction (0.602 OD_{600}), 1 h post-induction (1.136 OD_{600}), 2 h post-induction (1.607 OD_{600}), 3 h post-induction (1.883 OD_{600}) and 4 h post-induction (2.059 OD_{600}).

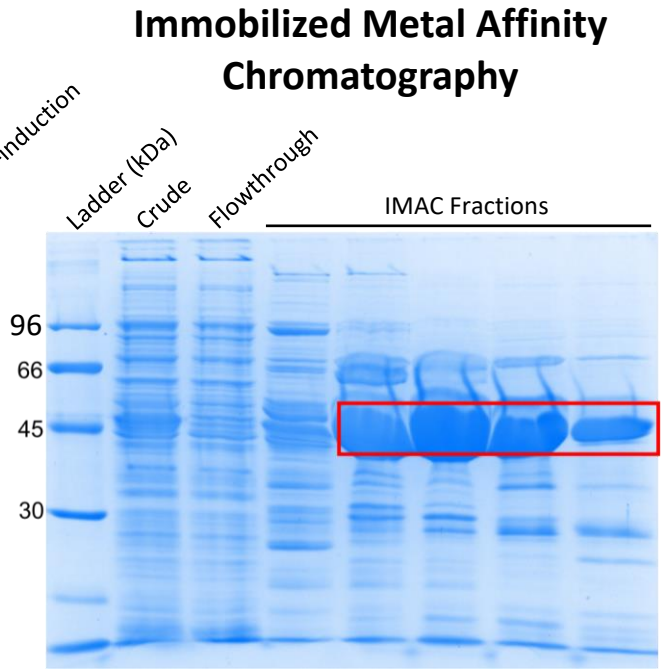

Figure 19: IMAC selected fractions of IreK Kinase Domain from *E. faecium* on a 12% SDS-PAGE gel. Samples were normalised up to 40 µg for gel analysis. Lanes left to right: Crude extract, Flow through after column run, Protein containing IMAC fractions. Pooled fractions are highlighted in red.

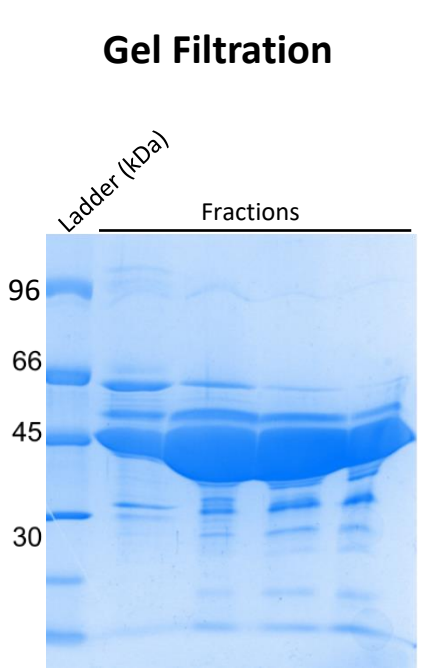

Figure 20: Gel filtrated select fractions of IreK Kinase Domain from *E. faecium* on a 12% SDS-PAGE gel. Samples were normalised up to 40 µg for gel analysis. Lanes left to right: *E. faecium* IreK protein containing fractions. All factions were pooled and concentrated.

3.3.3 *C. difficile* eSTK kinase domain

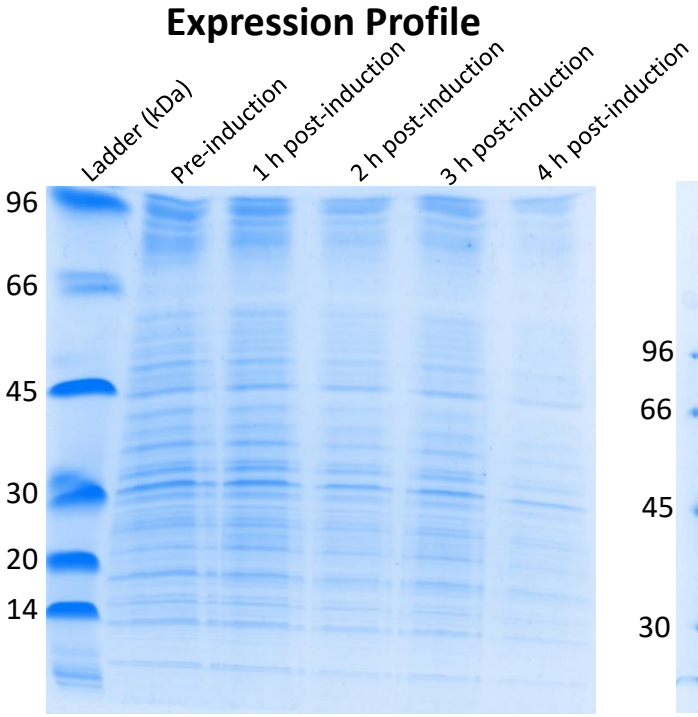

Figure 21: Expression profile of eSTK Kinase Domain from *C. difficile* in BL21 (DE3) cells on a 12% SDS-PAGE gel. Cells were normalised to OD 0.6 at 600nm for gel analysis. Lanes left to right: 0 h pre-induction (0.660 OD_{600}), 1 h post-induction (0.735 OD_{600}), 2 h post-induction (0.694 OD_{600}), 3 h post-induction (0.673 OD_{600}) and 4 h post-induction (0.659 OD_{600}).

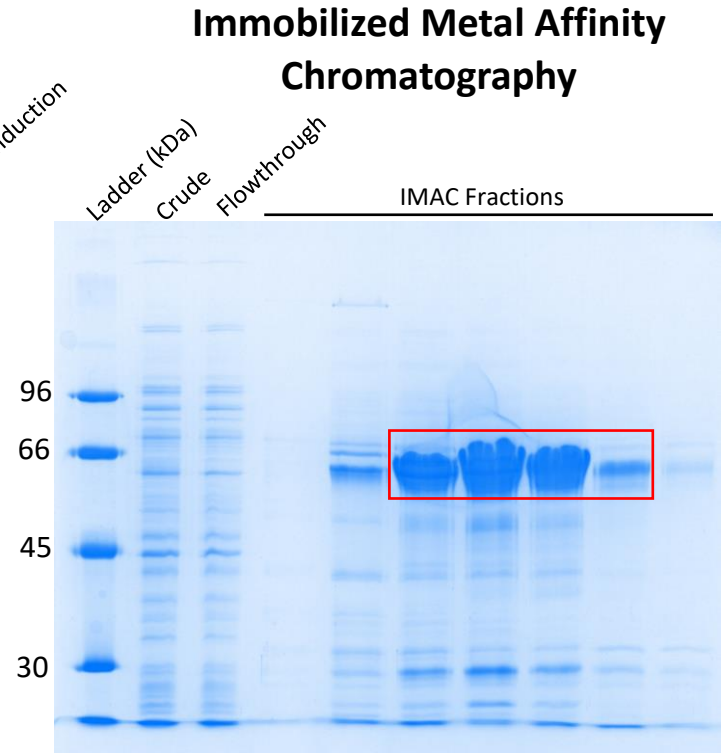

Figure 22: IMAC purification of eSTK (*C. difficile*) on a 12% SDS-PAGE gel. Lanes left to right: Crude extract, Flow through, IMAC fractions. Stained with Coomassie blue

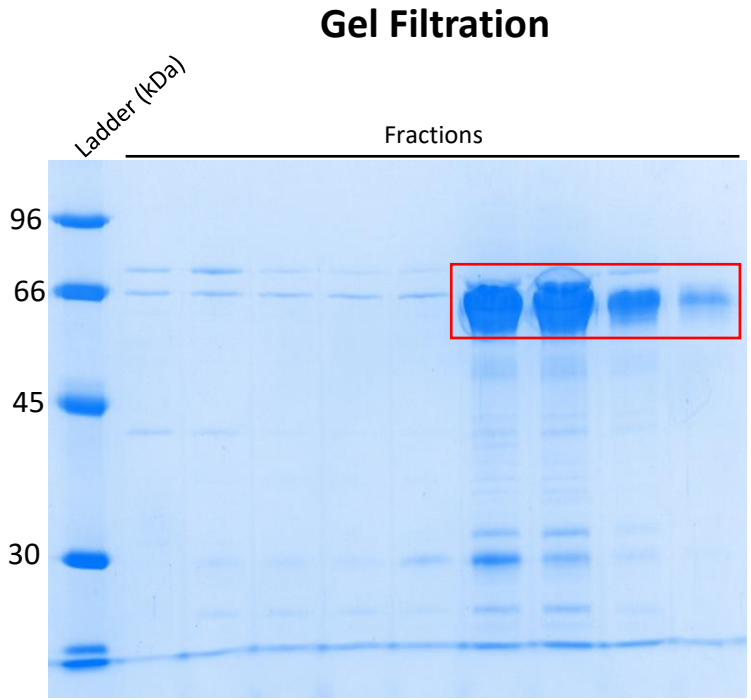

Figure 23: IMAC purification of eSTK (*C. difficile*) on a 12% SDS-PAGE gel. Lanes left to right: IMAC fractions. Stained with Coomassie blue

3.3.4 Optimisation of kinase domain protein expression and purification

The kinase domains from *E. faecalis* and *E. faecium* have previously been expressed and purified (Thoroughgood, 2018) and are stable cytosolic proteins from aerobic bacteria. Both proteins expressed to a sufficient level to appear on SDS-PAGE gels (**figure 15** and **18**). Immobilized metal affinity chromatography and gel filtration chromatography were sufficient to purify the kinase domains to a suitable level for activity and binding assays. Gel filtration chromatography was required for all three kinase purifications to remove contaminating proteins. The final purity (**figure 17** and **20**) was judged to be sufficient for planned assays and any impurities are at an irrelevant low concentration.

The kinase domain from *C. difficile* was more difficult to purify as however. The expression of *C. difficile* kinase domain was explored in a range of expression strains of *E. coli* including BL21(DE3), C41(DE3) and C43(DE3) at a range of induction durations and temperatures. In all cell lines, expression of the kinase domain was unclear (**figure 39**, appendix). In a first attempt to express and purify, BL21 (DE3) cells were used and purification was performed (**figure 40** and **43**, appendix). The kinase domain however appeared to degrade after each purification stage and was present at low concentrations.

As the kinase domain from *C. difficile* was found to be significantly less stable with a reduced expression than its *Enterococcal* counterparts, the purification needed to be optimised. Firstly, increasing the *E. coli* growth to 6 L increased the amount of protein expressed. Secondly, all protein extraction, SDS-PAGE analysis and purification steps were performed in one day at 4°C and in the presence of protease inhibitors in all purification buffers (**table 5**). This more cautious approach resulted in the successful expression and purification of the kinase domain from *C. difficile*. (**figure 23**)

3.3.5 Purified kinase domains

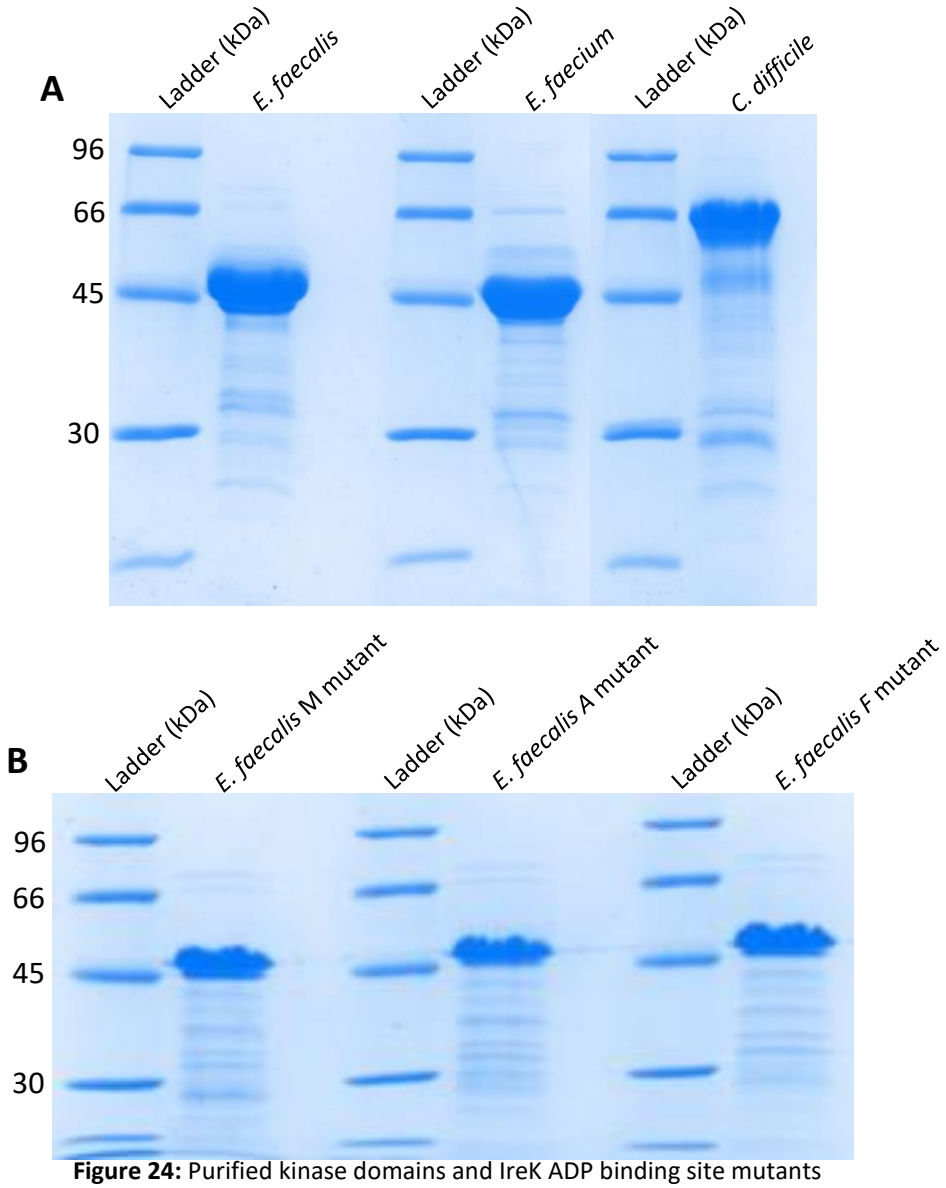

Figure 24: Purified kinase domains and IreK ADP binding site mutants (*E. faecalis*) on a 12 % SDS-PAGE gel. Lanes left to right: (**A**) IreK Kinase domain (*E. faecalis*), IreK kinase domain (*E. faecium*), eSTK kinase domain (*C. difficile*), (**B**) IreK M mutant, IreK A mutant, IreK F mutant.

As a result of successful expression and purification, the three primary kinase domains from *E. faecalis, E. faecium* and *C. difficile* are presented in **figure 24A**. The proteins are at sufficient purity to perform activity and binding assays. From a previous unfinished project (Thoroughgood, 2018), there are also three secondary *E. faecalis* IreK ADP binding site mutants (**figure 24B**). The mutants appear to have a greater concentration of impurities, which could be removed either by another round of gel filtration or reverse immobilised metal affinity chromatography if they interfered with future experiments.

3.4 Discussion and future work

The aim of this chapter was to express and purify the eSTK kinase domains from three Gram-positive bacteria and expand upon the kinase repertoire in (Goss, 2013).

The cloning process required several repeats before a successful result was obtained. The problems appear to arise from colony PCR analysis. Although the primers were checked for annealing suitability to the construct, they did not appear to produce the desired PCR output even though sanger sequencing proved the presence of gene insert. Primer redesign and optimisation of colony PCR conditions (including primer annealing temperature) are required, as potentially, the initial cloning attempts using the amplified PCR gene inserts produced the same 200 base pair outputs as the successful gBlock cloning attempts, indicating the initial attempts may have been successful should they have been sequenced.

The expression and purification of eSTK kinase domains from *E. faecalis*, *E. faecium* and *C. difficile* was successful. This was the first time that the eSTK kinase domain from *C. difficile* was expressed and purified in this laboratory. Expression in *E. coli* was difficult and appears to be present in the insoluble fraction of the cell lysate (**figure 40**, appendix). The kinase domain could potentially have issues folding in the *E. coli* cytoplasm. Expressing the protein in competent cell lines like BL21(DE3)pLysS (Thermofisher) may provide greater control over expression promoting the proper folding of the protein. Unlike *Enterococci*, *C. difficile* is an organism which grows under anaerobic conditions, which may cause proteins expressed and exposed to oxygen to degrade. This could have been avoided by forcing out oxygen with pressurised nitrogen in all storage containers to increase protein stability. The degradation of the *C. difficile* kinase domain could also be the result of an additional domain structure not found in the *Enterococcal* kinases. This would explain the increased molecular weight of compared to the other kinases. The stability of the kinase domain may be a misfolding of the structural domains which is not facilitated during expression in *E. coli*. Further investigation into the structure of the *C. difficile* kinase may provide insight into this hypothesis.

Ultimately, the successful method of purification was to perform all cell lysate extraction and purification events to flash freezing in one day. As none of these kinases have yet to be crystallised, further purification steps could be implemented such as reverse immobilised metal affinity chromatography. Another purification method could use an intein-chitin binding domain fusion and use chitin resin as a method to produce highly pure protein for crystallisation.

It is worth noting that the ADP binding site *E. faecalis* IreK mutants were created in (Thoroughgood, 2018) to recreate the sterically hindered ADP binding site of an IreK homolog in *S. aureus*. The idea of the mutants was to address why the *S. aureus* homolog has relatively large residues in the centre of a highly conserved region between IreK and the homolog.

The optimised conditions constructed in this chapter could be explored into other Gram-positive bacterial eSTKs. For example, with the successful purification of the eSTK kinase domain from *C. difficile*, other *Clostridium spp* like *Clostridium botulinum* or *tetani* could be investigated for the presence of eSTKs. Furthermore, expression of the human CDK2 would be a useful eukaryotic comparison to the prokaryotic systems. The expanding of the kinase domain molecular library would be an opportunity to compare eSTK signalling systems between bacterial species and between prokaryotes and eukaryotes.

4.0 Results and discussion chapter 2: Characterisation and effect of phosphorylation of kinase domains

4.1 Introduction

This chapter involves the investigation of the second project aim in which we investigate the phosphorylation of the purified kinase domains. The autophosphorylation activity of the kinase domains are essential for their activation, dimerisation and downstream signalling activity. The ability to dephosphorylate these domains is also crucial in terms of deactivating kinase signalling activity *in vivo* and *in vitro*, the availability of the ADP binding site for binding studies. The biological questions tested the phosphorylation status of the kinase domains out of expression in *E. coli* which eSTK kinase domains have been documented to become phosphorylated during overexpression in *E. coli* (Young et al., 2003). The chapter also includes the optimisation kinase domain dephosphorylation using IreP Lambda Protein Phosphatase, and lastly, the effect of phosphorylation on the oligomerisation of kinase domains. The phosphorylation of kinase proteins has traditionally been followed using radiolabelling using ^{35}S or ^{32}P labelled ATP and SDS-PAGE analysis. In this project we investigated the use of a fluorescent technique to detect phosphorylated proteins using a commercially available reagent from Thermofisher called Pro-Q Diamond stain. (A high-resolution two-dimensional Gel- and Pro-Q DPS-based proteomics workflow for phosphoprotein identification and quantitative profiling. (Ganesh K. Agrawal & Thelen, 2009)

4.2 Pro-Q Diamond stain analysis

The Pro-Q Diamond phosphate stain (Thermofisher) effectively detects phosphorylated serine, threonine and tyrosine residues. This is a useful technique to assess the phosphorylation status of all the purified kinase domains out of expression in *E. coli*.

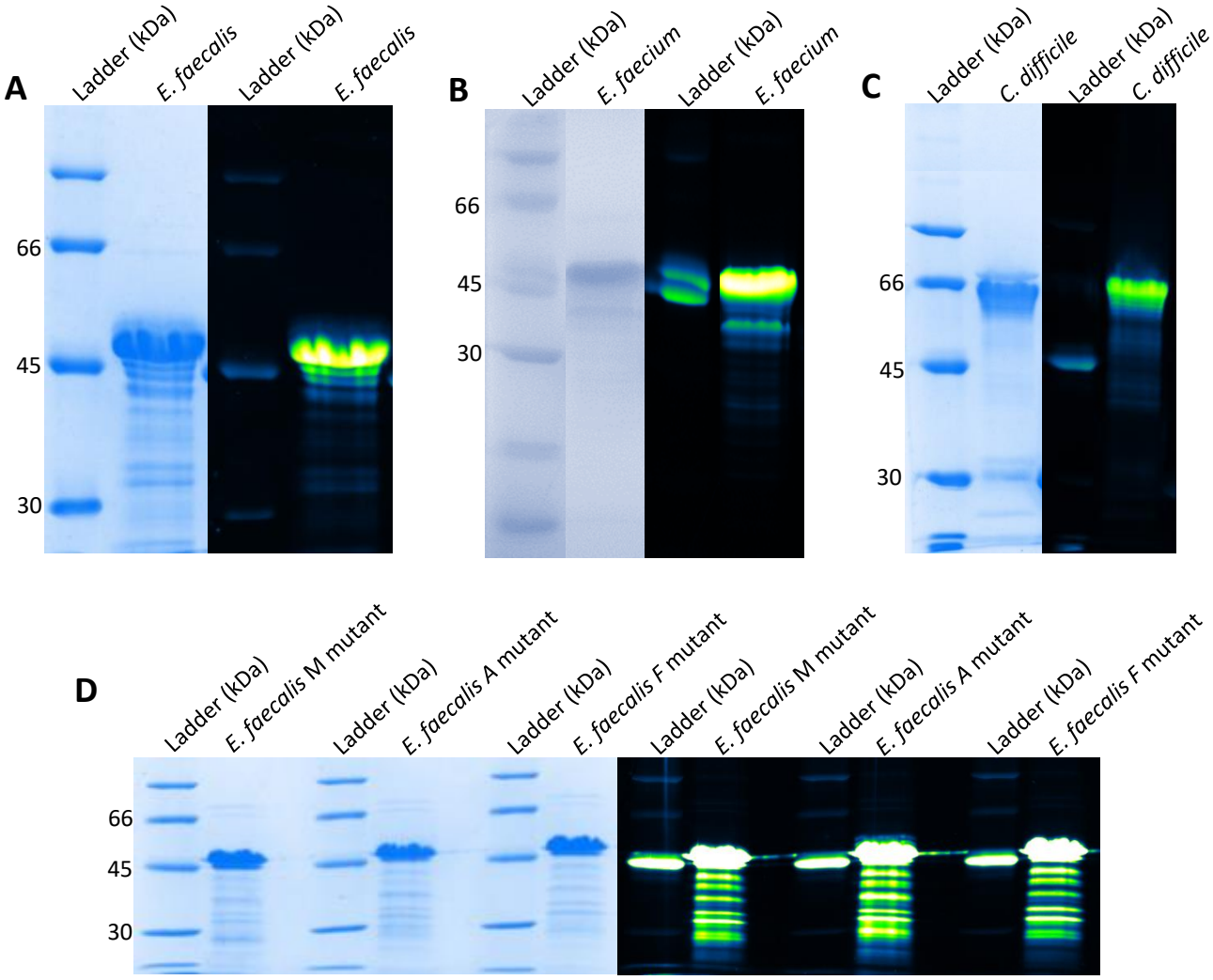

Figure 25: Pro-Q Diamond phosphorylation assay of purified kinase domains from *E. faecalis, E. faecium, C. difficile* and *E. faecalis* ADP binding site mutant kinase domains. Stained with Coomassie blue (left) and Pro-Q Diamond phosphate stain (right). Lanes from left: (**A**) *E. faecalis* IreK kinase domain, (**B**) *E. faecium* IreK kinase domain, (**C**) *C. difficile* eSTK kinase domain, (**D**) *E. faecalis* ADP binding site kinase M mutant, A mutant and F mutant.

As exhibited by **figure 25ABC**, all six kinase domains are phosphorylated during expression in *E. coli* which was initially unexpected. It is entirely conceivable that the unregulated kinase domains autophosphorylate themselves when expressed recombinantly in *E. coli* or are perhaps are being phosphorylated by another kinase present in *E. coli*. To note, in the protein ladder used in all figures using the Pro-Q diamond stain, there is a phosphorylated protein, Ovalbumin, which is used as a positive phosphorylation control at 45 kDa. The Coomassie blue staining performed after Pro-Q Diamond staining is used to prove the presence of total protein, this is the case for all Pro-Q Diamond staining. It is worth noting, that the ADP binding site mutants have a several bands corresponding to impurities which were mentioned in **3.3.5** on how to remove them if required. With the knowledge that the kinase domains were already phosphorylated following expression in *E. coli*, the next logical course was to investigate methods of dephosphorylation should the comparison between phosphorylated and dephosphorylated protein be required in future experiments.

4.3 Optimisation of dephosphorylation of kinase domains

The combination of staining methods using Coomassie blue and Pro-Q Diamond allow the detection of dephosphorylated protein. All three of the primary kinase domains were tested to whether they could be dephosphorylated using either IreP (IreK cognate phosphatase from *E. faecalis*, purified by (Thoroughgood, 2018)) or Lambda protein phosphatase (NEB) (Mn2+-dependent protein phosphatase, Lambda PP, targeting phosphorylated serine, threonine and tyrosine residues). Firstly, kinase domains from *E. faecalis* and *E. faecium* were reacted with both phosphatases (**figure 26A**). Both kinases were dephosphorylated to a degree, IreP was most effective with minimal phosphorylation fluorescence detected. Lambda PP was less effective in dephosphorylating *E. faecalis* IreK especially with around 30 % phosphorylation fluorescence residue remaining (**figure 26B**).

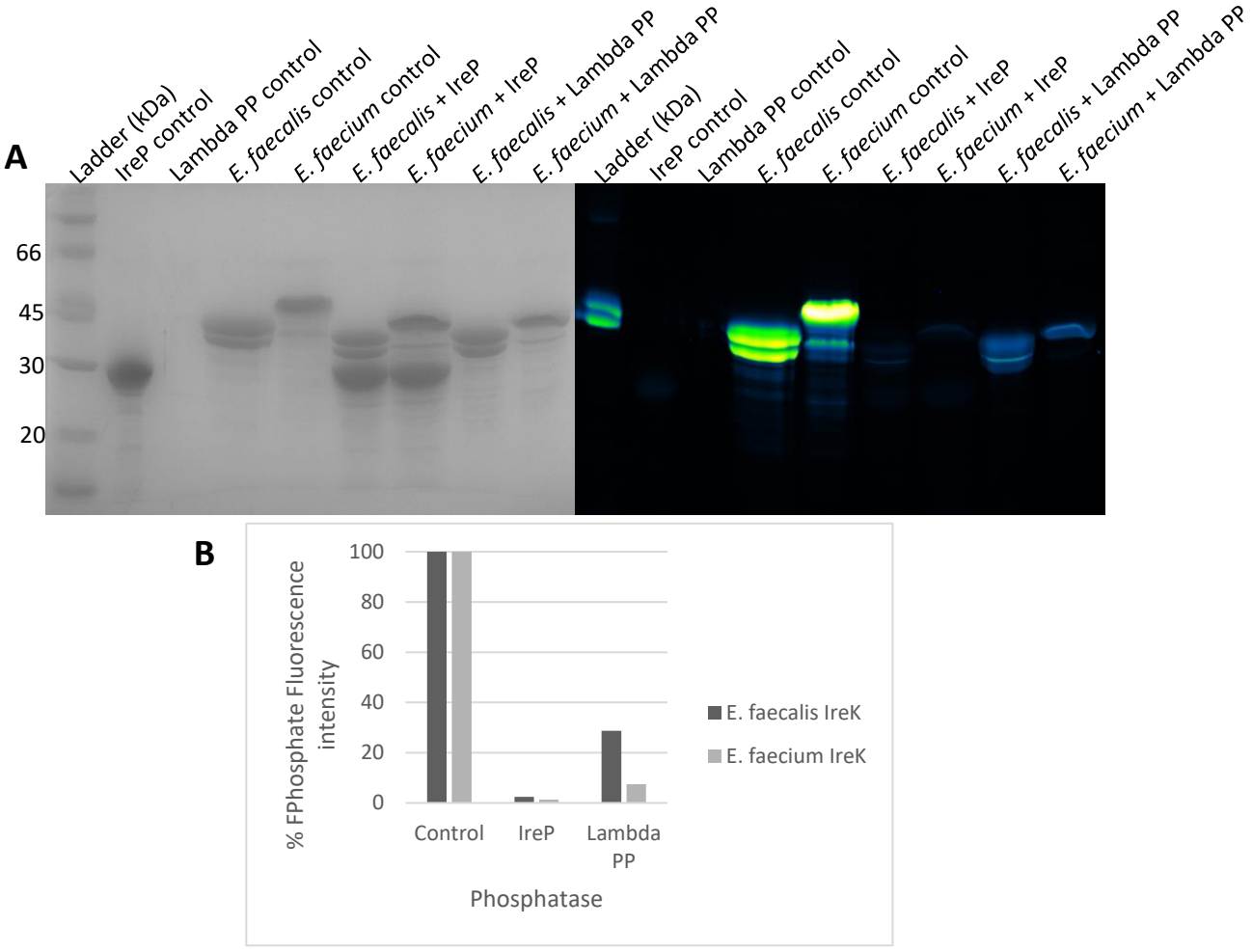

Figure 26: Optimisation of Phosphatase activity of IreP and Lambda phosphatase on phosphorylated IreK from *E. faecium* and *E. faecalis* on a 12% SDS-PAGE gel. Lanes left to right: (**A**) IreP control, Lambda PP control, phosphorylated *E. faecalis* IreK, phosphorylated *E. faecium* IreK, *E. faecalis* IreK + IreP, *E. faecium* IreK + IreP, *E. faecalis* IreK + Lambda PP, *E. faecium* IreK + Lambda PP. Coomassie blue (left) and Pro-Q stain analysis (right), (**B**) Quantification of the phosphatase assay in (**A**) where the data is compared to the phosphorylated control.

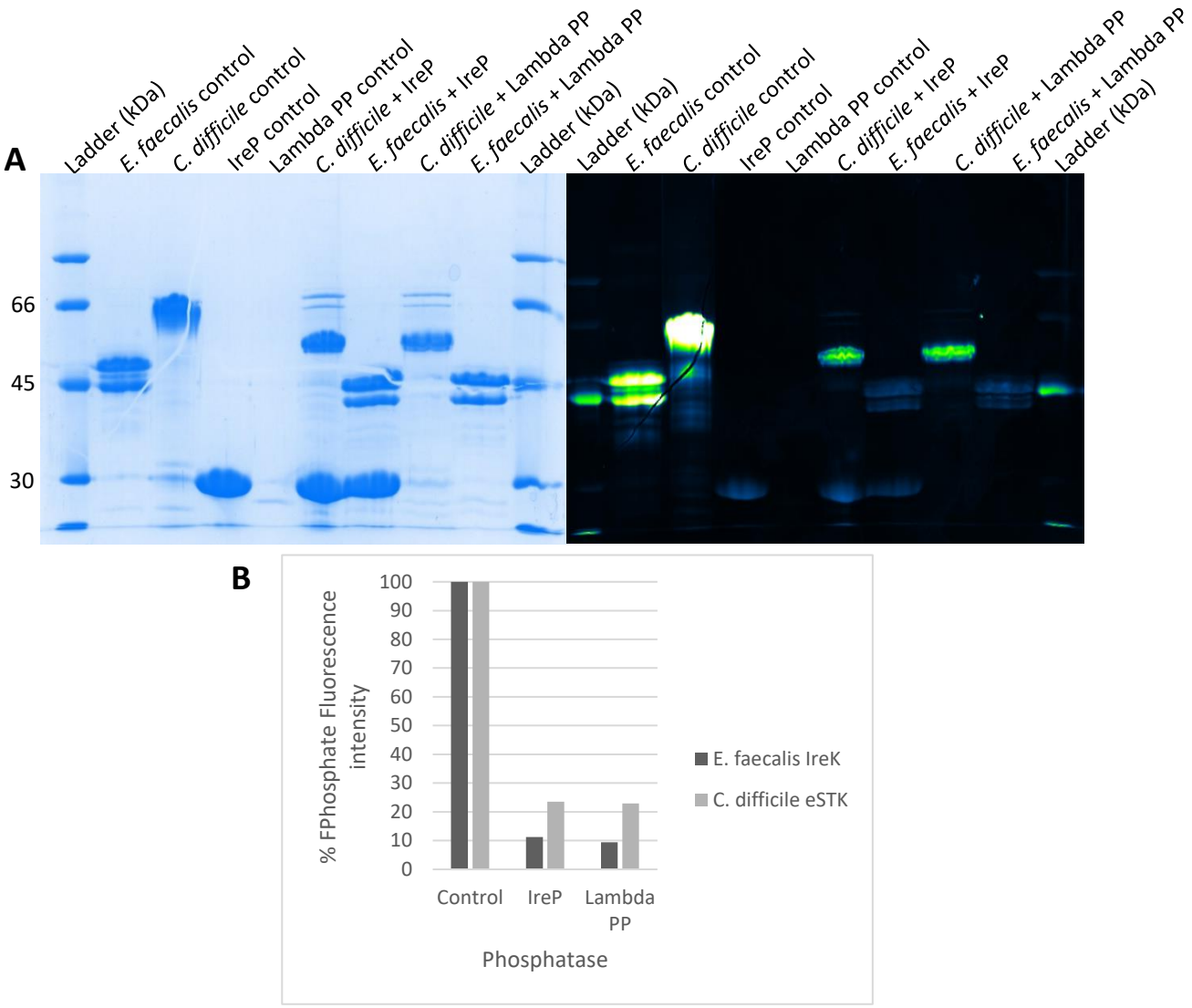

Figure 27: Optimisation of Phosphatase activity of IreP and Lambda phosphatase on phosphorylated IreK from *E. faecium* and eSTK kinase domain from *C. difficile* on a 12% SDS-PAGE gel. Lanes left to right: (**A**) IreP control, Lambda PP control, phosphorylated *E. faecalis* IreK, phosphorylated *C. difficile* eSTK, *E. faecalis* IreK + IreP, *C. difficile* eSTK + IreP, *E. faecalis* IreK + Lambda PP, *C. difficile* eSTK + Lambda PP. Coomassie blue (left) and Pro-Q stain analysis (right), (**B**) Quantification of the phosphatase assay in (**A**) where the data is compared to the phosphorylated control.

Following the successful dephosphorylation of *E. faecalis* and *E. faecium* kinase domains, the work could be repeated with *C. difficile*. The dephosphorylation of the *C. difficile* kinase domain by either IreP and Lambda PP was compared against an *E. faecalis* IreK control. As expected, IreP and Lambda PP mostly dephosphorylated IreK, with around 10 % fluorescence remaining, however this was not the case with *C. difficile.* Both phosphatases had a similar effect with around 25 % phosphorylation fluorescence remaining. The eSTK kinase domain appeared to have been partially dephosphorylated to produce a reduced fluorescence single band around 55 kDa, from the original 66 kDa. This may have occurred for several possible reasons: firstly, this kinase may have a greater number of phosphorylation sites compared to the *Enterococci* kinase domains, secondly, these phosphorylation sites maybe in a site(s) that are poorly recognised by either IreP or Lambda PP. Finally, it is entirely possible that the dephosphorylation reaction may need to be optimised under different conditions to the other kinases for maximum phosphatase activity. These reactions led to the optimisation of the dephosphorylation reaction. The original reaction was for 30 minutes at 30 °C. The conditions of future reactions were changed to 1 hour at 30 °C.

4.4 Native protein conformation analysis

As described in section **1.5.3.2**, eukaryotic-like serine threonine kinase domains activate by dimerisation and autophosphorylation. Oligomerisation of the kinase domains of eSTKs is assumed to occur however the effect of phosphorylation on this oligomerisation activity has not been explored. For a preliminary view on the effect of phosphorylation on oligomerisation, native-PAGE analysis (**2.6.4**) was performed to visualise the native conformations of the kinase domains. This method can also be used with Coomassie blue and Pro-Q Diamond staining for optimum identification of phosphorylated and dephosphorylated proteins. All three of the primary kinase domains were incubated with IreP and run on an SDS free acrylamide gel (**figure 28**).

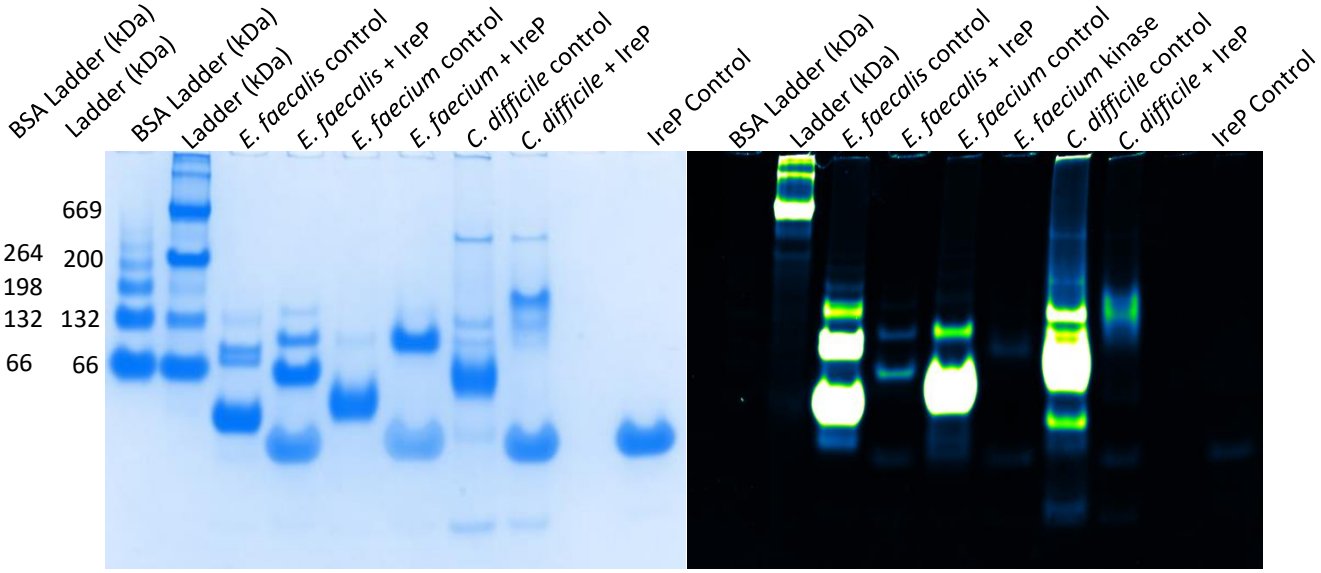

Figure 28: Effect of phosphorylation of the oligomerisation of kinase domains. Lanes left to right: (**A**) IreP control, Lambda PP control, phosphorylated *E. faecalis* IreK, *E. faecalis* IreK + IreP, phosphorylated *E. faecium* IreK, *E. faecium* IreK + IreP, phosphorylated *C. difficile* eSTK, *C. difficile* eSTK + IreP, IreP control. Coomassie blue (left) and Pro-Q stain analysis (right).

The protein ladders used included Bovine Serum albumin (BSA), which is known to form oligomers at high concentrations. The first information obtained from this assay is that all three kinases reside primarily in their monomeric form, indicated by the large bands at the bottom of the control lanes. There are however smaller bands present indicating possible dimer and trimer forms. All forms of the kinases are phosphorylated however. The effect of dephosphorylation on the oligomerisation appears minimal. All the kinases run slower on the gel due to a reduced charge from fewer phosphate groups. The oligomerisation does remain after dephosphorylation indicating that phosphorylation does not control this process. The *E. faecalis* and *C. difficile* kinases seem to be majority dephosphorylated but still produce a fluorescent signal indicating that the dephosphorylation reaction should be further optimised for greater concentrations of protein required for Native-PAGE analysis. The conditions of future reactions were changed to 1.5 hours at 30 °C with gentle shaking at 350 RPM to try and improve dephosphorylation efficiency.

4.5 Identification of phosphorylation sites of *C. difficile* eSTK

The kinase domains of eSTKs from have limited information regarding their autophosphorylation site. The autophosphorylation sites of the kinase domain of *C. difficile* have yet to be characterised. Considering this is the first time this eSTK kinase domain has been expressed and purified, it was the main target to investigate with the limited time of the project. Using electrospray ionisation mass spectrometry, a preliminary analysis of phosphorylated *C. difficile* kinase domain sites of phosphorylation was performed (**figure 29**).

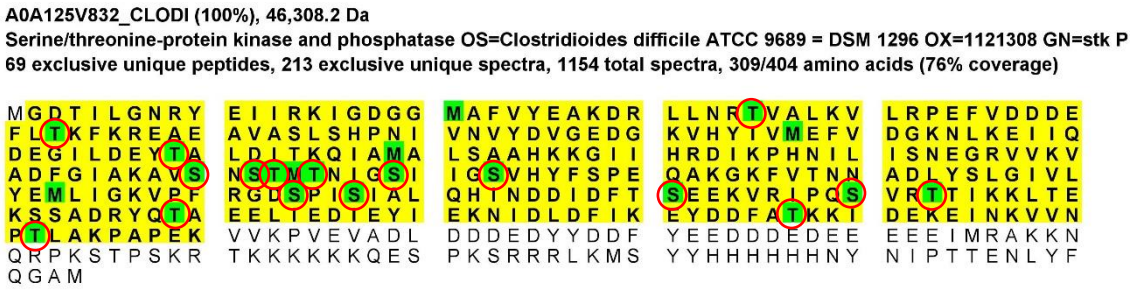

Figure 29: Scaffold analysis of mass spectrometry data from the *C. difficile* kinase domain. Yellow indicates fragment coverage of the eSTK protein sequence. Green highlights are modified residues with either phosphorylation (red circle) and oxidation (no circle).

Although the data only covers 76 % of the *C. difficile* kinase domain protein sequence, the information does suggest multiple phosphorylation sites, up to 17 residues. All red circled residues were detected as phosphorylated. As is the case of eSTKs, only serine and threonine residues were phosphorylated. Which resides are primary sites of phosphorylation required for kinase function are unknown and some could be secondary phosphorylation as a result from expression in *E. coli*. For a quantitative residue phosphorylation analysis, fully dephosphorylated kinase domain could be used as a control for a comparison to autophosphorylated kinase. Additionally, this analysis was only performed once, requiring further replicates to make clearer interpretations.

4.6 Discussion and future work

This chapter discussed the characterisation of phosphorylation in the eSTK kinase domains of *E. faecalis*, *E. faecium* and *C. difficile*. The Pro-Q Diamond phosphate staining technique was used to determine that all three kinases were fully phosphorylated during expression in *E. coli*. The cause of this could be due to a kinase present in *E. coli* targeting the eSTK kinase domains or the activation and autophosphorylation of the domains alone. Should the kinases be acting alone, it would indicate that these domains are not reliant on the extracellular PASTA domains to promote activation and autophosphorylation. The sites of which have become phosphorylated however may not be the same residues in normal wild-type expression. This suggests that as part of the purification process, all purified kinase should be dephosphorylated to ensure the biological relevance of further experiments.

The dephosphorylation of IreK by IreP was been previously achieved (Kristich et al., 2011; Thoroughgood, 2018) and has been successfully recreated in this work using Pro-Q Diamond staining for analysis. This work expanded the work however to exploring the dephosphorylation of *C. difficile* eSTK kinase domain and using a general serine/threonine/tyrosine phosphatase; Lambda PP (NEB). Firstly, Lambda PP had a reduced dephosphorylation activity compared to IreP across all kinase domains, due to its non-specific activity. Secondly, only partial dephosphorylation of *C. difficile* was achieved, requiring further optimisation of this reaction in the future. Interestingly, both IreP and Lambda appeared to have similar effects on *C. difficile* KD, indicating the structure of the kinase to contain more and/or harder to access phosphorylation sites than its *E. faecalis* and *E. faecium* KD counterparts.

This led to mass spectrometry analysis of the *C. difficile* KD. The data suggested that 17 or more residues were phosphorylated in the phosphorylated kinase out of *E. coli* expression. Although, without a direct comparison between dephosphorylated *C. difficile* KD and the kinases from the other two strains, no clear conclusion can be drawn. Further investigation would involve mass spectrometry repeats using dephosphorylated kinases from all three strains as a control to compare against the phosphorylated kinases. This would help quantify the phosphorylation sites between the kinases for a clear comparison, and possibly hint to key activation residues involved in signalling cascades.

The current dogma in the literature is that dimerisation of the eSTK kinase domains is essential for their activation and autophosphorylation activity. To investigate this with the bacterial eSTK kinase domains, the successful dephosphorylation activity of IreP was then redeployed to investigate the effects of dephosphorylation of the kinase domains. The Native-PAGE analysis indicated minimal difference in oligomerisation of the kinase domains of all three strains aside from changing the speed which the proteins ran on the gel, an effect of the lost phosphate groups. The native conformation analysis indicates that autophosphorylation activity does not appear to affect the oligomerisation of the kinase domains and they mostly residue in their monomeric form. This could indicate that the dimerisation is not a consequence of the phosphorylation status, however repeats and full dephosphorylation of the kinase domains are required for a clearer interpretation along with an orthogonal method of analysis. Further analysis on the kinase domain oligomerisation could include analytical gel filtration to determine the abundance of each oligomer or analytical centrifugation analysis which would provide information on native molecular weight in solution independent of gel or chromatography matrix interactions.

5.0 Results and discussion chapter 3: Kinase inhibitor binding and effect of kinase autophosphorylation activity

5.1 Introduction

This work in this chapter is to characterise the autophosphorylation activity of *E. faecalis* IreK and its phenylalanine ADP binding site mutant and the effect of Staurosporine on this activity. This was followed up by microscale thermophoresis to examine the binding affinity of Staurosporine on *E. faecalis* IreK. Lastly, the *in vivo* effect of Staurosporine on Cephalosporin resistance in *C. difficile* is also investigated this is chapter. Unfortunately, due to time constraints of the project, the other purified kinases were not investigated in said experiments. The work on Staurosporine and its effect on IreK is a continuation of work performed in (Thoroughgood, 2018).

5.2 *E. faecalis* IreK kinase domain

As the all the kinases were found to be already phosphorylated during expression in *E. coli* (**4.2**), the dephosphorylation reaction required to be optimised and a method devised to remove the phosphatase to leave a purified dephosphorylated kinase in solution. Firstly, the phosphatase was chosen; Lambda PP was used as although it was less efficient than IreP, it does not contain a His-tag, and could therefore be removed from IreK after the dephosphorylation reaction. As described in **2.7.3**, nickel Sepharose beads were used to purify out the Lambda PP after the dephosphorylation reaction with *E. faecalis* IreK. The dephosphorylation control of **figure 30** shows the successful dephosphorylation of IreK using Lambda PP.

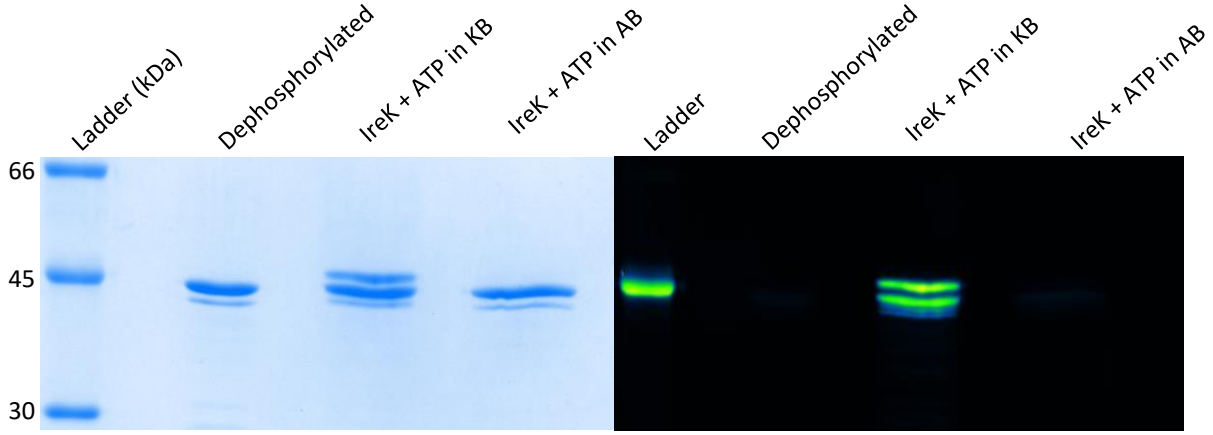

Figure 30: Optimisation of dephosphorylation, purification and autophosphorylation of IreK (*E.faecalis*) on a 12 % SDS-PAGE gel stained with Coomassie blue (top) and Pro-Q Diamond Phosphate stain (bottom). Reactions used 50 µM IreK in 10 µl at 37 °C. Lanes from left to right: Dephosphorylated IreK control, IreK + 1 mM ATP in kinase buffer incubated for 30 min, IreK + 1 mM ATP in assay buffer incubated for 30 min. Ladder contains phosphorylated protein Ovalbumin as a control.

The autophosphorylation buffer was the second optimisation to perform to prove the activity of the kinase domain IreK. There were two buffers tested, an assay buffer for general kinase activity and a kinase buffer adapted from (Goss, 2013) (**table 6**). The kinase buffer was successful in facilitating the autophosphorylation of IreK in the presence of 1 mM ATP (**figure 30**). The rate of autophosphorylation was the next question to investigate. By using the same kinase buffer as before but using timepoints up to 30 minutes with 25 µM of IreK in 10 µl reactions, an autophosphorylation time course was constructed (**figure 31**).

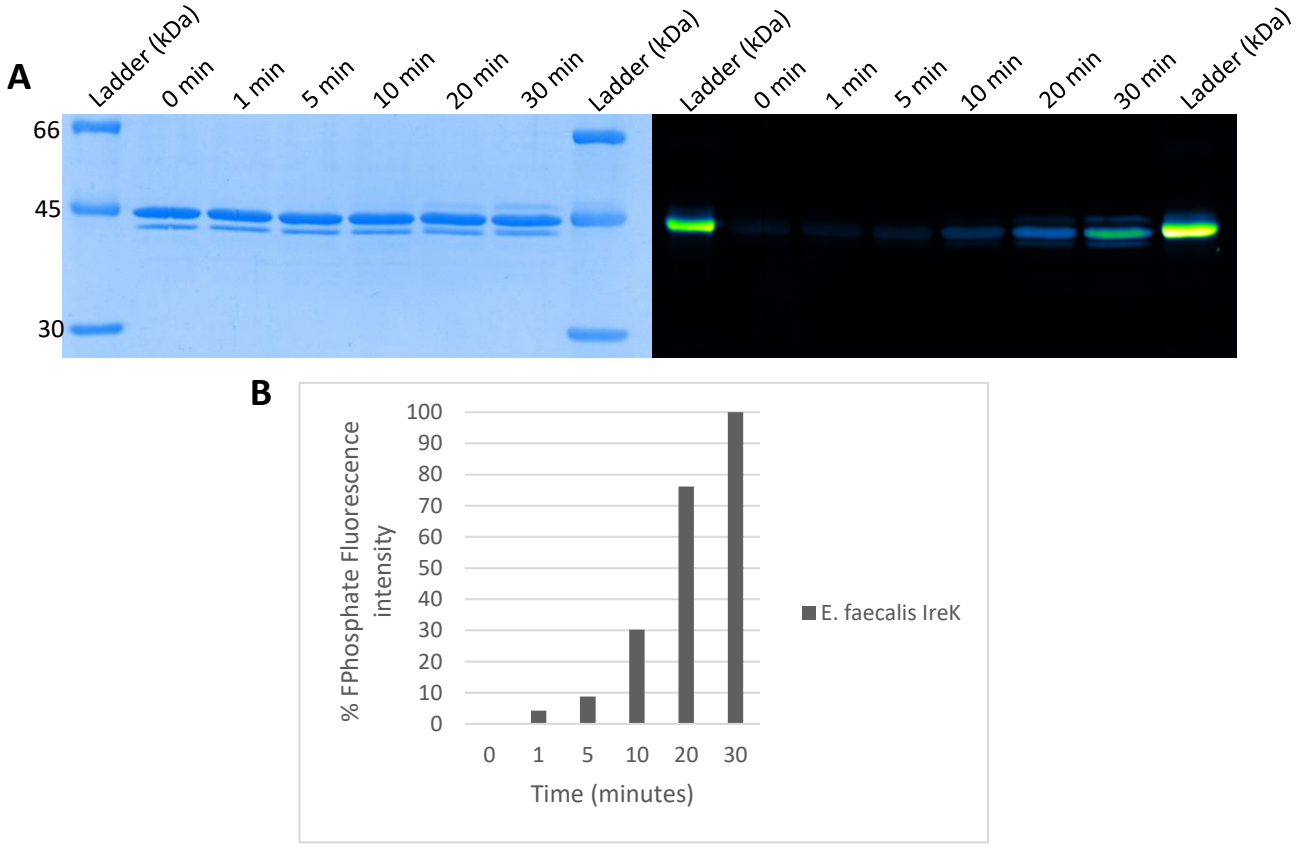

Figure 31: Kinase autophosphorylation assay of dephosphorylated IreK (*E.faecalis*) on a 12 % SDS-PAGE gel stained with Coomassie blue (top) and Pro-Q Diamond Phosphate stain (bottom). All reactions were performed at 37 °C with 25 µM IreK in 10 µl reactions. Lanes left to right: Dephosphorylated IreK control, IreK + 1 mM ATP incubated for 1, 5, 10, 20 and 30 min. Ladder contains phosphorylated protein Ovalbumin as a control. (**A**) Coomassie blue (left) and Pro-Q stain analysis (right), (**B**) Quantification of the phosphatase assay in (**A**) where the data is normalised to the 30-minute phosphorylation maximum

Although there is a clear increase in phosphorylation fluorescence up to 30 minutes, upon visual examination, the kinase does not become fully phosphorylated, indicating a longer incubation time is required. Fluorescence intensity analysis indicated rapid increase in phosphorylation after 20 minutes onwards further indicating a longer incubation time. The assay however had shown that the recombinant IreK had active autophosphorylation activity. The reaction was repeated with incubation time up to 1 hour (**figure 32**).

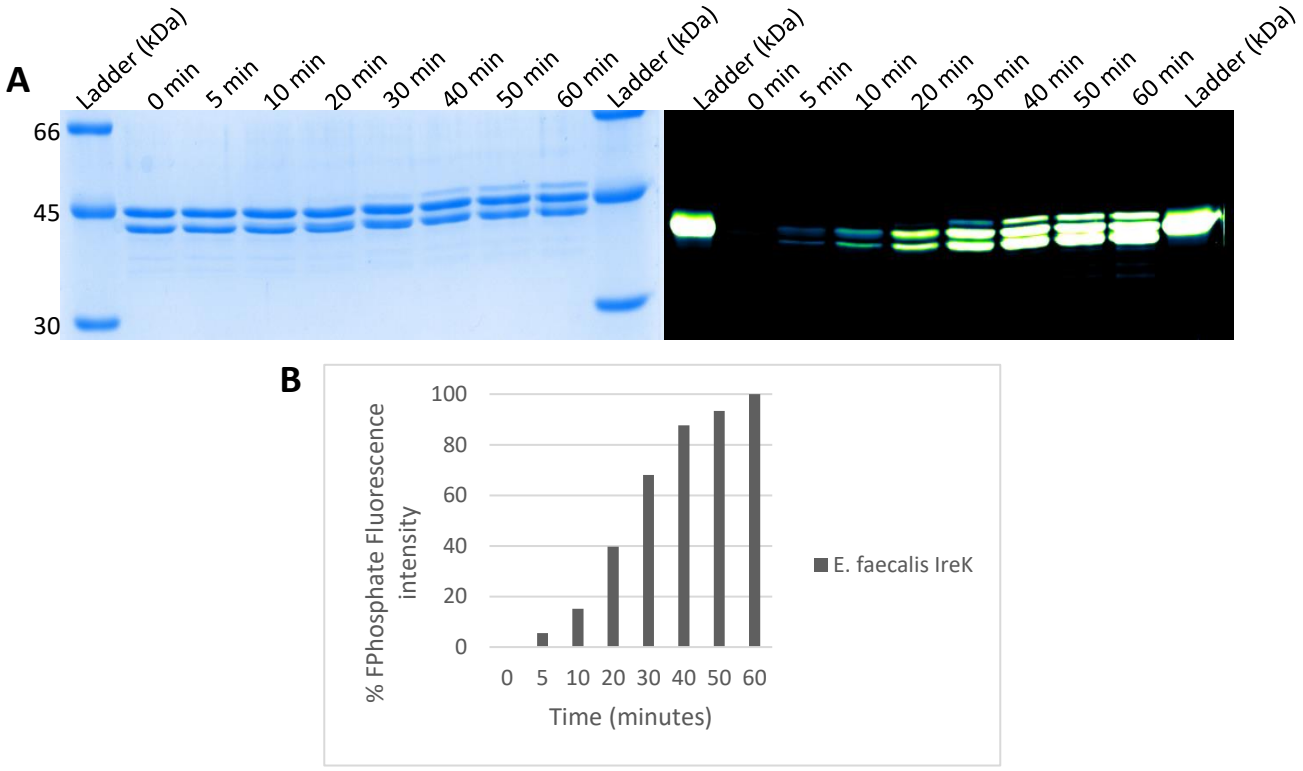

Figure 32: Kinase autophosphorylation assay of dephosphorylated IreK (*E.faecalis*) on a 12 % SDS-PAGE gel stained with Coomassie blue (top) and Pro-Q Diamond Phosphate stain (bottom). All reactions were performed at 37 °C with 25 µM IreK in 10 µl reactions. Lanes left to right: Dephosphorylated IreK control, IreK + 1 mM ATP incubated for 5, 10, 20, 30, 40, 50 and 30 min. Ladder contains phosphorylated protein Ovalbumin as a control. (**A**) Coomassie blue (left) and Pro-Q stain analysis (right), (**B**) Quantification of the phosphatase assay in (**A**) where the data is normalised to the 60-minute phosphorylation maximum and dephosphorylation control minimum.

The longer incubation times were required for full phosphorylation of IreK with 1 hour at the highest phosphorylation fluorescence. A single band appears above the original two IreK bands because of autophosphorylation. Fluorescence analysis shows that autophosphorylation begins to reach its maximum after 40 minutes. The two protein bands could however be IreK in a partially degraded state hence the two major bands present in both stain images in **figure 32**. The work here preliminarily characterises autophosphorylation which led the work onto the effect of kinase inhibitors on the effect of this phosphorylation activity

5.3 Effect of Staurosporine on autophosphorylation of *E. faecalis* IreK kinase domain

As previously mentioned (**1.5.3.7**), Staurosporine is a kinase inhibitor which prevents ATP binding and has an ATP-competitive inhibitory action. The inhibitor has a stronger affinity to the ADP-binding sites of kinases compared to ATP (Tanramluk et al., 2009). It is therefore an interesting inhibitor to use against the autophosphorylation activity of IreK. The effect of Staurosporine was determined against the autophosphorylation activity of dephosphorylated IreK kinase domain. The initial test involved incubating 50 mM Staurosporine for 15 minutes then repeating the ATP autophosphorylation reaction up to 30 minutes (**figure 33**).

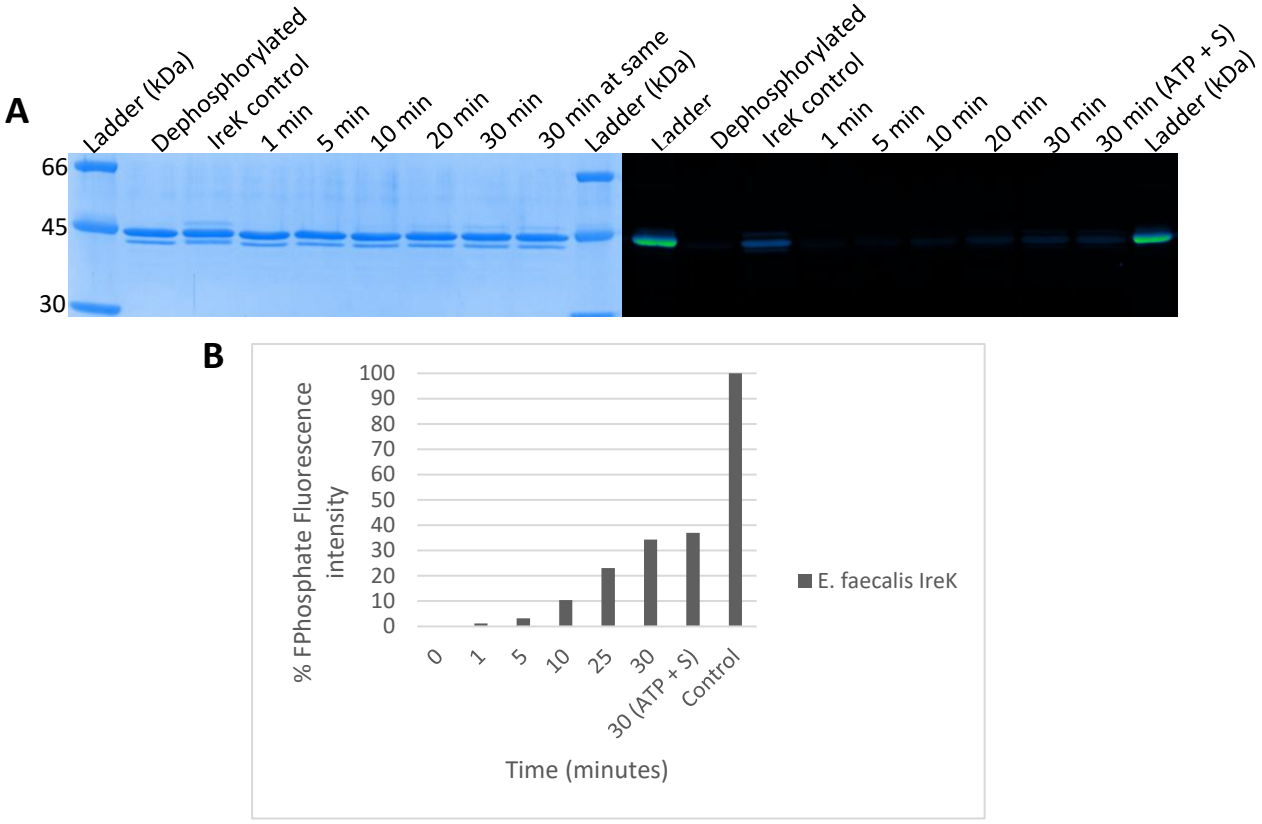

Figure 33: Effect of Staurosporine on kinase autophosphorylation of dephosphorylated IreK (*E. faecalis*) on a 12 % SDS-PAGE gel stained with Coomassie blue (top) and Pro-Q Diamond Phosphate stain (bottom). All reactions were performed at 37 °C with 25 µM IreK in 10 µl reactions. Lanes left to right: Dephosphorylated IreK control, Autophosphorylation IreK DMSO control, IreK + 50 µM Staurosporine for 15 min then incubated with 1 mM ATP for 1, 5, 10, 20, 30 min and 30 min (with inhibitor added at the same time. (**A**) Coomassie blue (left) and Pro-Q stain analysis (right), (**B**) Quantification of the phosphatase assay in (**A**) where the data is normalised to the 30-minute phosphorylation control maximum and dephosphorylation control minimum.

The fluorescence signals of all lanes were less clear in this assay. In comparison to **figure 32**, Staurosporine has decreased the autophosphorylation activity of IreK with minimal phosphorylated kinase present at the 30-minute mark. The incubation of IreK with Staurosporine reduced the phosphorylation signal by over 50 % in the fluorescence analysis suggesting that the inhibitor is decreasing the efficiency of IreK autophosphorylation activity. It is also worth noting that adding the inhibitor at the same time as ATP had no significant difference compared to the 15-minute pre-incubation. This is expected for an ATP-competitive inhibitor as it competes for the ATP active site. For a clearer interpretation of the effect of Staurosporine, the ATP incubation time was increased to 1 hour for increased fluorescent signal in **figure 34**. This assay investigated the effect of increasing concentration of Staurosporine after 1 hour of ATP incubation.

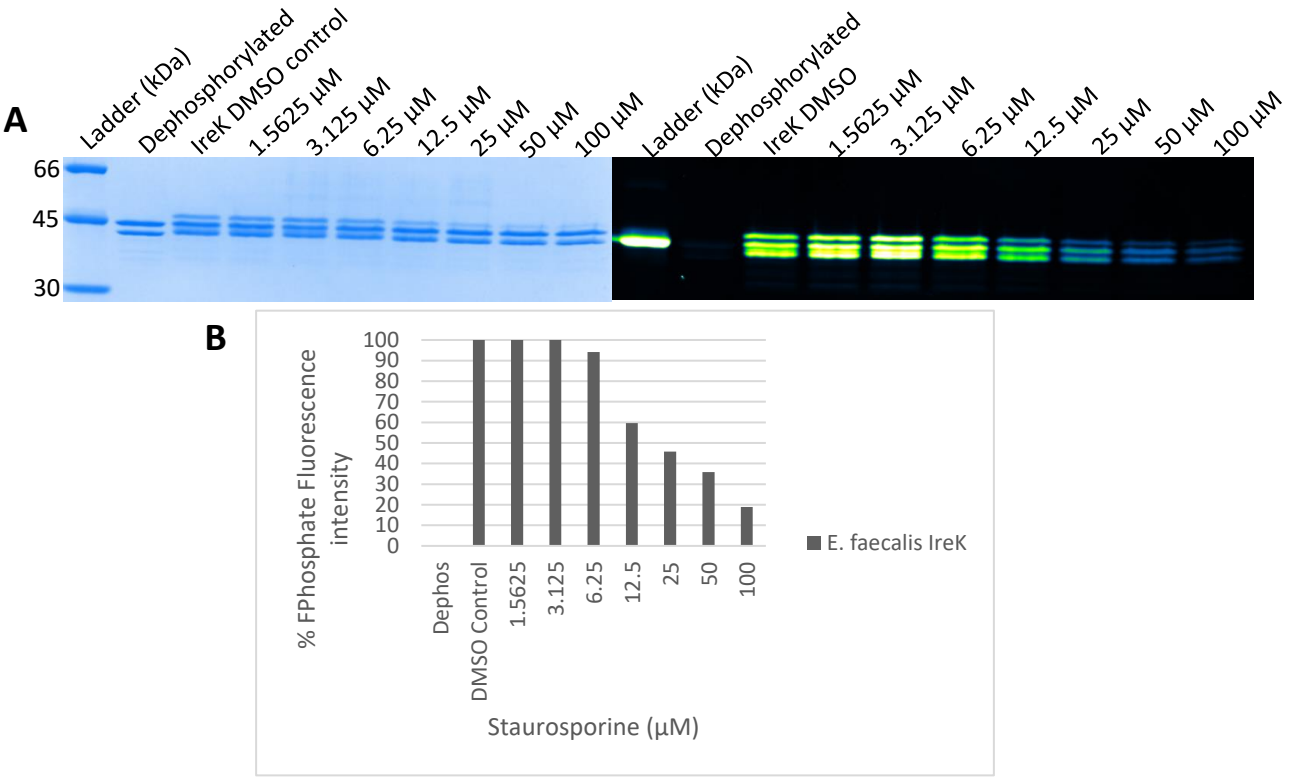

Figure 34: Effect of Staurosporine on kinase autophosphorylation of dephosphorylated IreK (*E.faecalis*) on a 12 % SDS-PAGE gel stained with Coomassie blue (top) and Pro-Q Diamond Phosphate stain (bottom). All reactions were performed at 37 °C with 25 µM IreK in 10 µl reactions. Lanes left to right: Dephosphorylated IreK control, Autophosphorylation IreK DMSO control, IreK + 1.5625, 3.125, 6.25, 12.5, 25, 50 and 100 µM Staurosporine for 15 min then incubated with 1 mM ATP for 1 hour respectively. (**A**) Coomassie blue (left) and Pro-Q stain analysis (right), (**B**) Quantification of the phosphatase assay in (**A**) where the data is normalised to the 1-hour phosphorylation control maximum and dephosphorylation control minimum.

As Staurosporine is suspended in DMSO, an Irek DMSO control was performed to determine any impact that DMSO has on the autophosphorylation activity of IreK. There appeared to be no detectable effect of DMSO on IreK activity, indicated by strong fluorescence in **figure 34** DMSO control. As expected, Staurosporine increases its inhibitory effect as the concentration increases, resulting in a steady decrease in fluorescence signal. This effect is clearly shown in the fluorescence analysis where the lowest concentration of inhibitor has no noticeable effect but from there the increasing concentration brings the signal down to below 20 % at 100 µM compared to the DMSO control. Even at 100 µM however, there is still some phosphorylation detected, perhaps due to unspecific phosphorylation on secondary sites.

5.4 Effect of Staurosporine on *E. faecalis* IreK phenylalanine ADP binding site mutant autophosphorylation activity

To further investigate where Staurosporine binds to IreK, the most sterically hindered ADP binding site mutant of IreK has a phenylalanine residue in the ADP binding site. By repeating the previous autophosphorylation and inhibitor binding studies, the effect of a modified ADP binding site can be explored.

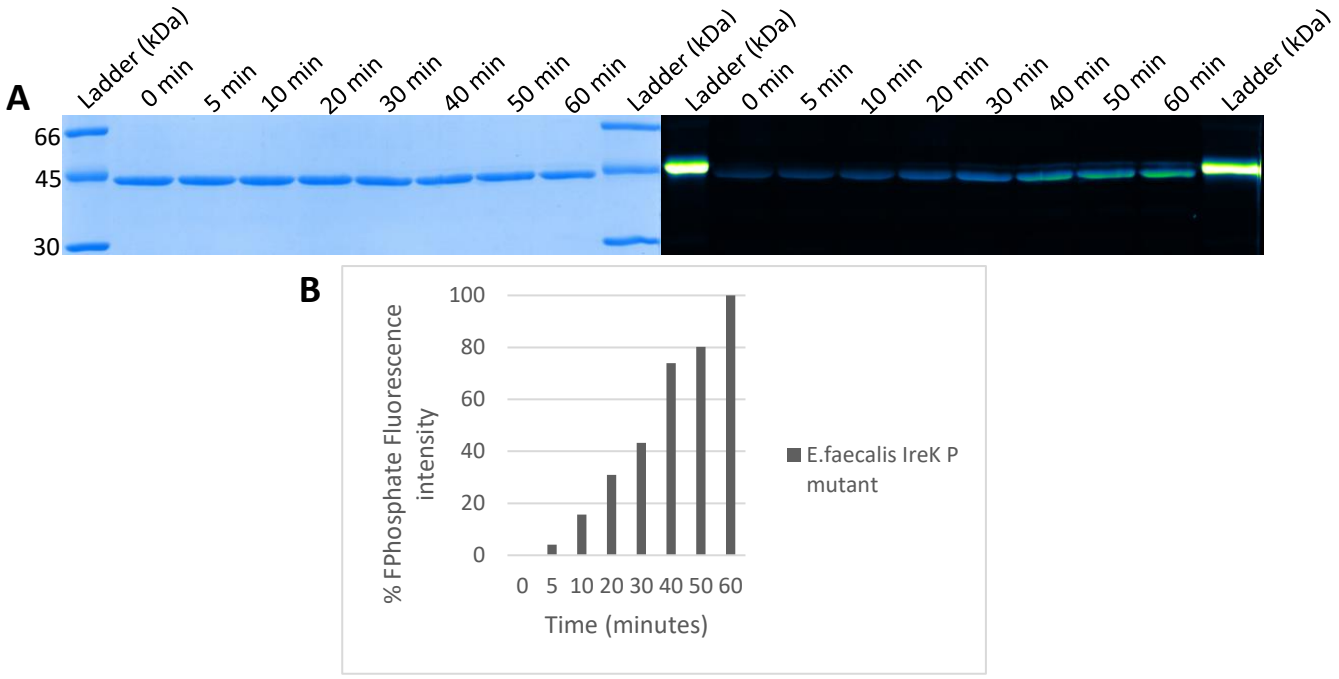

Figure 35: Kinase autophosphorylation assay of dephosphorylated ADP binding site phenylalanine mutant IreK (*E.faecalis*) on a 12 % SDS-PAGE gel stained with Coomassie blue (top) and Pro-Q Diamond Phosphate stain (bottom). All reactions were performed at 37 °C with 25 µM IreK mutant in 10 µl reactions. Lanes left to right: Dephosphorylated P mutant IreK control, IreK P mutant + 1 mM ATP incubated for 5, 10, 20, 30, 40, 50 and 30 min. Ladder contains phosphorylated protein Ovalbumin as a control. (**A**) Coomassie blue (left) and Pro-Q stain analysis (right), (**B**) Quantification of the phosphatase assay in (**A**) where the data is normalised to the 60-minute phosphorylation maximum and dephosphorylation control minimum.

The P mutant of IreK has retained its autophosphorylation activity with phosphate fluorescence increasing over time (**figure 35**). The rate of autophosphorylation appears to be slower in comparison to wild type with fluorescence analysis showing a delayed increase in phosphorylation at 40 and 50-minute incubation times compared to **figure 35B**. Considering the steric hinderance of a phenylalanine residue, this result was expected. A direct comparison between the wild type and this mutant would provide a clearer interpretation on the effect of the mutation.

By using the autophosphorylation time course of the P mutant as a control, a concentration dependent effect of Staurosporine could be examined (**figure 36**). During visual examination, the effect of Staurosporine has been reduced, requiring a higher concentration to cause a significant change in fluorescence.

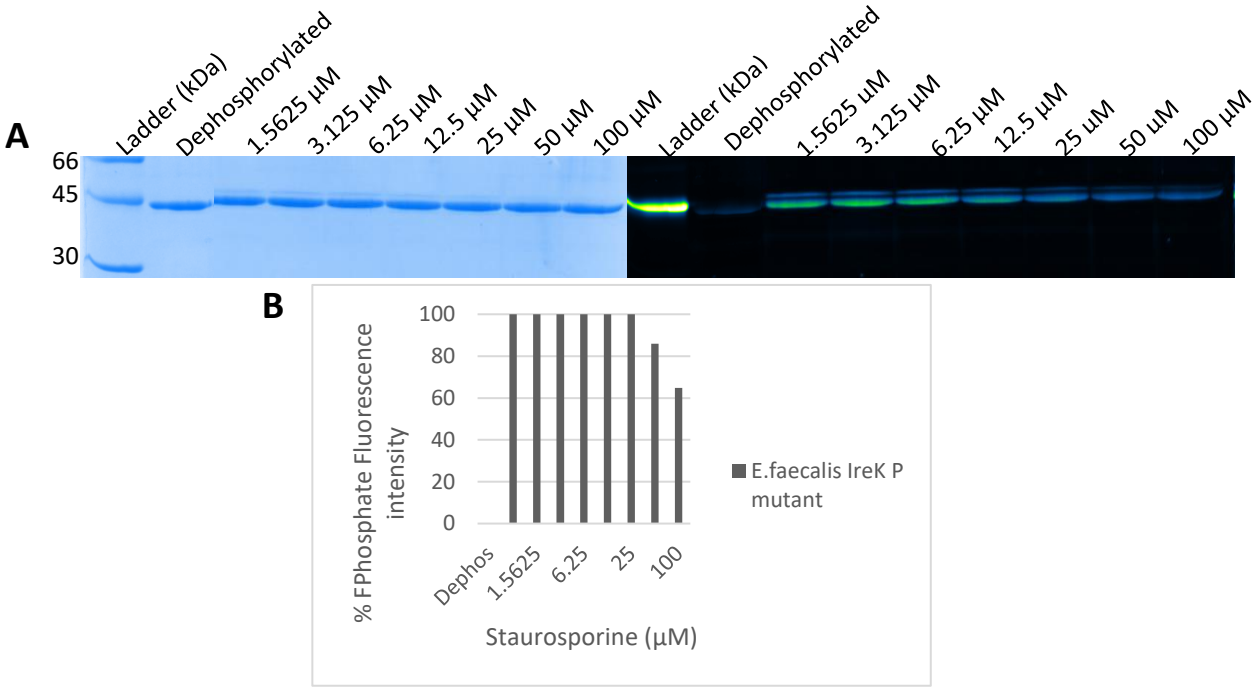

Figure 36: Effect of Staurosporine on kinase autophosphorylation of dephosphorylated ADP binding site phenylalanine mutant IreK (*E.faecalis*) on a 12 % SDS-PAGE gel stained with Coomassie blue (top) and Pro-Q Diamond Phosphate stain (bottom). All reactions were performed at 37 °C with 25 µM IreK mutant in 10 µl reactions. Lanes left to right: Dephosphorylated IreK control, P mutant IreK + 1.5625, 3.125, 6.25, 12.5, 25, 50 and 100 µM Staurosporine for 15 min then incubated with 1 mM ATP for 1 hour respectively. (**A**) Coomassie blue (left) and Pro-Q stain analysis (right), (**B**) Quantification of the phosphatase assay in (**A**) where the data is normalised to the 1-hour phosphorylation control maximum

This is supported by fluorescence analysis which indicates that a decrease in autophosphorylation occurs only after 50 µM or higher of inhibitor was added. Unfortunately, a DMSO control was not performed in this experiment due to time constraint and human error, therefore fluorescence analysis was performed using the 60-minute maximum from **figure 35**. Aside from this, the assay indicated that the steric hinderance caused by the phenylalanine present in the ADP binding site possibly blocked Staurosporine binding allowing the smaller ATP molecule to react to the binding site.

5.5 Binding affinities of Staurosporine to *E. faecalis* IreK

To investigate the binding of Staurosporine to *E. faecalis* IreK, a set of binding studies were performed to determine the dissociation constant using microscale thermophoresis (**2.8.1**). The experiments were performed in duplicate. To minimise variation between results, capillary scans (**figure 44**, appendix) were performed to detect ligand induced fluorescence changes and variation between capillaries produced by the protein dye. The variation detected was within 10 % which is acceptable in these types of experiments.

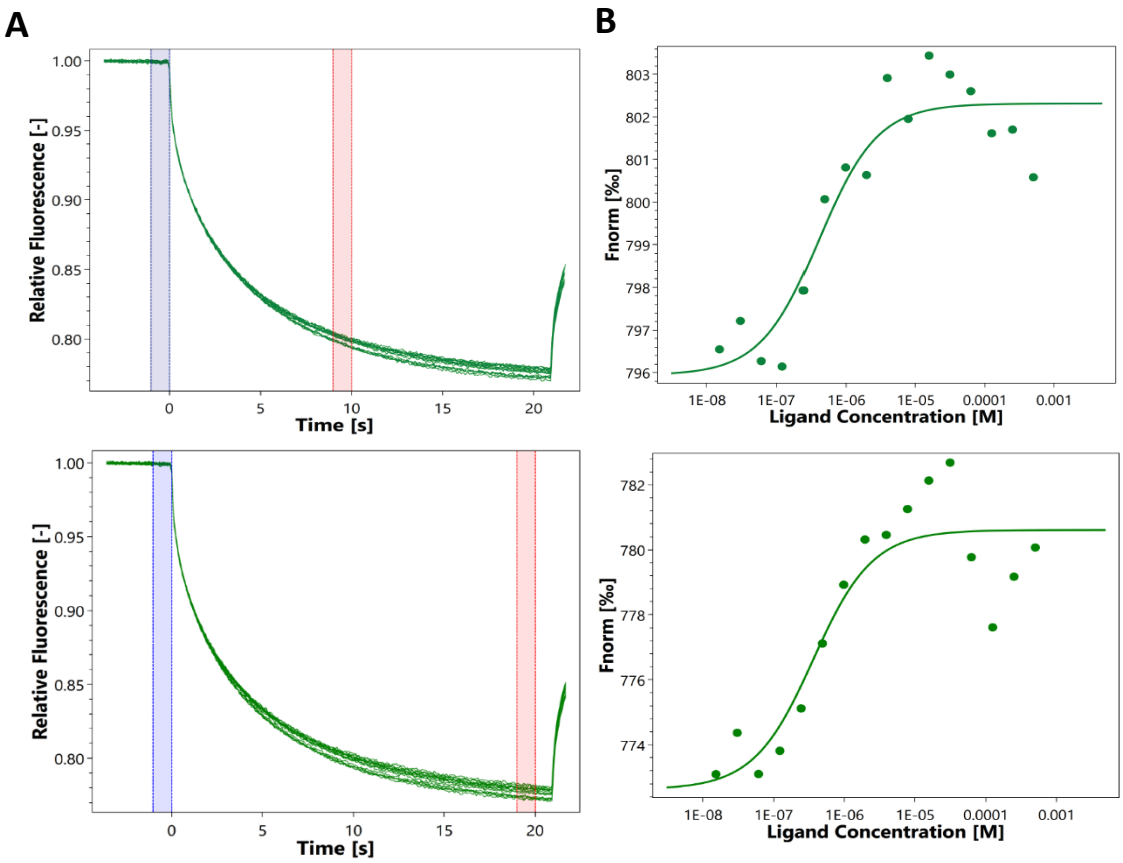

Figure 37: Staurosporine binding affinities to *E. faecalis* detected by microscale thermophoresis. (**A**) MST traces detecting the movement of dyed protein away from the projected heat source. (**B**) Dose response curves fitted with the Kd model, top right is taken from 10 seconds in the first replicate and top left is taken from time 20 seconds in the second replicate. Ligand is Staurosporine. The dose response Y-axis is normalised by dividing the fluorescence by the amplitude in the binding curve.

In both reactions, 50 nM *E. faecalis* phosphorylated IreK was incubated with 0.5 mM Staurosporine. The MST traces both exhibit no aggregation of the protein and no ligand induced photobleaching rate change. The dose response curves had acceptable signal to noise ratios. The average Kd of Staurosporine binding to IreK from both replicates was calculated to be 359 nM. The inhibitor therefore has a very strong binding affinity for IreK, in the ADP binding site which is expected of an ATP-competitive kinase inhibitor. This activity supports the inhibitory effect of Staurosporine on the autophosphorylation of *E. faecalis* IreK. The reduced inhibitory effect of the inhibitor on the phenylalanine ADP binding site mutant of IreK is also supported by this low Kd, further binding experiments using this mutant would however be required to fully deduce the effect of the mutation.

5.6 Effect of Staurosporine on Clostridium difficile Cephalosporin Minimal inhibitory concentrations

All the Staurosporine inhibitor experiments thus far have been under *in vitro* conditions. It was previously discovered that IreK in *E. faecalis* and *E. faecium* regulates Cephalosporin resistance (Kristich et al., 2011). The effect of Staurosporine on Cephalosporin resistance *in vivo* in *E. faecalis* and *E. faecium* has also been previously documented in (Thoroughgood, 2018). The treated *Enterococci* exhibited a similar phenotype to knockout IreK mutants, sensitivity to Cephalosporin treatments. This work however has not been replicated in *C. difficile* to see whether the eSTKs in this bacterial pathogen regulates the intrinsic resistance to Cephalosporins.

Table 8: Minimum inhibitory concentration assay of *C. difficile* under Cephalosporin treatment. Assay performed with and without Staurosporine kinase inhibitor

***Clostridium difficile* Toxin A & B Strain**	**Minimal inhibitory concentrations using Cefotaxime (µg/ml)**
- Staurosporine	8
+ Staurosporine	0.03125

A minimum inhibitory concentration assay using Cefotaxime was performed on *C. difficile* in the presence of Staurosporine (**table 8**). In the absence of kinase inhibitor, the bacteria showed an intrinsic resistance to Cephalosporins with 8 µg/ml MIC. In the presence of Staurosporine however, the MIC decreases over 100-fold to 0.03125 µg/ml. This suggests that the kinase inhibitor is binding to a kinase which may regulate Cephalosporin resistance, possibly an eSTK. The inhibitor however could be binding to several kinases including those in two-component signalling systems. In addition, this experiment will need to be repeated further as it was only performed once due to time constraint and difficulty growing *C. difficile* in artificial anaerobic environments.

5.7 Discussion and future work

This chapter characterised the autophosphorylation activity of both *E. faecalis* IreK and its ADP binding site phenylalanine mutant. After adapting the kinase activity buffer from (Goss, 2013), a autophosphorylation time course was constructed. The time of 1 hour was determined to produce the highest phosphorylation state. Interestingly, as the incubation time increased, a third band appeared because of the autophosphorylation activity. The three protein bands produced could be three different phosphorylation states of the kinase, or perhaps phosphorylation of secondary sites. Without information on the exact residues becoming phosphorylated, it is difficult to interpret.

The autophosphorylation activity of the phenylalanine IreK is reduced compared to the wild-type. The steric hinderance of the large phenylalanine side chain, preventing ATP from binding effectively, could be the cause of this. This would also the explain the reduced effect Staurosporine on the autophosphorylation activity on the IreK mutant. The kinase inhibitor has a negative effect on both IreK constructs however the large structure of the inhibitor would have significant trouble fitting into the ADP binding site of the mutant. Should the inhibitory effect of this drug occur at the same level of activity *in vivo* it could significantly decrease the signalling efficiency of the eSTK. This is supported by the MIC experiments in (Thoroughgood, 2018) showing Staurosporine treatment significantly decreases the Cephalosporin resistance in *E. faecalis* and *E. faecium*. The inhibition of autophosphorylation of IreK kinase domain could be the cause of this phenotype. This is further supported by the nanomolar concentration Kd of Staurosporine binding found during microscale thermophoresis binding studies of wild-type *E. faecalis* IreK. Further evidence could be gathered from replicates of the Pro-Q Diamond staining autophosphorylation Staurosporine assays and binding assays on the IreK mutants. For an overview of the activities of eSTKs in other bacterial strains, the experiments in this chapter could be repeated using the *E. faecium* and *C. difficile* kinase domains.

As a preliminary investigation into the effect of Staurosporine on *C. difficile* Cephalosporin resistance, the MIC experiment in this chapter provided an insight into a possibly conserved mechanism. The 100-fold decrease in Cephalosporin resistance in *C. difficile* because of Staurosporine treatment could be the result of the inhibition of any number of important kinases which regulate Cephalosporin resistance mechanisms. The similar effect in *E. faecalis* and *E. faecium* however suggests a conserved eSTK regulation mechanism, however the effect of Staurosporine on the *C. difficile* eSTK kinase autophosphorylation activity and the binding affinities between the protein and inhibitor would have to be investigated.

6.0 Discussion and conclusions

This project was a preliminary expansion of previous work performed by (Goss, 2013; Thoroughgood, 2018) into further characterisation of the eSTK kinase domains from *E. faecalis* and *E. faecium* but also the first characterisation of the *C. difficile* eSTK kinase domains. The eukaryotic serine/threonine kinase signalling system has been documented to regulate a wide range of cellular processes including antibiotic resistances.

After the successful expression and purification of eSTK kinase domains from *E. faecalis*, *E. faecium* and *C. difficile*, several experiments characterised the domains in terms of phosphorylation and kinase activity. The *E. coli* overexpressed kinase domains were found to be already phosphorylated. These phosphorylated kinases were successfully dephosphorylated in IreK of *E. faecalis* and *E. faecium* IreK and partially dephosphorylated in *C. difficile* KD. The effect of dephosphorylation on the oligomerisation of the kinase domains was deemed minimal, indicating no effect of phosphorylation on the activation dimerisation of these kinases.

The ATP-competitive kinase inhibitor anti-cancer drug, Staurosporine, has clinically relevant effects on eSTKs and Cephalosporin resistance in Gram-positive bacteria. In this work it has been found to inhibit autophosphorylation activity in *E. faecalis* IreK with a reduced effect in a mutant of the ADP binding site. This negative effect of the drug can be explained by the high binding affinity to wild-type IreK. Previous MIC experiments in (Thoroughgood, 2018) indicated a significant decrease in Cephalosporin resistance in *E. faecalis* and *E. faecium* after Staurosporine treatment. The same occurrence is found in this work with *C. difficile* although these are only preliminary findings.

The work in this project can be expanded in multiple ways. Firstly, this project can be finalised by exploring the autophosphorylation activity and the inhibitory effect of Staurosporine in already purified *E. faecium* and *C. difficile* kinase domains. Followed by binding studies in both kinases exploring the dissociation constant with Staurosporine as the ligand. This could be repeated using less toxic kinase inhibitors such as AZ compounds or Rottlerin against other kinase domains from other bacterial strains or even humans. The greater implications of this work could result in a combinational treatment using kinase inhibitors and antibiotics together to provide a method to tackle multi-drug resistance Gram-positive bacterial infections.

References

1. Agrawal, Ganesh K., & Thelen, J. J. (2009). A High-Resolution Two Dimensional Gel- and Pro-Q DPS-Based Proteomics Workflow for Phosphoprotein Identification and Quantitative Profiling. In *Phospho-Proteomics* (pp. 3–19). Humana Press. https://doi.org/10.1007/978-1-60327-834-8_1

2. Agrawal, Ganesh Kumar, & Thelen, J. J. (2009). A Modified Pro-Q Diamond Staining Protocol for Phosphoprotein Detection in Polyacrylamide Gels. In *The Protein Protocols Handbook* (pp. 579–585). Humana Press, Totowa, NJ. https://doi.org/10.1007/978-1-59745-198-7_54

3. Alber, T. (2009). Signaling mechanisms of the Mycobacterium tuberculosis receptor Ser/Thr protein kinases. *Current Opinion in Structural Biology*, *19*(6), 650–657. https://doi.org/10.1016/j.sbi.2009.10.017

4. Av-Gay, Y., & Everett, M. (2000). The eukaryotic-like Ser/Thr protein kinases of Mycobacterium tuberculosis. *Trends in Microbiology*, *8*(5), 238–244. https://doi.org/10.1016/S0966-842X(00)01734-0

5. Bakal, C. J., & Davies, J. E. (2000). No longer an exclusive club: eukaryotic signalling domains in bacteria. *Trends in Cell Biology*, *10*(1), 32–38. https://doi.org/10.1016/S0962-8924(99)01681-5

6. Barford, D. (1995). Protein phosphatases. *Current Opinion in Structural Biology*, *5*(6), 728–734. https://doi.org/10.1016/0959-440X(95)80004-2

7. Barthe, P., Mukamolova, G. V., Roumestand, C., & Cohen-Gonsaud, M. (2010). The Structure of PknB Extracellular PASTA Domain from Mycobacterium tuberculosis Suggests a Ligand-Dependent Kinase Activation. *Structure*, *18*(5), 606–615. https://doi.org/10.1016/j.str.2010.02.013

8. Beeby, M., Gumbart, J. C., Roux, B., & Jensen, G. J. (2013). Architecture and assembly of the Gram-positive cell wall. *Molecular Microbiology*, *88*(4), 664–672. https://doi.org/10.1111/mmi.12203

9. Beltramini, A. M., Mukhopadhyay, C. D., & Pancholi, V. (2009). Modulation of Cell Wall Structure and Antimicrobial Susceptibility by a Staphylococcus aureus Eukaryote-Like Serine/Threonine Kinase and Phosphatase. *Infection and Immunity*, *77*(4), 1406–1416. https://doi.org/10.1128/IAI.01499-08

10. Bennett, A. F., Dao, K. M., & Lenski, R. E. (1990). Rapid evolution in response to high-temperature selection. *Nature*, *346*(6279), 79–81. https://doi.org/10.1038/346079a0

11. Bertani, G. (1951). STUDIES ON LYSOGENESIS I. *Journal of Bacteriology*, *62*(3), 293–300.

12. Bizzini, A., Zhao, C., Auffray, Y., & Hartke, A. (2009). The Enterococcus faecalis superoxide dismutase is essential for its tolerance to vancomycin and penicillin. *Journal of Antimicrobial Chemotherapy*, *64*(6), 1196–1202. https://doi.org/10.1093/jac/dkp369

13. Bonnet, R. (2004). Growing group of extended-spectrum beta-lactamases: the CTX-M enzymes. *Antimicrobial Agents and Chemotherapy*, *48*(1), 1–14.

14. Bork, P., Brown, N. P., Hegyi, H., & Schultz, J. (1996). The protein phosphatase 2C (PP2C) superfamily: Detection of bacterial homologues. *Protein Science*, *5*(7), 1421–1425. https://doi.org/10.1002/pro.5560050720

15. Brewer, N. S., & Hellinger, W. C. (1991). The monobactams. *Mayo Clinic Proceedings*, *66*(11), 1152–1157.

16. Brown, L., Wolf, J. M., Prados-Rosales, R., & Casadevall, A. (2015). Through the wall: extracellular vesicles in Gram-positive bacteria, mycobacteria and fungi. *Nature Reviews Microbiology*, *13*(10), 620–630. https://doi.org/10.1038/nrmicro3480

17. Burnside, K., Lembo, A., Reyes, M. de los, Iliuk, A., BinhTran, N.-T., Connelly, J. E., … Rajagopal, L. (2010). Regulation of Hemolysin Expression and Virulence of Staphylococcus aureus by a Serine/Threonine Kinase and Phosphatase. *PLOS ONE*, *5*(6), e11071. https://doi.org/10.1371/journal.pone.0011071

18. Canova, M. J., Baronian, G., Brelle, S., Cohen-Gonsaud, M., Bischoff, M., & Molle, V. (2014). A novel mode of regulation of the Staphylococcus aureus Vancomycin-resistance-associated response regulator VraR mediated by Stk1 protein phosphorylation. *Biochemical and Biophysical Research Communications*, *447*(1), 165–171. https://doi.org/10.1016/j.bbrc.2014.03.128

19. CDC. (2016, January 1). CDC Press Releases. Retrieved 22 May 2018, from https://www.cdc.gov/media/releases/2015/p0225-clostridium-difficile.html

20. Cole, J. L. (2007). Activation of PKR: An open and shut case? *Trends in Biochemical Sciences*, *32*(2), 57–62. https://doi.org/10.1016/j.tibs.2006.12.003

21. Đapa, T., Leuzzi, R., Ng, Y. K., Baban, S. T., Adamo, R., Kuehne, S. A., … Unnikrishnan, M. (2013). Multiple Factors Modulate Biofilm Formation by the Anaerobic Pathogen Clostridium difficile. *Journal of Bacteriology*, *195*(3), 545–555. https://doi.org/10.1128/JB.01980-12

22. Dar, A. C., Dever, T. E., & Sicheri, F. (2005). Higher-Order Substrate Recognition of eIF2α by the RNA-Dependent Protein Kinase PKR. *Cell*, *122*(6), 887–900. https://doi.org/10.1016/j.cell.2005.06.044

23. Das, A. K., Helps, N. R., Cohen, P. T., & Barford, D. (1996). Crystal structure of the protein serine/threonine phosphatase 2C at 2.0 A resolution. *The EMBO Journal*, *15*(24), 6798–6809.

24. De Biase, D., & Lund, P. A. (2015). The Escherichia coli Acid Stress Response and Its Significance for Pathogenesis. *Advances in Applied Microbiology*, *92*, 49–88. https://doi.org/10.1016/bs.aambs.2015.03.002

25. Dessen, A., Mouz, N., Gordon, E., Hopkins, J., & Dideberg, O. (2001). Crystal Structure of PBP2x from a Highly Penicillin-resistant Streptococcus pneumoniae Clinical Isolate A MOSAIC FRAMEWORK CONTAINING 83 MUTATIONS. *Journal of Biological Chemistry*, *276*(48), 45106–45112. https://doi.org/10.1074/jbc.M107608200

26. Didier, J.-P., Cozzone, A. J., & Duclos, B. (2010). Phosphorylation of the virulence regulator SarA modulates its ability to bind DNA in Staphylococcus aureus. *FEMS Microbiology Letters*, *306*(1), 30–36. https://doi.org/10.1111/j.1574-6968.2010.01930.x

27. Dridi, L., Tankovic, J., & Petit, J.-C. (2004). CdeA of Clostridium difficile, a new multidrug efflux transporter of the MATE family. *Microbial Drug Resistance (Larchmont, N.Y.)*, *10*(3), 191–196. https://doi.org/10.1089/mdr.2004.10.191

28. Dupuy, B., & Sonenshein, A. L. (1998). Regulated transcription of Clostridium difficile toxin genes. *Molecular Microbiology*, *27*(1), 107–120.

29. Eades, C., Hughes, S., Heard, K., & SP Moore, L. (2017, December 9). Antimicrobial therapies for Gram-positive infections. Retrieved 22 May 2018, from https://www.pharmaceutical-journal.com/research/antimicrobial-therapies-for-gram-positive-infections/20203363.article

30. Eliopoulos, G. M., & Gold, H. S. (2001). Vancomycin-Resistant Enterococci: Mechanisms and Clinical Observations. *Clinical Infectious Diseases*, *33*(2), 210–219. https://doi.org/10.1086/321815

31. Fernandez, P., Saint-Joanis, B., Barilone, N., Jackson, M., Gicquel, B., Cole, S. T., & Alzari, P. M. (2006). The Ser/Thr protein kinase PknB is essential for sustaining mycobacterial growth. *Journal of Bacteriology*, *188*(22), 7778–7784. https://doi.org/10.1128/JB.00963-06

32. Freeman, J., Baines, S. D., Saxton, K., & Wilcox, M. H. (2007). Effect of metronidazole on growth and toxin production by epidemic Clostridium difficile PCR ribotypes 001 and 027 in a human gut model. *Journal of Antimicrobial Chemotherapy*, *60*(1), 83–91. https://doi.org/10.1093/jac/dkm113

33. Gagnon, S., Lévesque, S., Lefebvre, B., Bourgault, A.-M., Labbé, A.-C., & Roger, M. (2011). vanA-containing Enterococcus faecium susceptible to vancomycin and teicoplanin because of major nucleotide deletions in Tn1546. *The Journal of Antimicrobial Chemotherapy*, *66*(12), 2758–2762. https://doi.org/10.1093/jac/dkr379

34. Gianfrilli, P., Luzzi, I., Pantosti, A., Occhionero, M., Gentile, G., & Panichi, G. (1984). Cytotoxin and enterotoxin production by Clostridium difficile. *Microbiologica*, *7*(4), 375–379.

35. Gilmore, M. S., Clewell, D. B., & Courvalin, P. (2002). *The Enterococci: Pathogenesis, Molecular Biology, and Antibiotic Resistance*. ASM Press.

36. Goss, L. A. (2013). Threonine Phosphorylation Regulates Two-Component Systems Involved in Cell Wall Metabolism. Retrieved from https://academiccommons.columbia.edu/catalog/ac%3A188993

37. Greenstein, A. E., Echols, N., Lombana, T. N., King, D. S., & Alber, T. (2007). Allosteric Activation by Dimerization of the PknD Receptor Ser/Thr Protein Kinase from Mycobacterium tuberculosis. *Journal of Biological Chemistry*, *282*(15), 11427–11435. https://doi.org/10.1074/jbc.M610193200

38. Hall, C. L., Tschannen, M., Worthey, E. A., & Kristich, C. J. (2013). IreB, a Ser/Thr kinase substrate, influences antimicrobial resistance in Enterococcus faecalis. *Antimicrobial Agents and Chemotherapy*, *57*(12), 6179–6186. https://doi.org/10.1128/AAC.01472-13

39. Hall, I., & O'Toole, E. (1935). Intestinal flora in newborn infants with a description of a new pathogenic anaerobe, Bacillus difficilis. *Am J Dis Child*, (49), 390.

40. Hanahan, D. (1983). Studies on transformation of Escherichia coli with plasmids. *Journal of Molecular Biology*, *166*(4), 557–580.

41. Healy, V. L., Lessard, I. A., Roper, D. I., Knox, J. R., & Walsh, C. T. (2000). Vancomycin resistance in enterococci: reprogramming of the d-Ala–d-Ala ligases in bacterial peptidoglycan biosynthesis. *Chemistry & Biology*, *7*(5), R109–R119. https://doi.org/10.1016/S1074-5521(00)00116-2

42. Hegstad, K., Mikalsen, T., Coque, T. M., Werner, G., & Sundsfjord, A. (2010). Mobile genetic elements and their contribution to the emergence of antimicrobial resistant Enterococcus faecalis and Enterococcus faecium. *Clinical Microbiology and Infection*, *16*(6), 541–554. https://doi.org/10.1111/j.1469-0691.2010.03226.x

43. Heinlen, L., & Ballard, J. D. (2010). Clostridium difficile Infection. *The American Journal of the Medical Sciences*, *340*(3), 247–252. https://doi.org/10.1097/MAJ.0b013e3181e939d8

44. Hennequin, C., Porcheray, F., Waligora-Dupriet, A., Collignon, A., Barc, M., Bourlioux, P., & Karjalainen, T. (2001). GroEL (Hsp60) of Clostridium difficile is involved in cell adherence. *Microbiology (Reading, England)*, *147*(Pt 1), 87–96. https://doi.org/10.1099/00221287-147-1-87

45. Hollenbeck, B. L., & Rice, L. B. (2012). Intrinsic and acquired resistance mechanisms in enterococcus. *Virulence*, *3*(5), 421–569. https://doi.org/10.4161/viru.21282

46. Huse, M., & Kuriyan, J. (2002). The Conformational Plasticity of Protein Kinases. *Cell*, *109*(3), 275–282. https://doi.org/10.1016/S0092-8674(02)00741-9

47. Huycke M, M., Sahm F, D., & Gilmore S, M. (1998). Multiple-Drug Resistant Enterococci: The Nature of the Problem and an Agenda for the Future - Volume 4, Number 2—June 1998 - Emerging Infectious Disease journal - CDC. https://doi.org/10.3201/eid0402.980211

48. Jackson, S., Calos, M., Myers, A., & Self, W. T. (2006). Analysis of Proline Reduction in the Nosocomial Pathogen Clostridium difficile. *Journal of Bacteriology*, *188*(24), 8487–8495. https://doi.org/10.1128/JB.01370-06

49. Jung, K., Fabiani, F., Hoyer, E., & Lassak, J. (2018). Bacterial transmembrane signalling systems and their engineering for biosensing. *Open Biology*, *8*(4), 180023. https://doi.org/10.1098/rsob.180023

50. Juris, S. J., Rudolph, A. E., Huddler, D., Orth, K., & Dixon, J. E. (2000). A distinctive role for the Yersinia protein kinase: Actin binding, kinase activation, and cytoskeleton disruption. *Proceedings of the National Academy of Sciences*, *97*(17), 9431–9436. https://doi.org/10.1073/pnas.170281997

51. Kalantari, A., Mijakovic, I., Shi, L., & Derouiche, A. (2015). Serine/threonine/tyrosine phosphorylation regulates DNA binding of bacterial transcriptional regulators. *Microbiology*, *161*(9), 1720–1729. https://doi.org/10.1099/mic.0.000148

52. Kang, H.-K., & Park, Y. (2015). Glycopeptide Antibiotics: Structure and Mechanisms of Action. *Journal of Bacteriology and Virology*, *45*(2), 67. https://doi.org/10.4167/jbv.2015.45.2.67

53. Kellogg, S. L., & Kristich, C. J. (2018). Convergence of PASTA kinase and two-component signaling in response to cell wall stress in Enterococcus faecalis. *Journal of Bacteriology*, JB.00086-18. https://doi.org/10.1128/JB.00086-18

54. Kong, K.-F., Schneper, L., & Mathee, K. (2010). Beta-lactam Antibiotics: From Antibiosis to Resistance and Bacteriology. *APMIS : Acta Pathologica, Microbiologica, et Immunologica Scandinavica*, *118*(1), 1–36. https://doi.org/10.1111/j.1600-0463.2009.02563.x

55. Koul, A., Choidas, A., Treder, M., Tyagi, A. K., Drlica, K., Singh, Y., & Ullrich, A. (2000). Cloning and Characterization of Secretory Tyrosine Phosphatases of Mycobacterium tuberculosis. *Journal of Bacteriology*, *182*(19), 5425–5432. https://doi.org/10.1128/JB.182.19.5425-5432.2000

56. Kristich, C. J., Little, J. L., Hall, C. L., & Hoff, J. S. (2011). Reciprocal Regulation of Cephalosporin Resistance in Enterococcus faecalis. *MBio*, *2*(6), e00199-11. https://doi.org/10.1128/mBio.00199-11

57. Kristich, C. J., Rice, L. B., & Arias, C. A. (2014). Enterococcal Infection—Treatment and Antibiotic Resistance. In M. S. Gilmore, D. B. Clewell, Y. Ike, & N. Shankar (Eds.), *Enterococci: From Commensals to Leading Causes of Drug Resistant Infection*. Boston: Massachusetts Eye and Ear Infirmary. Retrieved from http://www.ncbi.nlm.nih.gov/books/NBK190420/

58. Kristich, C. J., Wells, C. L., & Dunny, G. M. (2007). A eukaryotic-type Ser/Thr kinase in Enterococcus faecalis mediates antimicrobial resistance and intestinal persistence. *Proceedings of the National Academy of Sciences*, *104*(9), 3508–3513. https://doi.org/10.1073/pnas.0608742104

59. Kuriyama, T., Karasawa, T., & Williams, D. W. (2014). Chapter Thirteen - Antimicrobial Chemotherapy: Significance to Healthcare. In *Biofilms in Infection Prevention and Control* (pp. 209–244). Boston: Academic Press. https://doi.org/10.1016/B978-0-12-397043-5.00013-X

60. Kuroda, M., Kuwahara-Arai, K., & Hiramatsu, K. (2000). Identification of the Up- and Down-Regulated Genes in Vancomycin-Resistant Staphylococcus aureus Strains Mu3 and Mu50 by cDNA Differential Hybridization Method. *Biochemical and Biophysical Research Communications*, *269*(2), 485–490. https://doi.org/10.1006/bbrc.2000.2277

61. Liu, Q., Fan, J., Niu, C., Wang, D., Wang, J., Wang, X., … Gao, Q. (2011). The Eukaryotic-Type Serine/Threonine Protein Kinase Stk Is Required for Biofilm Formation and Virulence in Staphylococcus epidermidis. *PLoS ONE*, *6*(9). https://doi.org/10.1371/journal.pone.0025380

62. Madhusudan, Akamine, P., Xuong, N.-H., & Taylor, S. S. (2002). Crystal structure of a transition state mimic of the catalytic subunit of cAMP-dependent protein kinase. *Nature Structural & Molecular Biology*, *9*(4), 273–277. https://doi.org/10.1038/nsb780

63. Manuse, S., Fleurie, A., Zucchini, L., Lesterlin, C., & Grangeasse, C. (2016). Role of eukaryotic-like serine/threonine kinases in bacterial cell division and morphogenesis. *FEMS Microbiology Reviews*, *40*(1), 41–56. https://doi.org/10.1093/femsre/fuv041

64. Maza, L. M. D. la, Pezzlo, M. T., & Shigei, J. T. (2004). *Color Atlas of Medical Bacteriology*. ASM Press.

65. Meggio, F., Donella Deana, A., Ruzzene, M., Brunati, A. M., Cesaro, L., Guerra, B., … Furet, P. (1995). Different susceptibility of protein kinases to staurosporine inhibition. Kinetic studies and molecular bases for the resistance of protein kinase CK2. *European Journal of Biochemistry*, *234*(1), 317–322.

66. Mieczkowski, C., Iavarone, A. T., & Alber, T. (2008). Auto-activation mechanism of the Mycobacterium tuberculosis PknB receptor Ser/Thr kinase. *The EMBO Journal*, *27*(23), 3186–3197. https://doi.org/10.1038/emboj.2008.236

67. Miller, V. L., Taylor, R. K., & Mekalanos, J. J. (1987). Cholera toxin transcriptional activator ToxR is a transmembrane DNA binding protein. *Cell*, *48*(2), 271–279. https://doi.org/10.1016/0092-8674(87)90430-2

68. Miroux, B., & Walker, J. E. (1996). Over-production of proteins in Escherichia coli: mutant hosts that allow synthesis of some membrane proteins and globular proteins at high levels. *Journal of Molecular Biology*, *260*(3), 289–298. https://doi.org/10.1006/jmbi.1996.0399

69. Muñoz-Dorado, J., Inouye, S., & Inouye, M. (1991). A gene encoding a protein serine/threonine kinase is required for normal development of M. xanthus, a gram-negative bacterium. *Cell*, *67*(5), 995–1006. https://doi.org/10.1016/0092-8674(91)90372-6

70. Navarre, W. W., & Schneewind, O. (1999). Surface Proteins of Gram-Positive Bacteria and Mechanisms of Their Targeting to the Cell Wall Envelope. *Microbiology and Molecular Biology Reviews*, *63*(1), 174–229.

71. Nguyen, T. N., Phan, Q. G., Duong, L. P., Bertrand, K. P., & Lenski, R. E. (1989). Effects of carriage and expression of the Tn10 tetracycline-resistance operon on the fitness of Escherichia coli K12. *Molecular Biology and Evolution*, *6*(3), 213–225. https://doi.org/10.1093/oxfordjournals.molbev.a040545

72. Ohlsen, K., & Donat, S. (2010). The impact of serine/threonine phosphorylation in Staphylococcus aureus. *International Journal of Medical Microbiology*, *300*(2), 137–141. https://doi.org/10.1016/j.ijmm.2009.08.016

73. Ortiz-Lombardía, M., Pompeo, F., Boitel, B., & Alzari, P. M. (2003). Crystal Structure of the Catalytic Domain of the PknB Serine/Threonine Kinase from Mycobacterium tuberculosis. *Journal of Biological Chemistry*, *278*(15), 13094–13100. https://doi.org/10.1074/jbc.M300660200

74. Palmer, K. L., Kos, V. N., & Gilmore, M. S. (2010). Horizontal Gene Transfer and the Genomics of Enterococcal Antibiotic Resistance. *Current Opinion in Microbiology*, *13*(5), 632–639. https://doi.org/10.1016/j.mib.2010.08.004

75. Papp-Wallace, K. M., Endimiani, A., Taracila, M. A., & Bonomo, R. A. (2011). Carbapenems: Past, Present, and Future ▿. *Antimicrobial Agents and Chemotherapy*, *55*(11), 4943–4960. https://doi.org/10.1128/AAC.00296-11

76. Paredes, C. J., Alsaker, K. V., & Papoutsakis, E. T. (2005). A comparative genomic view of clostridial sporulation and physiology. *Nature Reviews Microbiology*, *3*(12), 969–978. https://doi.org/10.1038/nrmicro1288

77. Paulsen, I. T., Banerjei, L., Myers, G. S. A., Nelson, K. E., Seshadri, R., Read, T. D., … Fraser, C. M. (2003). Role of Mobile DNA in the Evolution of Vancomycin-Resistant Enterococcus faecalis. *Science*, *299*(5615), 2071–2074. https://doi.org/10.1126/science.1080613

78. Pensinger, D. A., Schaenzer, A. J., & Sauer, J.-D. (2018). Do Shoot the Messenger: PASTA Kinases as Virulence Determinants and Antibiotic Targets. *Trends in Microbiology*, *26*(1), 56–69. https://doi.org/10.1016/j.tim.2017.06.010

79. Pereira, S. F. F., Goss, L., & Dworkin, J. (2011). Eukaryote-Like Serine/Threonine Kinases and Phosphatases in Bacteria. *Microbiology and Molecular Biology Reviews*, *75*(1), 192–212. https://doi.org/10.1128/MMBR.00042-10

80. Pope, C. F., McHugh, T. D., & Gillespie, S. H. (2010). Methods to Determine Fitness in Bacteria. In *Antibiotic Resistance Protocols* (pp. 113–121). Humana Press. https://doi.org/10.1007/978-1-60327-279-7_9

81. Prade, L., Engh, R. A., Girod, A., Kinzel, V., Huber, R., & Bossemeyer, D. (1997). Staurosporine-induced conformational changes of cAMP-dependent protein kinase catalytic subunit explain inhibitory potential. *Structure (London, England: 1993)*, *5*(12), 1627–1637.

82. Pubchem. (2018). Vancomycin. Retrieved 10 May 2018, from https://pubchem.ncbi.nlm.nih.gov/compound/14969

83. Rajagopal, L., Vo, A., Silvestroni, A., & Rubens, C. E. (2006). Regulation of cytotoxin expression by converging eukaryotic-type and two-component signalling mechanisms in Streptococcus agalactiae. *Molecular Microbiology*, *62*(4), 941–957. https://doi.org/10.1111/j.1365-2958.2006.05431.x

84. Rao, A., Jump, R. L. P., Pultz, N. J., Pultz, M. J., & Donskey, C. J. (2006). In vitro killing of nosocomial pathogens by acid and acidified nitrite. *Antimicrobial Agents and Chemotherapy*, *50*(11), 3901–3904. https://doi.org/10.1128/AAC.01506-05

85. Reynolds, P. E. (1989). Structure, biochemistry and mechanism of action of glycopeptide antibiotics. *European Journal of Clinical Microbiology & Infectious Diseases: Official Publication of the European Society of Clinical Microbiology*, *8*(11), 943–950.

86. Rice, L. B., Carias, L. L., Rudin, S., Laktičová, V., Wood, A., & Hutton-Thomas, R. (2005). Enterococcus faecium Low-Affinity pbp5 Is a Transferable Determinant. *Antimicrobial Agents and Chemotherapy*, *49*(12), 5007–5012. https://doi.org/10.1128/AAC.49.12.5007-5012.2005

87. Roberts, M. C. (2005). Update on acquired tetracycline resistance genes. *FEMS Microbiology Letters*, *245*(2), 195–203. https://doi.org/10.1016/j.femsle.2005.02.034

88. S. Tsutsumi, L., B. Owusu, Y., G. Hurdle, J., & Sun, D. (2014, January). Progress in the Discovery of Treatments for C. difficile Infection: A Clinical and Medicinal Chemistry Review [Text]. Retrieved 23 May 2018, from http://0-www.ingentaconnect.com.pugwash.lib.warwick.ac.uk/content/ben/ctmc/2014/00000014/00000001/art00011

89. Schlicker, C., Fokina, O., Kloft, N., Grüne, T., Becker, S., Sheldrick, G. M., & Forchhammer, K. (2008). Structural Analysis of the PP2C Phosphatase tPphA from Thermosynechococcus

elongatus: A Flexible Flap Subdomain Controls Access to the Catalytic Site. *Journal of Molecular Biology*, *376*(2), 570–581. https://doi.org/10.1016/j.jmb.2007.11.097

90. Schmidl, S. R., Gronau, K., Hames, C., Busse, J., Becher, D., Hecker, M., & Stülke, J. (2010). The Stability of Cytadherence Proteins in Mycoplasma pneumoniae Requires Activity of the Protein Kinase PrkC. *Infection and Immunity*, *78*(1), 184–192. https://doi.org/10.1128/IAI.00958-09

91. Shah, I. M., Laaberki, M.-H., Popham, D. L., & Dworkin, J. (2008). A Eukaryotic-like Ser/Thr Kinase Signals Bacteria to Exit Dormancy in Response to Peptidoglycan Fragments. *Cell*, *135*(3), 486–496. https://doi.org/10.1016/j.cell.2008.08.039

92. Shakir, S. M., Bryant, K. M., Larabee, J. L., Hamm, E. E., Lovchik, J., Lyons, C. R., & Ballard, J. D. (2010). Regulatory Interactions of a Virulence-Associated Serine/Threonine Phosphatase-Kinase Pair in Bacillus anthracis. *Journal of Bacteriology*, *192*(2), 400–409. https://doi.org/10.1128/JB.01221-09

93. Shi, L., Potts, M., & Kennelly, P. J. (1998). The serine, threonine, and/or tyrosine-specific protein kinases and protein phosphatases of prokaryotic organisms: a family portrait. *FEMS Microbiology Reviews*, *22*(4), 229–253. https://doi.org/10.1111/j.1574-6976.1998.tb00369.x

94. Sickmann, A., & Meyer, H. E. (2001). Phosphoamino acid analysis. *PROTEOMICS*, *1*(2), 200–206. https://doi.org/10.1002/1615-9861(200102)1:2<200::AID-PROT200>3.0.CO;2-V

95. Sifaoui, F., Arthur, M., Rice, L., & Gutmann, L. (2001). Role of Penicillin-Binding Protein 5 in Expression of Ampicillin Resistance and Peptidoglycan Structure in Enterococcus faecium. *Antimicrobial Agents and Chemotherapy*, *45*(9), 2594–2597. https://doi.org/10.1128/AAC.45.9.2594-2597.2001

96. Spigaglia, P. (2016). Recent advances in the understanding of antibiotic resistance in Clostridium difficile infection. *Therapeutic Advances in Infectious Disease*, *3*(1), 23–42. https://doi.org/10.1177/2049936115622891

97. Spigaglia, P., Carucci, V., Barbanti, F., & Mastrantonio, P. (2005). ErmB Determinants and Tn916-Like Elements in Clinical Isolates of Clostridium difficile. *Antimicrobial Agents and Chemotherapy*, *49*(6), 2550–2553. https://doi.org/10.1128/AAC.49.6.2550-2553.2005

98. Stock, J. B., Stock, A. M., & Mottonen, J. M. (1990). Signal transduction in bacteria. *Nature*, *344*(6265), 395–400. https://doi.org/10.1038/344395a0

99. Studier, F. W., & Moffatt, B. A. (1986). Use of bacteriophage T7 RNA polymerase to direct selective high-level expression of cloned genes. *Journal of Molecular Biology*, *189*(1), 113–130.

100. Tacconelli, E., Carrara, E., Savoldi, A., Harbarth, S., Mendelson, M., Monnet, D. L., … Zorzet, A. (2018). Discovery, research, and development of new antibiotics: the WHO priority list of antibiotic-resistant bacteria and tuberculosis. *The Lancet Infectious Diseases*, *18*(3), 318–327. https://doi.org/10.1016/S1473-3099(17)30753-3

101. Tanramluk, D., Schreyer, A., Pitt, W. R., & Blundell, T. L. (2009). On the Origins of Enzyme Inhibitor Selectivity and Promiscuity: A Case Study of Protein Kinase Binding to

Staurosporine. *Chemical Biology & Drug Design*, *74*(1), 16–24. https://doi.org/10.1111/j.1747-0285.2009.00832.x

102. Thoroughgood, C. (2018, April). *Functional and structural studies of an Enterococcal Serine/Threonine kinase and its contribution to antibiotic resistance mechanisms* (PhD). University of Warwick.

103. Treuner-Lange, A., Ward, M. J., & Zusman, D. R. (2001). Pph1 from Myxococcus xanthus is a protein phosphatase involved in vegetative growth and development. *Molecular Microbiology*, *40*(1), 126–140. https://doi.org/10.1046/j.1365-2958.2001.02362.x

104. Udo, H., Munoz-Dorado, J., Inouye, M., & Inouye, S. (1995). Myxococcus xanthus, a gram-negative bacterium, contains a transmembrane protein serine/threonine kinase that blocks the secretion of beta-lactamase by phosphorylation. *Genes & Development*, *9*(8), 972–983. https://doi.org/10.1101/gad.9.8.972

105. Ulrich, L. E., Koonin, E. V., & Zhulin, I. B. (2005). One-component systems dominate signal transduction in prokaryotes. *Trends in Microbiology*, *13*(2), 52–56. https://doi.org/10.1016/j.tim.2004.12.006

106. Ungureanu, V. (2010). [Macrolides, lincosamides, streptogramines (MLS): mechanisms of action and resistance]. *Bacteriologia, Virusologia, Parazitologia, Epidemiologia (Bucharest, Romania: 1990)*, *55*(2), 131–138.

107. Vicente, A. F., Antunes, J. M. A. P., Lara, G. H. B., Mioni, M. S. R., Allendorf, S. D., Peres, M. G., … Megid, J. (2014). Evaluation of Three Formulations of Culture Media for Isolation of Brucella spp. regarding Their Ability to Inhibit the Growth of Contaminating Organisms [Research article]. https://doi.org/10.1155/2014/702072

108. Vuotto, C., Moura, I., Barbanti, F., Donelli, G., & Spigaglia, P. (2016). Subinhibitory concentrations of metronidazole increase biofilm formation in Clostridium difficile strains. *Pathogens and Disease*, *74*(2). https://doi.org/10.1093/femspd/ftv114

109. Wamel, W. J. B. V., Hendrickx, A. P. A., Bonten, M. J. M., Top, J., Posthuma, G., & Willems, R. J. L. (2007). Growth Condition-Dependent Esp Expression by Enterococcus faecium Affects Initial Adherence and Biofilm Formation. *Infection and Immunity*, *75*(2), 924–931. https://doi.org/10.1128/IAI.00941-06

110. Wasels, F., Monot, M., Spigaglia, P., Barbanti, F., Ma, L., Bouchier, C., … Mastrantonio, P. (2014). Inter- and Intraspecies Transfer of a Clostridium difficile Conjugative Transposon Conferring Resistance to MLSB. *Microbial Drug Resistance*, *20*(6), 555–560. https://doi.org/10.1089/mdr.2014.0015

111. Watanakunakorn, C. (1984). Mode of action and in-vitro activity of vancomycin. *The Journal of Antimicrobial Chemotherapy*, *14 Suppl D*, 7–18.

112. Wehenkel, A., Bellinzoni, M., Schaeffer, F., Villarino, A., & Alzari, P. M. (2007). Structural and Binding Studies of the Three-metal Center in Two Mycobacterial PPM Ser/Thr Protein Phosphatases. *Journal of Molecular Biology*, *374*(4), 890–898. https://doi.org/10.1016/j.jmb.2007.09.076

113. Werner, G., Coque, T. M., Franz, C. M. A. P., Grohmann, E., Hegstad, K., Jensen, L., … Weaver, K. (2013). Antibiotic resistant enterococci—Tales of a drug resistance gene trafficker. *International Journal of Medical Microbiology*, *303*(6), 360–379. https://doi.org/10.1016/j.ijmm.2013.03.001

114. Wilson, K. H. (1993). The microecology of Clostridium difficile. *Clinical Infectious Diseases: An Official Publication of the Infectious Diseases Society of America*, *16 Suppl 4*, S214-218.

115. Yotsuji, A., Mitsuyama, J., Hori, R., Yasuda, T., Saikawa, I., Inoue, M., & Mitsuhashi, S. (1988). Mechanism of action of cephalosporins and resistance caused by decreased affinity for penicillin-binding proteins in Bacteroides fragilis. *Antimicrobial Agents and Chemotherapy*, *32*(12), 1848–1853.

116. Young, T. A., Delagoutte, B., Endrizzi, J. A., Falick, A. M., & Alber, T. (2003). Structure of Mycobacterium tuberculosis PknB supports a universal activation mechanism for Ser/Thr protein kinases. *Nature Structural & Molecular Biology*, *10*(3), 168–174. https://doi.org/10.1038/nsb897

117. Zapun, A., Contreras-Martel, C., & Vernet, T. (2008). Penicillin-binding proteins and β-lactam resistance. *FEMS Microbiology Reviews*, *32*(2), 361–385. https://doi.org/10.1111/j.1574-6976.2007.00095.x

118. Zhang, C.-C. (1996). Bacterial signalling involving eukaryotic-type protein kinases. *Molecular Microbiology*, *20*(1), 9–15. https://doi.org/10.1111/j.1365-2958.1996.tb02483.x

119. Zhang, W., & Shi, L. (2004). Evolution of the PPM-family protein phosphatases in Streptomyces: duplication of catalytic domain and lateral recruitment of additional sensory domains. *Microbiology*, *150*(12), 4189–4197. https://doi.org/10.1099/mic.0.27480-0

120. Zschiedrich, C. P., Keidel, V., & Szurmant, H. (2016). Molecular mechanisms of two-component signal transduction. *Journal of Molecular Biology*, *428*(19), 3752–3775. https://doi.org/10.1016/j.jmb.2016.08.003

7.0 Appendix

7.1 Kinase domain protein sequences

Table 9: Kinase domain protein sequences used for sequence analysis and bacterial sequences used for design of expression plasmid constructs

eSTK Kinase domain protein sequences
***Enterococcus faecalis* ATCC 29200 kinase domain**
YHIIGSIGSGGMANVYLAHDLILDRDVAVKVLRFDFQNDQAAIRRFQREALAATELVHPN IVSVYDVGEEDGLQYLVMEYVKGMDLKRYIQTHFPIPYSTVVDITQQILSAVAMAHEHRI IHRDLKPQNILIDEHGTVKITDFGIAIALSETSITQTNTMLGSVHYLSPEQARGSMATNQ SDIYAVGIILYEMLTGNVPFDGESAVTIALKHFQEEIPSVKMFDPGIPQSLENVVRHATA KDPSDRYKTANEMAEDLY
***Enterococcus faecium* E980 kinase domain**
YQITGNIGSGGMANVFLAHDLILDRDVAVKVLRFDFQNDQTAIRRFQREALAATELVHPN IVSVYDVGEEDNMQYLVMEYVKGMDLKRYIQTHYPVPYETAVNIMQQILSAISLAHNHQI IHRDLKPQNVLIDNEGVVKITDFGIAIALSETSITQTNTMLGSVHYLSPEQARGSMATKQ SDIYALGIILYEMLTGSVPFDGESAVTIALKHFQDDLPSIKALDPNVPQALENVILRATA KEPADRYKSAEEMSDDLS
***C. difficile* ATCC 9689 kinase domain**
MGDTILGNRYEIIRKIGDGGMAFVYEAKDRLLNRTVALKVLRPEFVDDDEFLTKFKREAE AVASLSHPNIVNVYDVGEDGKVHYIVMEFVDGKNLKEIIQDEGILDEYTALDITKQIAMA LSAAHKKGIIHRDIKPHNILISNEGRVVKVADFGIAKAVSNSTMTNIGSIIGSVHYFSPE QAKGKFVTNNADLYSLGIVLYEMLIGKVPFRGDSPISIALQHINDDIDFTSEEKVRIPQS VRTTIKKLTEKSSADRYQTAEELIEDIEYIEKNIDLDFIKEYDDFATKKIDEKEINKVVN PTLAKPAPEKVVKPVEVADLDDDEDYYDDFYEEDDDEDEEEEEIMRAKKNQRPKSTPSKR TKKKKKKQESPKSRRRLK
***Homo sapiens* CDK2 Human Cyclin-dependent Kinase**
MENFQKVEKIGEGTYGVVYKARNKLTGEVVALKKIRLDTETEGVPSTAIREISLLKELNH PNIVKLLDVIHTENKLYLVFEFLHQDLKKFMDASALTGIPLPLIKSYLFQLLQGLAFCHS HRVLHRDLKPQNLLINTEGAIKLADFGLARAFGVPVRTYTHEVVTLWYRAPEILLGCKYY STAVDIWSLGCIFAEMVTRRALFPGDSEIDQLFRIFRTLGTPDEVVWPGVTSMPDYKPSF PKWARQDFSKVVPPLDEDGRSLLSQMLHYDPNKRISAKAALAHPFFQDVTKPVPHLRL

7.2 gBlock sequences

Table 10: Designed and optimised gBlocks for expression in *E. coli*. Complementary overhangs highlighted in bold

eSTK Kinase domain gBlock sequences
***C. difficile* ATCC 9689 eSTK kinase domain**
TGT ATT TTC AGG GCG CC ATG GGA GAT ACG ATC TTG GGC AAT CGT TAC GAA ATT ATT CGT AAG ATC GGG GAT GGC GGA ATG GCA TTC GTT TAC GAG GCT AAG GAT CGT CTT TTG AAT CGT ACA GTC GCG TTG AAG GTA TTG CGC CCA GAG TTT GTC GAT GAT GAT GAA TTC CTT ACA AAG TTC AAA CGC GAG GCA GAA GCT GTT GCC TCC CTT TCA CAC CCT AAC ATT GTA AAC GTC TAT GAC GTG GGG GAG GAT GGG AAA GTC CAC TAC ATT GTA ATG GAG TTC GTT GAC GGC AAG AAC CTT AAA GAG ATC ATC CAA GAC GAG GGC ATT TTA GAC GAA TAC ACA GCT TTA GAT ATT ACT AAG CAG ATC GCC ATG GCG TTG TCT GCT GCA CAC AAG AAA GGT ATT ATC CAT CGC GAC ATC AAA CCA CAT AAT ATT TTG ATC TCG AAT GAG GGC CGC GTA GTG AAA GTA GCA GAT TTC GGG ATC GCG AAA GCA GTT TCT AAC TCC ACC ATG ACT AAC ATC GGA TCT ATT ATC GGC AGC GTG CAT TAT TTC AGC CCA GAG CAA GCG AAG GGA AAG TTT GTC ACA AAT AAT GCC GAC CTG TAC TCA TTG GGC ATT GTG CTG TAT GAA ATG CTG ATC GGT AAA GTC CCT TTT CGC GGC GAT TCT CCC ATC AGC ATC GCC TTA CAG CAC ATC AAT GAC GAT ATT GAT TTC ACT TCA GAA GAG AAA GTG CGT ATC CCC CAA AGT GTG CGT ACG ACG ATT AAA AAG TTG ACA GAA AAG TCA AGC GCT GAC CGT TAC CAA ACC GCT GAA GAG CTT ATC GAG GAT ATT GAG TAC ATC GAA AAA AAT ATC GAT TTG GAT TTT ATC AAG GAA TAC GAC GAT TTT GCG ACG AAA AAG ATC GAT GAA AAG GAG ATT AAC AAG GTC GTC AAC CCG ACC CTT GCT AAA CCG GCC CCG GAA AAG GTG GTT AAG CCA GTC GAG GTG GCA GAC CTT GAC GAT GAC GAA GAC TAT TAC GAT GAC TTT TAC GAG GAG GAT GAT GAT GAG GAC GAG GAA GAG GAA GAG ATC ATG CGT GCC AAA AAA AAC CAG CGC CCG AAG AGT ACA CCA TCC AAA CGC ACG AAA AAG AAA AAA AAA AAG CAA GAA TCA CCT AAA TCT CGT CGC CGT TTG AAG TGA **TAC AGA TTA AAT CAG AA**

7.3 First attempt at *C. difficile* eSTK expression, purification and Pro-Q Diamond stain analysis

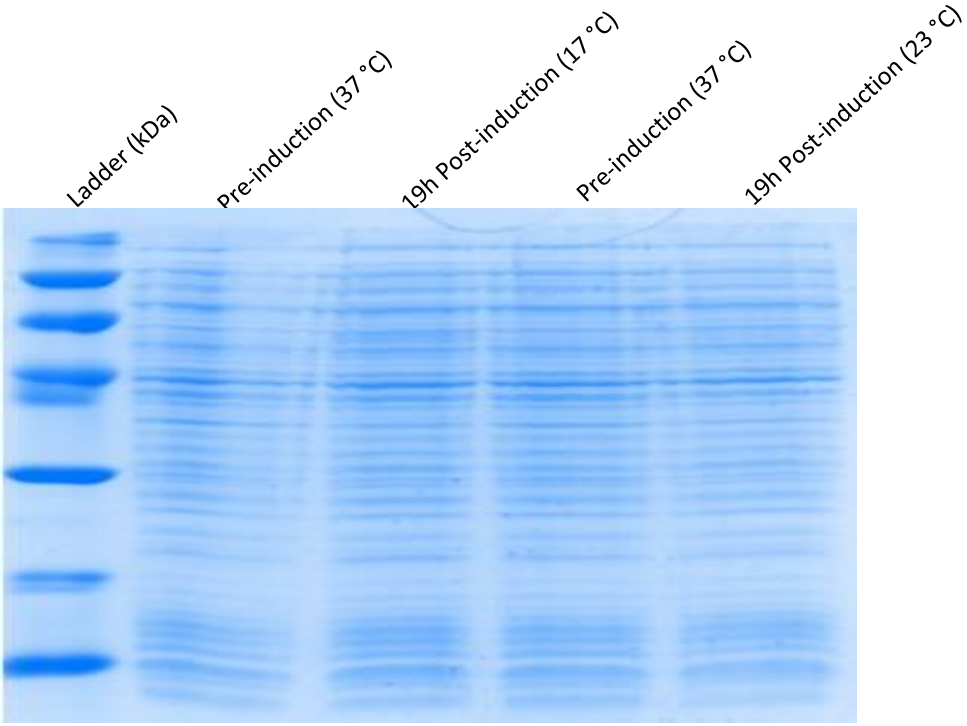

Figure 38: Expression profile of eSTK from *C. difficile* in BL21 (DE3) cells at different induction temperatures run on a 12% SDS-PAGE gel. Each lane equalised to OD 0.6 at 600nm. Lanes left to right: Pre-induction at 37°C growth, 19H post induction at 17°C, Pre-induction at 37°C growth, 19H Post-induction at 23°C. Stained with Coomassie blue.

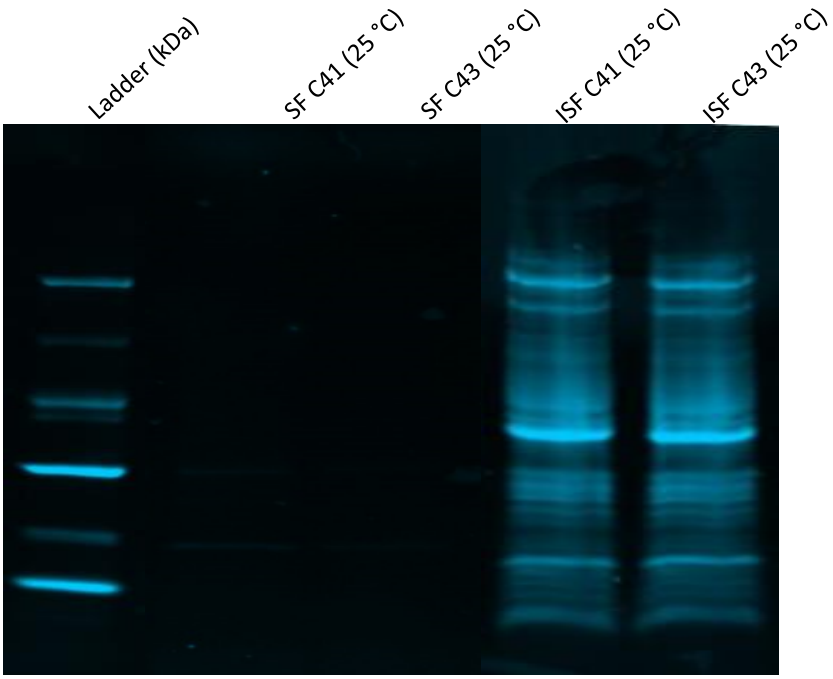

Figure 39: Expression profile of eSTK kinase domain from *C.difficile* in BL21 (DE3) cells on a 12% SDS-PAGE gel. Lanes left to right: 16.5h Induction C41 soluble fraction, 16.5h Induction C43 soluble fraction, 16.5h Induction C41 insoluble fraction, 16.5h Induction C43 insoluble fraction.

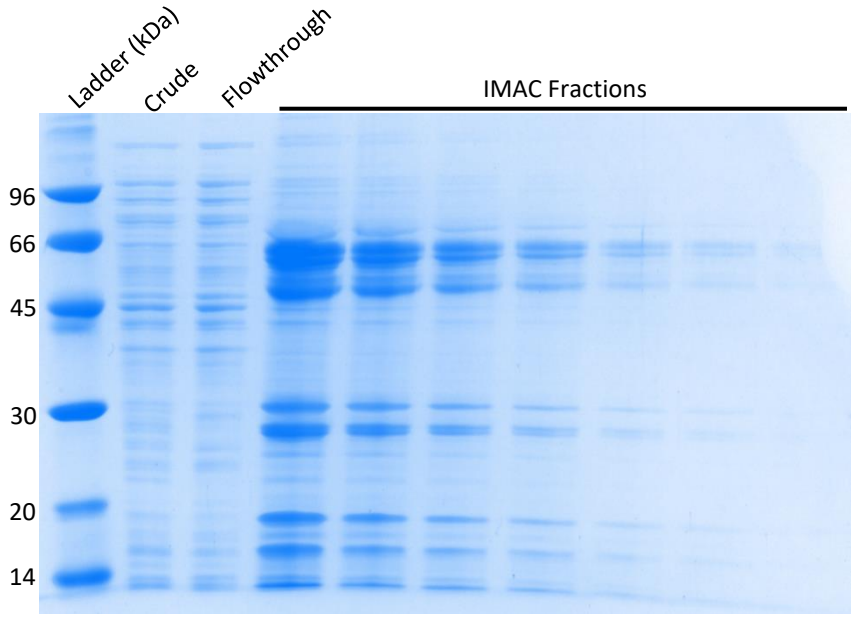

Figure 40: IMAC selected fractions of eSTK Kinase Domain from *C.difficile* on a 12% SDS-PAGE gel. Samples were normalised up to 20 µg for gel analysis. Lanes left to right: Crude extract, Flow through after column run, Pooled IMAC fractions over a serial dilution (40 µg to 1.25 µg) after column concentration.

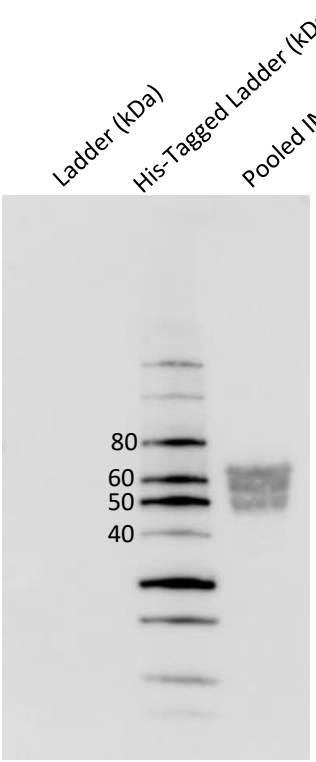

Figure 41: Western blot analysis of pooled IMAC selected fractions of eSTK Kinase Domain from *C.difficile* on a 12% SDS-PAGE gel. Lanes: IMAC pooled extract.

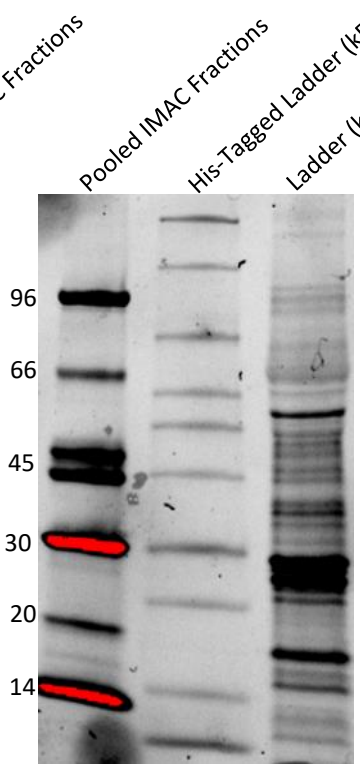

Figure 42: Pre western blot analysis of pooled IMAC selected fractions of eSTK Kinase Domain from *C.difficile* on a 12% SDS-PAGE gel. Lanes: IMAC pooled extract.

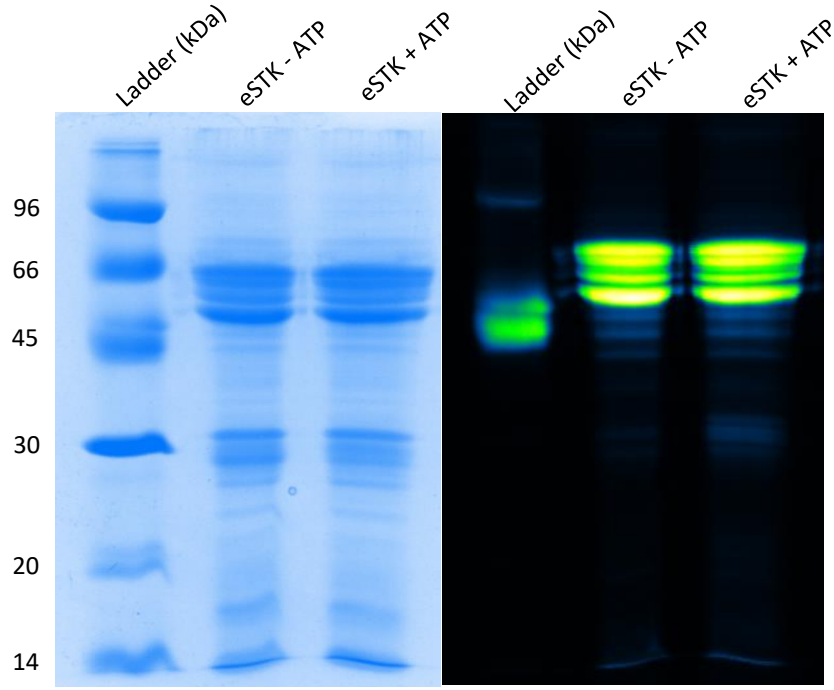

Figure 43: Autophosphorylation activity of eSTK Kinase Domain from *C. difficile* on a 12% SDS-PAGE gel. Coomassie blue staining (left) and Pro-Q Diamond staining (right) Lanes left to right: *C.difficile* eSTK protein incubated with ATP for 1 hour, *C.difficile* eSTK protein control without ATP.

7.4 Microscale Thermophoresis controls

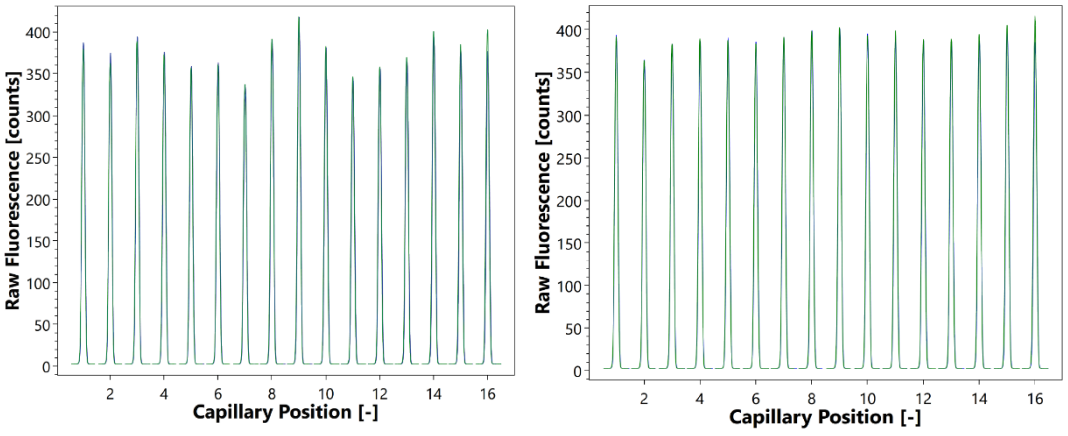

Figure 44: Capillary scans during microscale thermophoresis. Assesses variation between each capillary reaction, both sets of data are within the acceptable 10 % variation.